Chapter V

Host-Guest Complexes with Crown Ethers and a Cryptand

V.1 Introduction

A host-guest complex is a supramolecular assembly involving coordination of a receptor and a substrate by way of molecular recognition of mutually complimentary moieties. The area of supramolecular assemblies was discussed in **Chapter I**. This chapter discusses the specific area of host-guest complexation of crown ethers and a cryptand (receptors) with various secondary ammonium ion guests (substrates). Determination of stoichiometry and association constants using Nuclear Magnetic Resonance (NMR) spectroscopy are discussed for many of the systems.

V.1.1 Crown Ether Complexes

V.1.1.1 Historical Significance

Since Pedersen's discovery that crown ethers complexed alkali metals,[1,2] crown ethers have been the cornerstone of host-guest chemistry, a term first introduced by Cram.[3,4] Several reviews of complexes between crown ethers and molecular guests, both neutral and charged have been published.[5-11] Most crown ether complexes investigated were with alkali metals, but several small organic cations were also investigated as guests. Beyond the simple crown ether, crown ether moieties have been incorporated into larger molecules, such as lariat-crown ethers, oligomers, polymers, and their three-dimensional analogs, cryptands and spherands, which have been complexed with several smaller molecules and metal ions.

In 1967, Pedersen reported the first binding ability of crown ethers with dibenzo-18-crown-6 (**V-1**, **DB18C6**) and a potassium cation.[1,2] The host was defined as an ionophore. Ionophores are compounds that can bind and transport cations.[12] Pedersen also noticed that **DB18C6** was not very soluble in methanol alone, but was readily

soluble in methanol in the presence of sodium salts. Also, **DB18C6** made normally insoluble potassium permangenate soluble in benzene ("purple benzene") and chloroform.[8] Soon after this discovery the crown complexes were related to the naturally occuring complexes of cyclic antibiotics such as valinomycin and the potassium cation.[13] Crown ethers were synthesized to mimic many of the naturally occuring cyclic antibiotics.[14]

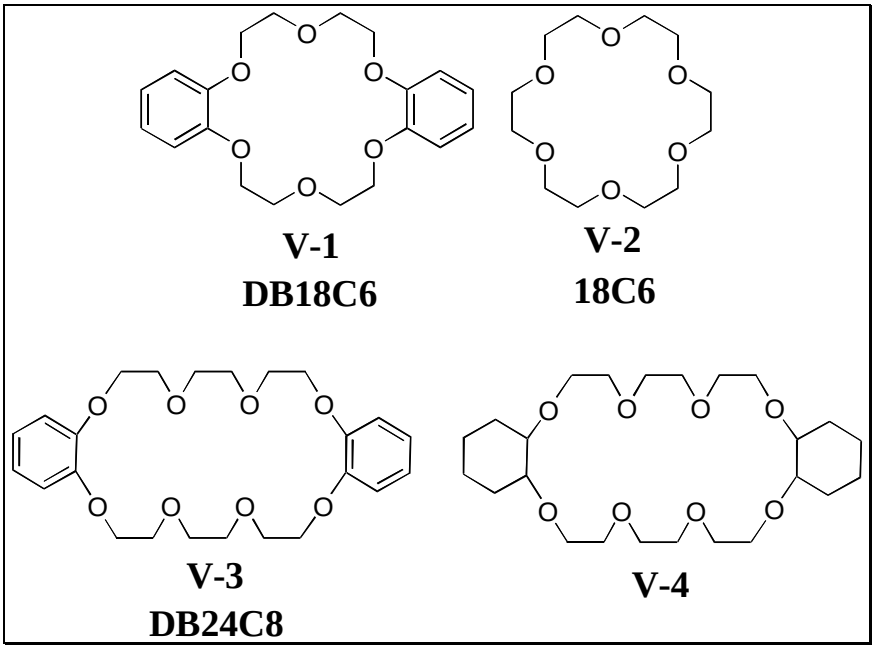

There do exist several structural and geometric requirements for the complexation of ions by the crown ether. The three most important characteristics of crown ether binding are: a) the number and type of donor atoms, b) the dimensions of the cavity, and c) the preorganization of the host molecule to create the most effective guest coordination. The last two characteristics define the *macrocycle effect* which will be discussed later.[6]

A tight fit for metal binding by crown ethers is not always a requirement, however.[12] Larger macrocycles form higher stochiometric complexes, whereas, smaller crown ethers form sandwich complexes. The crown ether can sometimes also undergo

extreme geometric conversion upon complexation. Normally the complexed and uncomplexed crowns are structurally very different.[12] "Nature abhors a vacuum;" therefore, as an example, 18-crown-6 (**V-2**, **18C6**), when complexed with the potassium cation (**Figure V-1**), exhibits D_{3d} symmetry (three ether oxgens are pointed upward and three are pointed downward permitting the favorable all-gauche conformation of the ethylene-oxy units and the alternating oxygen dipoles). **18C6** alone does not have an open cavity; the cavity is filled by two methylene groups to fill the void. The same phenomenon was observed for dibenzo-24-crown-8 (**V-3**, **DB24C8**) and dicyclohexano-18-crown-6 (**V-4**).

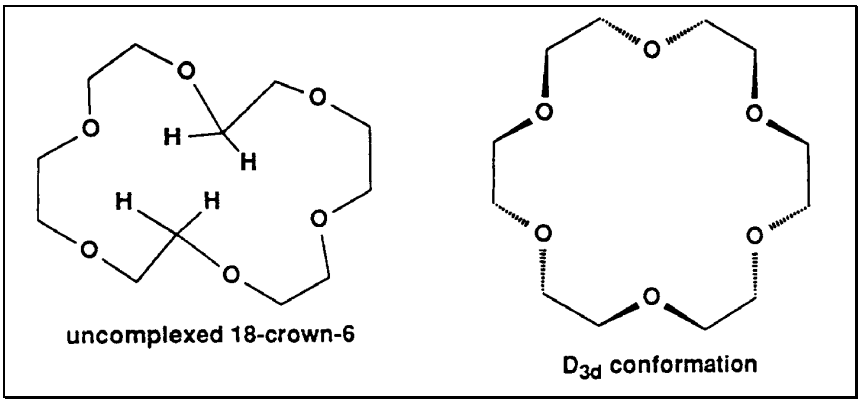

Figure V-1. Comparison of uncomplexed and complexed 18-crown-6 (**V-2**, **18C6)**.[12]

Pedersen realized early on that ammonium ions and thiourea could be complexed by his crowns.[12] The complexation with organic guests have weaker intermolecular interactions than with metal ions.[7] The first complex of an ammonium cation with a crown ether was reported in 1975 between a *t*-butylammonium ion and (2,6-dimethylylbenzoic acid)-18-crown-6.[15] Metcalfe, and others soon after reported the complexation of N,N-dimethyldiaza-12-crown-4 with several secondary ammonium ions (as perchlorates and thiocyanates).[16] Later, Cram and co-workers discovered that 27-crown-9 complexed guanidinium in a 1:1 stoichiometry.[12] Stoddart, Colquhoun, and

others revealed a "second sphere solvation" with the complex of 18-crown-6 and a transition metal bound ammonia molecule ($Pt(NH_3)_6$).[12]

Uses of crown ether complexes have been both microscopic and macroscopic. Crown ethers have been used as solvating agents for anions (masking cations at the same time). Specifically, selective acylation of secondary amines in the presence of primary amines has been reported in the presence of crown ethers.[8,17,18] Both solid-liquid (K permanganate into benzene) and liquid-liquid (salts partioned into chloroform layer of liquid-liquid extraction) phase transfer phenomena have been reported.[8,19,20] Crown ethers have been used in reactions as synthetic reagents such as: nucleophilic substitutions (e.g., halogen and pseudohalogen exchange, O, N, and S alkylation), reactions with carbanions, C-C bond formation (e.g. Darzens or Knoevenagel condensation), additions, eliminations, the generation of carbenes, extrusion of gases (N_2, CO_2), oxidations, reductions ('dissolving metals,' 'electrides,' metal hydrides), rearrangements (Favorskii, Cope), isomerizations, and polymerizations. Macroscopic uses have been primarily focused on chemical analysis such as: i) selective ion extractions, ii) ion-exchange chromatography, iii) ion-selective electrodes, iii) chromoionophores and fluoroionophores, iv) transport through membranes. [8] Crown ether-metal ion complexes have also been used in biological systems,[21] isotope chemistry and radiochemistry, [22] and in high-power batteries[23]

Complexes involving crown ethers are more stable than their linear counterparts, known as podands, due to what has been labeled the *macrocycle effect*. The *macrocycle effect* is simply defined as the preorganization of the host to complex the guest molecule.[12] The effect is a direct result of the entropy of complexation. The linear analogs must undergo comparably more conformational change to obtain a favorable complexation geometry, whereas the cyclic crown ethers are preorganized in a more favorable complexation geometry. Therefore, the conformational entropy is lower in the cyclics than in the linear analogs.

The *macrocycle effect* is also apparent for complexes involving cryptands. Cryptand complexes are termed cryptates. Topological control warrants that cryptates have higher selectivity due to their limited flexibility.[8,24] The conformational entropy of a cryptand is lower than its cyclic analog and even lower than its linear analog. Experimental results and molecular modeling calculations have demonstrated this effect as well.[25,26]

The *macrocycle effect* is a significant effect as illustrated in the following examples.[12] The comparison of the binding of the potassium cation with **18C6** and its podand equivalent, pentaethylene glycol dimethyl ether, reveals a 6000-fold increase (200 to 1,200,00) in binding strength for the crown (in anhydrous MeOH). Lehn showed that the binding of the potassium cation by the [2.2.2]-cryptand (in 95% MeOH) was 90,000-fold higher than its analogous open-chain lariat-crown.

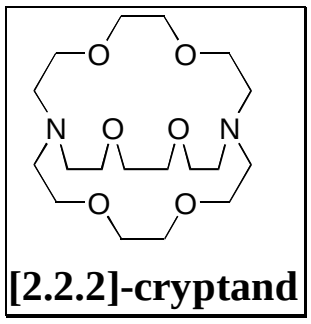

[2.2.2]-cryptand

The *'hole size'* concept "holds that when a cation's diameter and a crown ether's hole are the same size, the latter is selective for the former."[12] This implies a more stable complex forms when a tight fit is obtained. As can be inferred from **Figure V-2** 18-crown-6 is selective for all four ions Na^+, K^+, NH_4^+, and Ca^{2+} over the smaller and larger crown ethers since the fits are tightest. The concept can be applied to the complexation of organic ions with crown ethers.

However, these results contradict other investigations of crown ether complexes. Other investigations of crown ether complexes have shown that crown ethers did not form the most stable complexes with those metal ions where the best match between host

and guest dimensions was found. The best fit was made with the next smaller metal ion. As an example, the trends for decreasing stability of several crown ethers with several alkali metal ions are: 15-crown-5 = Li >> Na > K > Cs, 18-crown-6 = Na $\geq$ K > Li > Rb > Cs, and 21-crown-7 = K > Na $\geq$ Rb > Li > Cs.[27-29] This contradiction indicates the difficulty in comparing results obtained from different investigators. Caution must be taken in recreating precise experimental conditions to make valid comparisons.

Rebek *et al.* have described how the packing coefficient, the ratio of the guest volume to the host volume, can be a good estimate of the complexation properties of a molecular capsule with the substrate.[30] The best binding was achieved when the coefficient was within the range of 0.55 $\pm$ 0.09 and larger packing coefficients (up to 70%) can be achieved with complexes stabilized by strong intermolecular forces like hydrogen bonding. This phenomenon was called the "55% solution" because most organic liquids have packing coefficients of similar value.

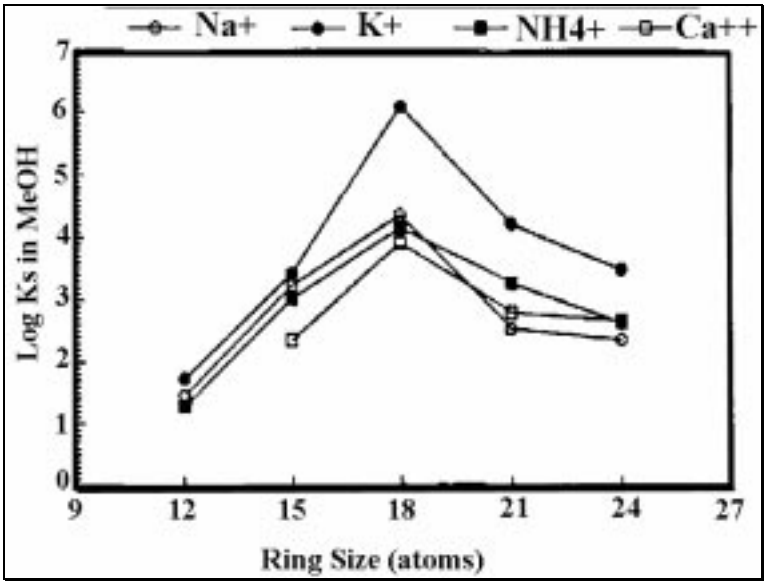

Figure V-2. Cation binding by crown ethers with various ring sizes.

As alluded to in the discussion of the *macrocycle effect* and '*hole size*' concept, thermodynamics play an important role in the complexation phenomenon. [12] Both

entropy and enthalpy must be considered together. Most chemists believe that the enthalpic term, which includes concepts such as inductive stabilization and steric congestion, predominates in host-guest chemistry. However, entropy concepts such as solvent effects and organization are equally or sometimes more important effects. As the strength of the host-guest interaction increases, a negative enthalpy change, the solvent must also become more ordered, a negative entropy change. Thus, cation binding constants may differ surprisingly little even though one expects a much stronger ligand-cation interaction in one case than in another. An example of this can be found in a comparison (**Table V-1**) of several bibracchial lariat ethers based on the 4,13-diaza-18-crown-6 system (**Figure V-3**). The binding constants for the potassium and sodium ions do not differ by much for each host due to *enthalpy-entropy compensation*. The enthalpy term is more negative for each complex for the potassium cation indicating a less favorable interaction, but the entropy term is also more negative, indicating a more favorable interaction. Therefore, the association constants do not differ by as much as might be expected.[12]

In an attempt to simplify the designation and abbreviation of the complexes discussed in this chapter, a systematic symbolism was used. A colon indicates a complex between the first and second component and subscripts indicate the number of molecules of each component. The host is the first abbreviation, usually a crown ether (e.g., **DB24C8** for dibenzo-24-crown-8) and the second abbreviation is the guest molecule (designated using the numeric values assigned in this chapter). Counterions are included, where appropriate, and are placed after a dot, • ; the number of which precedes the chemical abbreviation. For example, a one to two complex of bis-(*m*-phenylene)-32-crown-10 (**BMP32C10**, **BMP32C10**) to di-*n*-butyl ammonium hexafluorophosphate (**V-10•PF_6**) would be designated as **BMP32C10**:(**V-10•PF_6**)$_2$. Where the complexes are referred to as rotaxanes or pseudorotaxanes the suggested nomenclature described in **Chapter 1** was used.

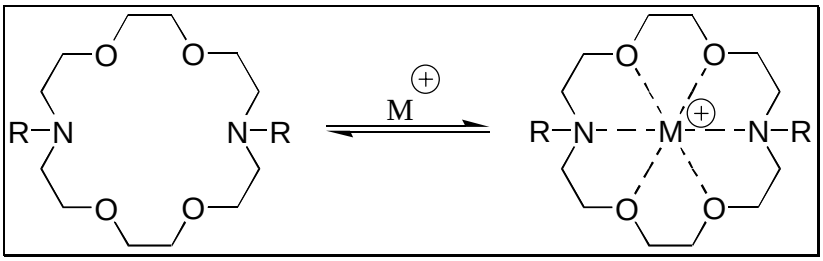

Figure V-3. Cation binding of bibracchial lariat ethers.[12]

Table V-1. Comparison of thermodynamic data and binding constants for bibracchial lariat ethers in **Figure V-3** (MeOH).[12]

Compound or R group	Cation	log K_S	ΔH (kJ/mol)	TΔS(J/mol)
18-crown-6	Na^+	4.35	-7.40 ± 0.11	-1.50 ± 0.09
(V-2)	K^+	6.08	-11.3 ± 0.02	-3.03 ± 0.04
R = CH_2-C≡CH	Na^+	3.61	-4.97 ± 0.04	-0.05 ± 0.12
	K^+	4.99	-10.0 ± 0.15	-4.21 ± 0.09
R = CH_2-C≡N	Na^+	2.69	-4.87 ± 0.08	-1.20 ± 0.10
	K^+	3.91	-9.54 ± 0.11	-3.29 ± 0.17

V.1.1.2 Crown Ether and Ammonium Ion Complexes

V.1.1.2.a Primary Ammonium Ions

As mentioned above the first structure reported for an ammonium cation complexed with a crown ether was between (2,6-dimethylylbenzoic acid)-18-crown-6 and a *t*-butylammonium ion.[15] Since then, numerous reports have been published describing the binding of primary ammonium ions with crown ethers.[9,10] The complexes were of the face-to-face type, where the primary ammonium hydrogens point toward the cavity of the crown ether ring but do not penetrate the plane of the ring. More specifically, in the complex of **18C6** with R-NH_3^+, the hydrogens are bonded to alternating oxygens with the R group extending away and perpendicular to the plane of the crown ether, a configuration often referred to as "perching" (**Figure V-4**).[31]

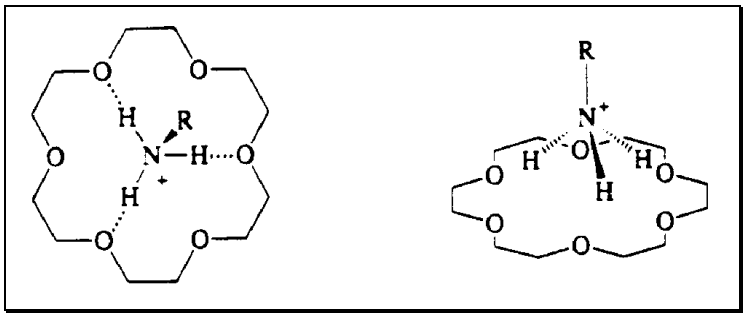

Figure V-4. Complex between **18C6** and R-NH_3^+.[31]

To understand, and possibly design predictable systems, with gained control, the binding constants as well as thermodynamic parameters ΔH and ΔS are important constants to measure and compare from system to system. Unfortunately, due to the differences between the complexation conditions, e.g., different solvents, or different counterions, and the difficulty in measuring the thermodynamic parameters by experimental methods, comparisons are extremely difficult. However, some systems can be compared. The binding constants (log K_s) varied greatly depending on what R was in the ammonium ion for the complexes between **18C6** and R-NH_3^+. For $MeNH_3^+$,[32] $EtNH_3^+$,[33] *t*-$BuNH_3^+$,[32] and $PhNH_3^+$[32] they were 4.25, 3.99, 2.90, and 3.80, respectively, in 100% methanol. Also, changing the host molecule's number and/or type of heteroatoms effected the binding constant (**Figure V-5**).[31] Izatt, Christensen, and co-workers determined numerous stability constants for crown ether/cation complexes.[12] A detailed discussion concerning the determination of association constants by NMR will be given in **Section V.1.2**.

Azacrown ethers, crown ethers containing one or more nitrogen atom in the "crown" ring, form stronger complexes with cations (especially transition metal cations) than macrocycles containing only oxygen atoms.[6] Their complexation with primary ammonium ions was demonstrated as early as 1979 when Bovill and co-workers reported the X-ray crystal structure of benzylammonium thiocyanate with diaza-24-crown-6.[34] Later their complexation and transport phenomena of primary and secondary ammonium

ions with diaza-crown ethers was demonstrated in 1984.[35] Several investigators found through the study of an array of aza- and diazacrown ethers that ammonium ion complexation was favored by 18-membered rings over 12- and 15-membered rings.[36-42] These findings concurred with Cram's earlier work.[43]

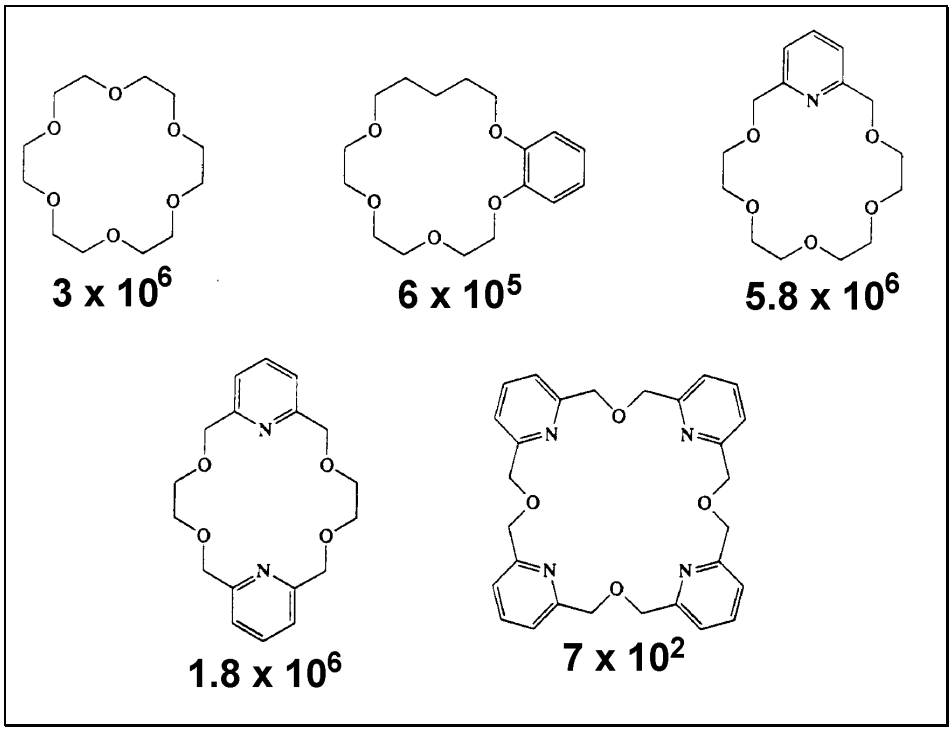

Figure V-5. Binding constants for crown-type hosts with *t*-butyl ammonium thiocyanate in MeOH.[31]

Other crown ether type hosts have been reported to bind with ammonium ions. Complexes between diammonium ions and lariat ether like crowns have been reported by Mageswaren, *et al.*[44] and Johnson, *et al.*[45] The earliest work reporting the complexation of ammonium ions with podands, linear analogs of crown ethers, in the gas phase occurred in 1983.[46]

Valinomycin is known to wrap around one potassium cation and transport it in *vivo*. This natural phenomenon demonstrates that a 3D complex is needed and assumed to be more stable by complete protection from the lipid environment.[12] Also, the *'hole size'* concept is better represented for cryptands. The fit for the potassium cation inside the [2.2.2]-cryptand is almost exact.[12] The internal size is about 2.8 Å and the diameter of the spherical potassium cation is 2.66 Å. This fit is better than observed for **18C6** whose internal diameter is 2.6 – 3.2 Å in the complex.[8] These factors contributed to the concept and design of cryptands, bicyclic crown ethers (see **Chapter IV**). Several reports have been published for the complexation of diammonium ions with cryptand-like bis-crowns.[47-49]

V.1.1.2.b Secondary Ammonium Ions

The earliest report of the complexation of secondary ammonium ions with a crown ether was in 1977.[16] However, the crown ether was an azacrown ether, more specifically N,N-dimethyldiaza-12-crown-4. The size of the ring allowed only an edge-to-face type complex. The stabilization of the complex presumably was achieved through the hydrogen bonding of the ammonium hydrogens to the azacrown ether's nitrogens. Izatt *et al*. reported that the selective binding of ammonium ions (primary, secondary, and tertiary) with **18C6** decreased in the order $RNH_3^+ > R_2NH_2^+ > R_3NH^+$, R_4N^+.[32] The complexation and transport phenomena of primary and secondary ammonium ions was also observed with diaza-crown ethers.[35] Brisdon *et al*. reported that extraction of secondary dialkylammonium salts from a mixture of protonated secondary and tertiary amines using polysiloxanes functionalized with 12-crown-4 side chains.[50] However, to date no edge-to-face complex has been observed between secondary ammonium ions and all oxygen crown ethers having rings sizes less than 24 atoms.

Stoddart *et al*. recently reported on the self-assembly complexation of *ortho*- and *para*-phenylene crown ethers with secondary ammonium ions to form pseudorotaxanes.[51-55] An extensive review of specific complexes was recently

published.[56] Various secondary ammonium ions having one or more ammonium centers were reported to complex with 24-, 34-, 51-, and 68-membered crown ethers in the solid, liquid, and "gas" phases. Most of the reported complexes existed as pseudorotaxanes as evidenced by X-ray crystallographic analysis of stable crystals. Complex stoichiometries ranged from 4:2 to 1:1 to 1:4. **Figure V-6** shows the "logical progression" from the simple [1.1]pseudorotaxane (**a**) to higher ordered pseudorotaxanes and rotaxanes.[56] The complexes resulted primarily through the hydrogen bonding between the ammonium protons and the ether oxygens of the crown ether. Further stabilization of the complexes was achieved in many cases through π-orbital interactions of the aromatic rings of both species.

The first example of a rotaxane synthesized from a crown ether and secondary ammonium ion was in 1995 by Busch, *et al.* (**Figure V-7**).[57] The synthesis was performed in a two-phase system of water and chloroform. The water soluble acylating agent reacted at the interface with the primary amine, forming the end blocked linear thread. Once the stable complex was formed between the crown ether and the secondary ammonium ion center some of the crown ether was trapped, leaving a rotaxane. Later, Stoddart *et al*. produced [1.1]rotaxanes and [2.1]rotaxanes also between secondary ammonium ions and crown ethers (**Figure V-8**).[55,58]

Stoddart, *et al.* have gone beyond the simple formation of pseudorotaxanes and rotaxanes whereby they designed supramolecular systems that utilized molecular recognition to assemble larger aggregates. Hydrogen-bonded polypseudorotaxanes between the dibenzylammonium ion **V-5** and **DB24C8** were shown to exist by X-ray crystallography (**Figure V-9**). The intermolecular hydrogen bonds formed between the terminal acid groups of the thread were arranged such that the resulting pseudorotaxanes, each one being considered a repeat unit, were aligned linearly. However, the system differed from a covalent polymer in that it was thermodynamically controlled and reversible.

Throughout the above discussion and the published literature never have *meta*-phenylene crown ethers been discussed. Bis(*meta*-phenylene) crown ethers are of special

interest to our group because we have developed syntheses of a number of (5-) mono-[60,61] and (5, 5'-) di-functional[62-66] derivatives of these crown ethers as precursors to self assembled supermolecules[67-71] and polymeric rotaxanes.[72] Due to their symmetric nature these substituted bis(*m*-phenylene) crown ethers can be prepared as pure compounds without isomer separation and have simpler NMR spectra than their substituted bis(*ortho*-) and bis(*para*-) analogs.

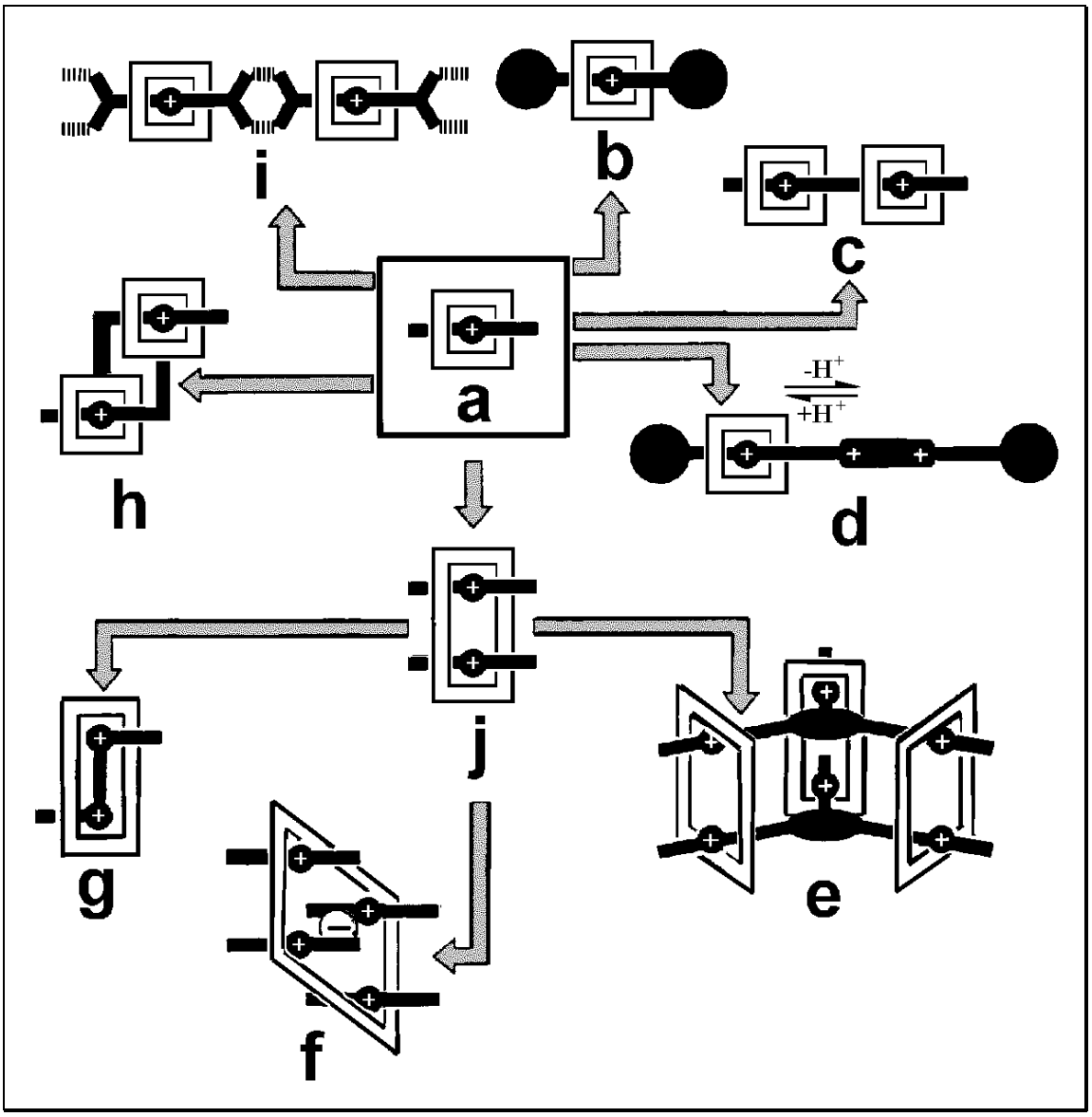

Figure V-6. Cartoon depicting "logical progression" from the simple [1.1]pseudorotaxane (**a**) to higher ordered pseudorotaxanes and rotaxanes: 1) [1.1]rotaxane (**b**), 2) [2.1]pseudorotaxane (**c**), 3) proposed acid-base-controlled [1.1]rotaxane (**d**), 4) [3.2]pseudorotaxane (**e**), 5) [1.4]pseudorotaxane (**f**), 6) "doubly-docked" [1.1]pseudorotaxane (**g**), 7) "dimeric daisy chain-like" supermolecule (**h**), 8) main-chain polypseudorotaxane (**i**), 9) [1.2]pseudorotaxane (**j**).[56]

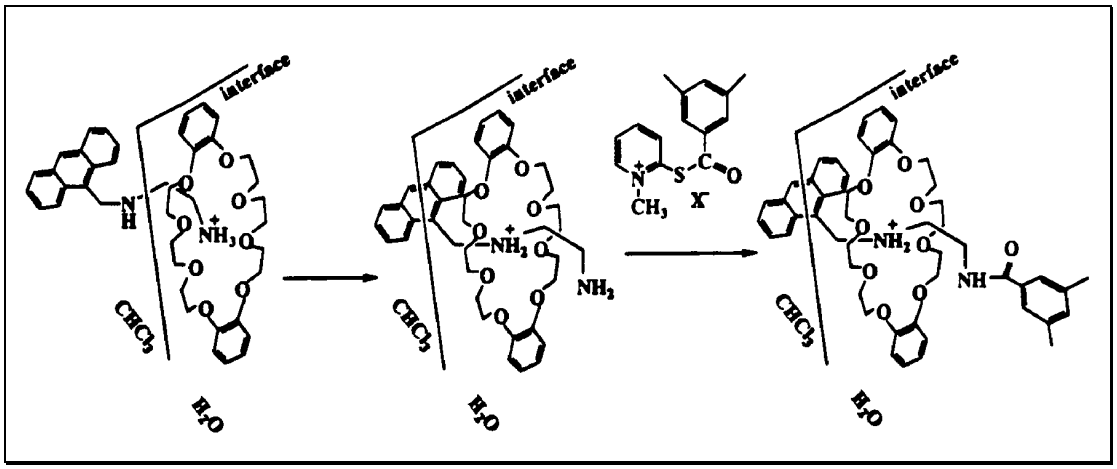

Figure V-7. First rotaxane formed between a secondary ammonium ion and **DB24C8**.[57]

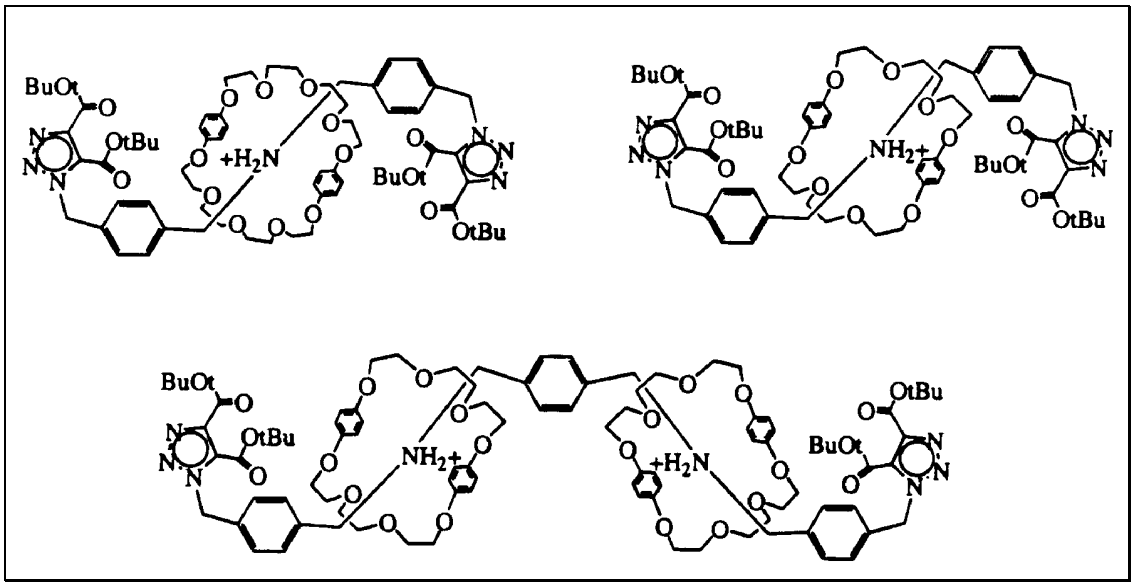

Figure V-8. Rotaxanes from secondary ammonium ions and crown ethers produced by Stoddart *et al.*[59]

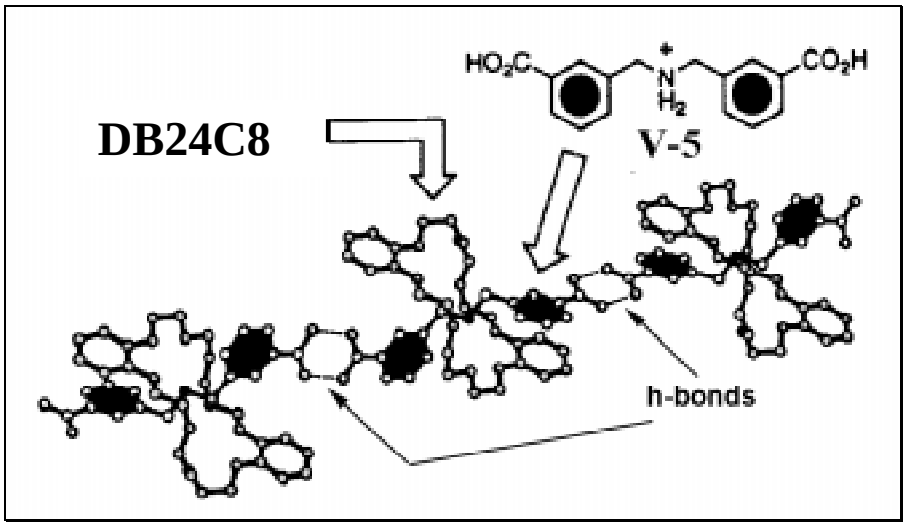

Figure V-9. Crystal structure of a hydrogen-bonded polypseudorotaxane from the dibenzylammonium ion **V-5** and **DB24C8**.

V.1.2 Determination of Association Constants for Molecular Complexes

As mentioned earlier, measuring association constants and thermodynamic parameters allows for comparison of systems to better design supramolecular complexes, specifically rotaxanes, polyrotaxanes, etc… The complexes discussed in this work all exist in equilibrium and are simply represented by the equilibrium **Equation 1**. The crown ether has been designated as ***R***, the receptor, the secondary ammonium ion(s) as ***S***, the substrate, and the complex as $\boldsymbol{R_nS_m}$, each having n and m number of components in the complex, respectively. If the stoichiometry of the complex(s) and the concentration of both the products and reactants can be determined under the equilibrium conditions then the overall association constant (K_a) can be calculated according to **Equation 2**. Usually this is not an easy task.

$$nR + mS \leftrightharpoons R_nS_m \qquad (\mathbf{1})$$

$$K_a = \frac{[R_nS_m]}{[R]^n[S]^m} \qquad (\mathbf{2})$$

The first techniques used for studying the equilibrium complexation of crown ethers were pioneered by Pedersen and Frensdorff.[12] They developed the extraction and ion selective electrode techniques. Since then, several other techniques have been employed. They include spectroscopic (NMR, UV/visible, fluorescence/phosphorescence, CD, and mass), electrochemical (potentiometry, polarography, and ionic conductivity), thermodynamic (calorimetry, ion exchange, solubility, and partial pressure), and other (reaction kinetics and competition methods) techniques.[73]

An excellent review of techniques for determining association constants was published by Tsukube *et al.*[73] More specifically, they discuss in detail how the stoichiometry and the association constant(s) of the complexes can be determined using NMR from the changes in the chemical shifts of the proton signals. There are two different extremes of exchange rates that can exist for the complexation relative to the NMR time scale, fast- and slow-exchange (**Figure V-10**). In the case of slow-exchange, for a 1:1 complex (**Figure V-10a**), two peaks are observed for one proton for component ***R***. One peak is observed at the expected chemical shift for a proton on the uncomplexed component ***R*** and another "new" peak is observed for the same component in the complex ***RS***. In an equal molar solution of both complexing components one can calculate the concentration of [***S***], [***R***], and [***RS***] directly using the integration values of both peaks. Both the stoichiometry and association constant(s) can be determined from one NMR experiment. This method of calculating the association constant has been commonly referred to as the single point method. However, this phenomenon is not often observed. More common is the fast-exchange process (**Figure V-10b**).

In the fast exchange process only one peak is observed for the proton of interest. No longer observed is a peak at the expected chemical shift for ***R***. The peak is shifted by Δ, where Δ equals the difference between the observed chemical shift, $\delta_{observed}$, and the chemical shift of the "free" or uncomplexed component ***R***, δ_{R} ($\Delta = \delta_{observed} - \delta_{R}$). A necessary constant not easily obtained is Δ_o, the difference between the chemical shift of

the complex ***RS***, δ_{RS}, and δ_R ($\Delta_o = \delta_{RS} - \delta_R$). To determine the stoichiometry, Δ_o, and the association constant(s) several NMR experiments must be conducted.

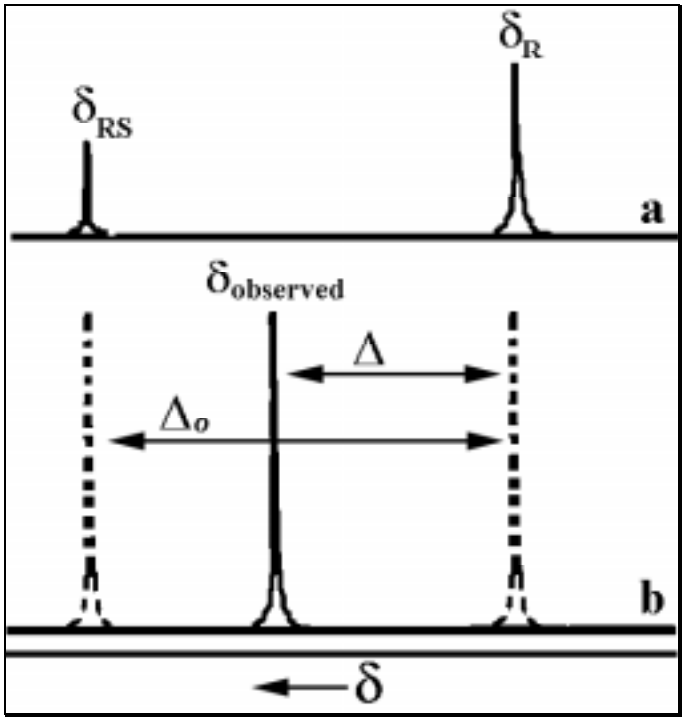

Figure V-10. Two different exchange rates, a) slow- and b) fast-exchange, relative to NMR time scale for complexation.

Both Sutherland and Stoddart reported several complexes that exhibited fast exchange. Sutherland *et al*. reported several complexation induced shifts of proton signals as observed by ^{1}H-NMR for primary diammonium ions and crown ethers.[74,75] The research by Stoddart *et al.*[51-55] discussed in **Section V.1.1.2.b** also reported the same fast-exchange complexation for secondary ammonium ions and crown ethers. However, Stoddart *et al*.[51-55] also reported several complexes that exhibited slow exchange on the NMR time scale.

V.1.2.1 Determination of Stoichiometry for Fast-Exchange Complexes

Under fast-exchange conditions one method for determining the stoichiometry of the complex(es) is the mole ratio method.[76] The total concentration of the receptor $[\boldsymbol{R}]_o$ is held constant and the total concentration of the substrate $[\boldsymbol{S}]_o$ is varied. The subscript "*o*" indicates initial conditions or concentrations of each component. This method is commonly referred to as the titration method. A plot of the ratio $[\boldsymbol{S}]_o/[\boldsymbol{R}]_o$ versus the chemical shift of a proton of ***R*** should yield a curve with an abrupt change in the slope or discontinuity which corresponds to the stoichiometric ratio of the complex. In cases where the association constant is low the plot becomes more rounded, thus, an extrapolation using only the linear parts of the curve is required to find the break point.[77] As an example, the complex formed between the bicyclic molecule **V-6** and *p*-nitrophenol exhibited a discontinuity in the curve at a stoichiometric ratio of 1:1 (**Figure V-11**). Historically the data obtained for the mole ratio method has been plotted incorrectly (normally the dependent variable is plotted on the y-axis). This is probably due to the fact that the results from NMR experiments plot the chemical shift data on the x-axis.

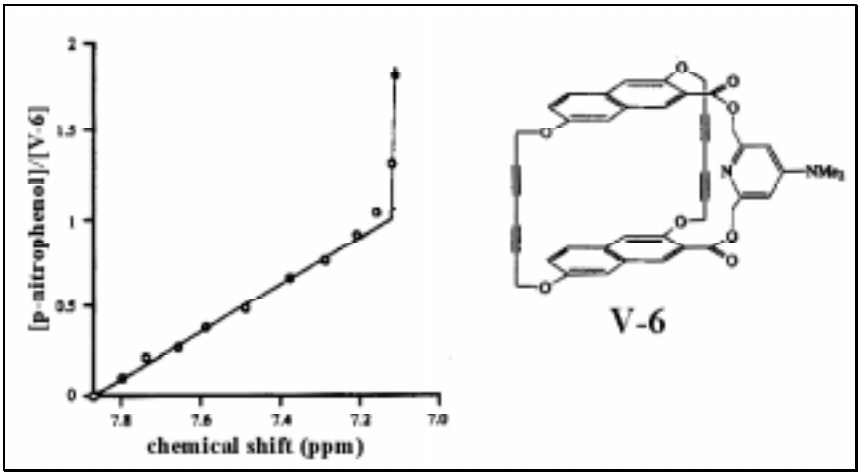

Figure V-11. Mole ratio plot for complex formed between the bicyclic molecule **V-6** and *p*-nitrophenol.[78]

As the association constant increases for the 1:1 complex the "break point" of the mole ratio plot is more apparent (**Figure V-12**). The vertical lines of **Figure V-12** indicate the theoretical maximum for the chemical shift of the bimolecular complex. At lower K_a values the curves would be more rounded experimentally making it more difficult to establish the stoichiometry.

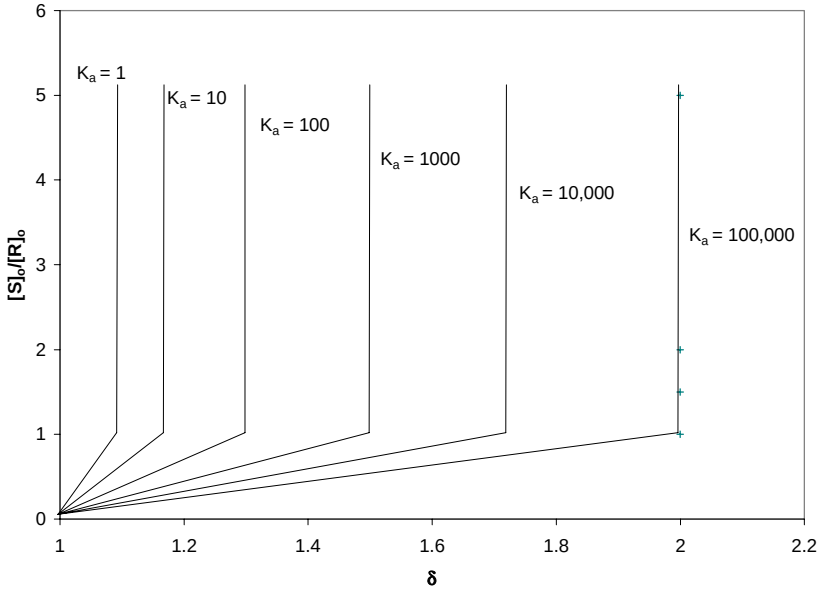

Figure V-12. Plot of $[\mathbf{S}]_o/[\mathbf{R}]_o$ versus δ for various K_a values.

V.1.2.2 Determination of Association Constants for 1:1 Complexes with Fast-Exchange

Once the stoichiometry of the complex is established in a fast exchange process the association constant can be determined. Again, however, several NMR experiments must be conducted since there are two (or more) unknowns, the K_a(s) and Δ_o(s). One attractive feature of determining the stoichiometry by the mole ratio method is that, if designed properly, the data obtained can be used directly for calculating the association constant. For a 1:1 complex **Equation 1** can be simplified to **Equation 3**.

$$R + S \rightleftharpoons RS \qquad (3)$$

Equation 2 then becomes:

$$K_a = \frac{[RS]}{[R][S]} \qquad (4)$$

If the concentration of one component, **R**, is held constant, for example at 10 mM, then the concentration of the complex **RS** increases more rapidly at higher K values with increasing [**S**] (**Figure V-13**).

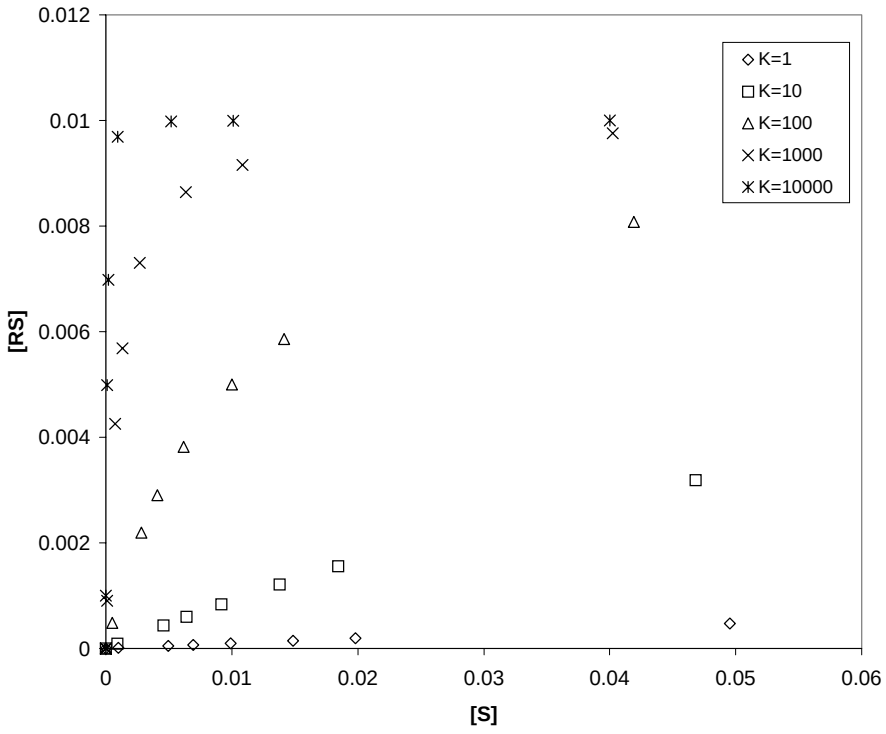

Figure V-13. Plot of [**RS**] versus [**S**] at various K_a values. $[\mathbf{R}]_o$ = 10mM

The chemical shift for a proton of one component of the complex, in this case **R**, can be observed in all of the NMR experiments. **Equation 5** relates the observed chemical shift, $\delta_{observed}$, to the chemical shift of the pure component, $\delta_{\mathbf{R}}$, and the

complexed signal, $\delta_{\boldsymbol{RS}}$, according to the mole fraction of ***R***, $N_{\boldsymbol{R}}$, and ***RS***, $N_{\boldsymbol{RS}}$, in the system.

$$\delta_{obs} = N_R \delta_R + N_{RS} \delta_{RS} \quad (\mathbf{5})$$

$N_{\boldsymbol{R}}$ and $N_{\boldsymbol{RS}}$ are defined as

$$N_R = \frac{[R]}{[R]+[RS]} \quad (\mathbf{6})$$

$$N_{RS} = \frac{[RS]}{[R]+[RS]} \quad (\mathbf{7})$$

where the sum of $N_{\boldsymbol{R}}$ and $N_{\boldsymbol{RS}}$ is unity,

$$N_R + N_{RS} = 1 \quad (\mathbf{8})$$

Substituting **Equations 6** and **7** into **Equation 5** for $N_{\boldsymbol{R}}$ and $N_{\boldsymbol{RS}}$ gives:

$$\delta_{obs} = \delta_R + \frac{[RS]}{[R]+[RS]}(\delta_{RS} - \delta_R) \quad (\mathbf{9})$$

The initial concentrations of ***R*** and ***S***, $[\boldsymbol{R}]_o$ and $[\boldsymbol{S}]_o$, respectively, are:

$$[R]_o = [R]+[RS] \quad (\mathbf{10})$$

$$[S]_o = [S]+[RS] \quad (\mathbf{11})$$

Substituting **Equations 10** into **9** and solving for [***RS***], we obtain

$$[RS] = \frac{[R]_o(\delta_{observed} - \delta_R)}{(\delta_{RS} - \delta_R)} \quad \textbf{(12)}$$

Recalling that $\Delta = \delta_{observed} - \delta_{\boldsymbol{R}}$ and $\Delta_o = \delta_{\boldsymbol{RS}} - \delta_{\boldsymbol{R}}$ **Equation 12** can be rewritten as

$$[RS] = [R]_o\left(\frac{\Delta}{\Delta_o}\right) \quad \textbf{(13)}$$

The ratio Δ/Δ_o is called the saturation factor and is equal to $N_{\boldsymbol{RS}}$. Solving **Equation 4** for [***R***] and substituting into **Equation 10** gives

$$[R]_o = \frac{[RS]}{K[S]} + [RS] = [RS]\left(\frac{1}{K_a[S]} + 1\right) \quad \textbf{(14)}$$

Plugging **Equation 14** into **Equation 13** for $[\boldsymbol{R}]_o$ and rearranging we obtain

$$\frac{1}{\Delta} = \frac{1}{\Delta_o K_a[S]} + \frac{1}{\Delta_o} \quad \textbf{(15)}$$

Equation 15 is known as the Benesi-Hildebrand equation.[79,80] A plot of $1/\Delta$ versus $1/[\boldsymbol{S}]$ yields a straight line with an intercept of $1/\Delta_o$ and a slope of $1/\Delta_o K_a$. Multiplying **Equation 15** by $\Delta\Delta_o K_a$ and rearranging gives the Scatchard equation

$$\frac{\Delta}{[S]} = -K_a\Delta + \Delta_o K_a \quad \textbf{(16)}$$

Plotting the data using the Scatchard equation is an excellent way of determining if the complex that is observed is indeed a 1:1 complex.[81] Any curvature ($R^2 < 0.98$) indicates that the complexation is of higher order than a 1:1.

Both the Benesi-Hildebrand and the Scatchard equations require that the concentrations of ***S*** be known. However, under fast-exchange conditions the values of [***S***] are not easily known. Often times $[\boldsymbol{S}]_o$ can be substituted for [***S***] if $K_a[\boldsymbol{R}] << 1$ and $[\boldsymbol{S}]_o >> [\boldsymbol{R}]_o$ when K_a is relatively low.[73] For complexes with high association constants a large excess of ***S*** is not essential.[82] An improved method of calculating the association constant using the Benesi-Hildebrand equation is to first use $[\boldsymbol{S}]_o$ for [***S***] and calculate both Δ_o and K_a. Then the calculated Δ_o and K_a are used to calculate a new value for [***S***]. This new value is then used to give improved Δ_o and K_a values. The iterative method is repeated until the Δ_o and K_a values converge.

The Rose-Drago graphical method for determining the association constant has been applied to systems where the assumption $[\boldsymbol{S}] = [\boldsymbol{S}]_o$ cannot be used.[83,84] The Rose-Drago equation is

$$(\Delta_o - \Delta)K_a = \frac{\Delta\Delta_o}{\Delta_o[S]_o - \Delta[R]_o} \qquad (\mathbf{17})$$

In the Rose-Drago equation $[\boldsymbol{S}]_o$ is used instead of [***S***]. Arbitrarily chosen values of Δ_o are plugged into the equation and $1/K_a$ values are calculated using the known values of $[\boldsymbol{R}]_o$, $[\boldsymbol{S}]_o$, and Δ. This is repeated for each data set. The curves of each data set for each chosen Δ_o value cross at the theoretical value of $1/K_a$. Since normally the data has scatter the mean crossing value is calculated to arrive at K_a.

Another method used for determining K_a using a graphical method was developed by Creswell and Allred.[85] A detailed outline of the technique and explanation of the data treatment using the Creswell-Allred method as well as its effective application in determining the method for determining association constant(s) was reported by Horman and Dreux.[86] The Creswell-Allred equation is

$$K_a = \frac{1}{\left(\frac{\Delta_o}{\Delta} - 1\right)[S]_o - \left(1 - \frac{\Delta}{\Delta_o}\right)[R]_o} \quad \textbf{(18)}$$

Solving **Equation 13** for Δ and substituting into the equation $\Delta = \delta_{observed} - \delta_{\boldsymbol{R}}$ gives

$$\delta_{observed} = \frac{[RS]}{[R]_o}\Delta_o + \delta_R \quad \textbf{(19)}$$

[***RS***] can be calculated from the second order polynomial equation

$$[RS] = \frac{\left(\left([R]_o + [S]_o + \frac{1}{K_a}\right) \pm \sqrt{\left([R]_o + [S]_o + \frac{1}{K_a}\right)^2 - 4[R]_o[S]_o}\right)}{2} \quad \textbf{(20)}$$

[***RS***] is calculated by arbitrarily choosing values of K_a. A plot of $\delta_{observed}$ versus [***RS***]/[***R***]$_o$ gives a straight line. Δ_o is calculated from the slope and $\delta_{\boldsymbol{R}}$ is calculated from the intercept. K_a is adjusted until the calculated value of $\delta_{\boldsymbol{R}}$ agrees with the experimental value of $\delta_{\boldsymbol{R}}$. It must be pointed out that since the chemical shift of a signal for a proton on ***R*** is tracked in each solution [***R***]$_o$ < [***S***]$_o$. This is because if [***R***]$_o$ > [***S***]$_o$ **Equation 20** can go negative, an unreal answer.

The discussed graphical methods are not inclusive, but are the methods of choice used in this work to calculate the association constants of some systems. It is advised that several methods be used to calculate K_a since there is an inherent error for each method.[73] The graphical methods also allow for helpful examination of the data for any suspect results or other insight into the behavior of the complex(es).

There are some constraints placed on choosing suitable concentrations for each component in the NMR solutions. When the association constant is low[87] ($K_a \leq 10^4$ M^{-1})

both Person[88] and Deranleau[89] separately demonstrated that the solutions should cover the region of 20 to 80% saturation. However, for complexes having low K_a values the receptor (the observed component) concentration is always a minor component.[87] A more rigorous and accurate method for choosing the proper concentrations to use was developed by Weber.[90] Weber pointed out that a more important parameter to consider is **p**, the "probability of binding." The parameter **p** is defined as the ratio of the concentration of the complex, [***RS***], divided by the maximum concentration of the complex. It is also equal to the concentration of the complex, [***RS***], divided by the initial concentration of the minor component, $[\boldsymbol{R}]_o$ in this case, i.e., the fraction of **R** complexed. When using the titration method the definition of **p**, therefore, changes at the point where $[\boldsymbol{R}]_o$ is equal to $[\boldsymbol{S}]_o$.

$$p = \frac{[RS]}{[S]_o} \qquad \text{when } [\boldsymbol{R}]_o \geq [\boldsymbol{S}]_o \tag{21}$$

$$p = \frac{[RS]}{[R]_o} \qquad \text{when } [\boldsymbol{R}]_o < [\boldsymbol{S}]_o \tag{22}$$

Using **Equation 13**, **Equation 22** becomes

$$p = \frac{\Delta}{\Delta_o} \tag{23}$$

The most information about the complex is obtained from data that has a **p** value between 0.2 and 0.8. Choosing the "correct" concentrations to be used does involve an initial assumption of K_a. Best results are obtained when the concentration of the minor component (the fixed component), $[\boldsymbol{R}]_o$, is kept at a concentration equal to about one tenth of the equilibrium dissociation constant, K_d (= $1/K_a$). The titrant (substrate, ***S***) is then first added at a concentration equal to that concentration and then increased to a concentration of about ten times K_d (**Table V-2**). As an example, if one assumes an

association constant, K_a, of 10 then $[\boldsymbol{R}]_o$ should be held at 0.010 while $[\boldsymbol{S}]_o$ should be varied from 0.03 to 0.3 (**Table V-3**). This criteria has been applied to the determination of the association constants for several of the systems discussed below.

Entry	$[\boldsymbol{R}]_o/K_d$	$[\boldsymbol{S}]_o/K_d$															
↓	↓	0.1	0.2	0.3	0.4	0.5	0.6	0.7	0.9	1.0	2.0	3.0	5.0	10	20	40	100
		p															
1	0.1	0.08	0.16	0.22	0.27	0.32	0.36	0.40	0.46	0.50	0.66	0.75	0.83	0.92	0.95	0.98	0.99
2	1.0	0.49	0.48	0.46	0.45	0.44	0.43	0.42	0.39	0.38	0.59	0.70	0.81	0.90	0.95	0.98	0.99
3	10.0	0.91	0.91	0.91	0.91	0.91	0.90	0.90	0.90	0.90	0.89	0.88	0.85	0.73	0.92	0.97	0.99
4	$[\boldsymbol{S}]_o/K_d$[a]	0.08	0.14	0.19	0.23	0.27	0.30	0.32	0.36	0.38	0.50	0.57	0.64	0.73	0.80	0.85	0.90

Table V-2. Dependence of Weber's "probability of binding" upon experimental conditions.[87] Black entries are suitable **p** values. [a]In this example $[\boldsymbol{R}]_o$ and $[\boldsymbol{S}]_o$ are always equal.

Table V-3. Suitable concentrations (M) for $[\boldsymbol{S}]_o$ and $[\boldsymbol{R}]_o$ for given values of K_a.

$\boldsymbol{K_a}$ ($\mathbf{M^{-1}}$)	$\boldsymbol{K_d}$ ($\mathbf{M^{-1}}$)	$\boldsymbol{[R]_o}$	$\boldsymbol{[S]_o}$
1	1	0.1	0.3 - 3.0
10	0.1	0.01	0.03 - 0.3
100	0.01	0.001	0.003 - 0.03
1000	0.001	0.0001	0.0003 - 0.003
10000	0.0001	0.00001	0.00003 - 0.0003

V.2 Results and Discussions

V.2.1 Complexation of Bis-(*m*-phenylene)-26-crown-8 (V-7) with Secondary Ammonium Ions

As stated in the **Chapter I**, the cyclic component of a rotaxane must have a minimum number of 22 carbon, nitrogen, and/or oxygen atoms in the ring to be threaded by a linear poly(methylene) chain. Therefore, it was assumed that bis-(*m*-phenylene)-26-crown-8 (**V-7**, **BMP26C8**) was a suitable candidate for the formation of rotaxanes. The synthesis of **BMP26C8** was discussed in **Chapter II**. The complexation behavior of **BMP26C8** with diphenethyl- (**V-8•PF$_6$**), dibenzyl- (**V-9•PF$_6$**), and di-*n*-butyl ammonium hexafluorophosphate (**V-10•PF$_6$**) salts are discussed here.

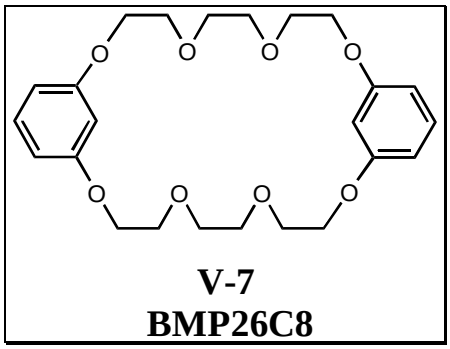

V-7
BMP26C8

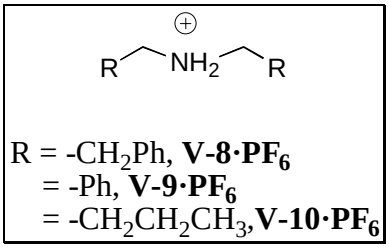

R = -CH_2Ph, **V-8·PF$_6$**
= -Ph, **V-9·PF$_6$**
= -$CH_2CH_2CH_3$,**V-10·PF$_6$**

Stoddart *et al*. have demonstrated by ^{1}H NMR and fast-atom bombardment mass spectroscopy (FAB-MS) that dibenzo-24-crown-8 (**V-3**, **DB24C8**) complexed with the dibenzyl ammonium salt **V-9•PF$_6$** and the di-*n*-butyl ammonium salt **V-10•PF$_6$**. [51-55] The stoichiometry for the complex between **DB24C8** and **V-9•PF$_6$** was determined to be

1:1 since the exchange was slow on the NMR time scale. However, the stoichiometry was not determined for the complex in solution. Both complexes were shown to exist in a pseudorotaxane conformation in the solid state. However, we observed that when the 26-membered *meta* analog **BMP26C8** was placed in solution (CD_3CN, $CDCl_3$, or acetone-d_6) with **V-8•PF$_6$**, **V-9•PF$_6$**, or **V-10•PF$_6$** there was no change in the chemical shifts of the proton signals. The ^{1}H NMR plots (400 MHz, CD_3CN, ambient *T*) of the ethyleneoxy region are compared in **Figure V-14** for **BMP26C8** and **V-9•PF$_6$**.

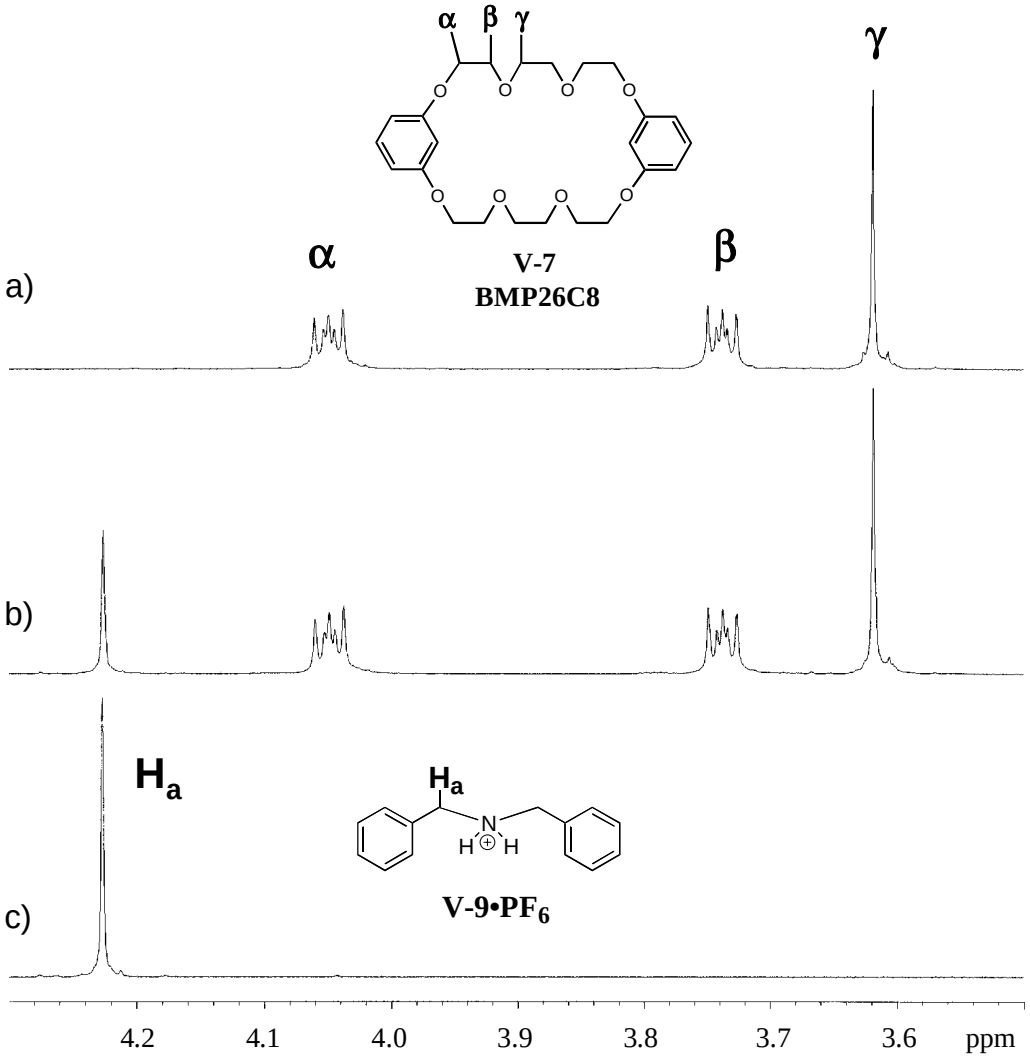

Figure V-14. Stacked ^{1}H NMR plots (400 MHz, CD_3CN, ambient *T*) for a) **BMP26C8**, b) **BMP26C8** + **V-9•PF$_6$** (1:1 stoichiometry, 0.010 M), and c) **V-9•PF$_6$**.

It was believed that the internal hydrogens of the phenyl rings of **BMP26C8** might prohibit the aromatic termini of the ammonium ions **V-8** and **V-9** from threading through the cavity of **BMP26C8** to form a stable [1.1]pseudorotaxane. Therefore, ^{1}H NMR (**Figure V-15**) was used to investigate the complexation of **BMP26C8** with the smaller di-*n*-butyl ammonium ion **V-10**, which has a smaller cross sectional area than **V-8** or **V-9**. However, since the chemical shifts of the protons of neither component changed it was determined that complexation did not occur.

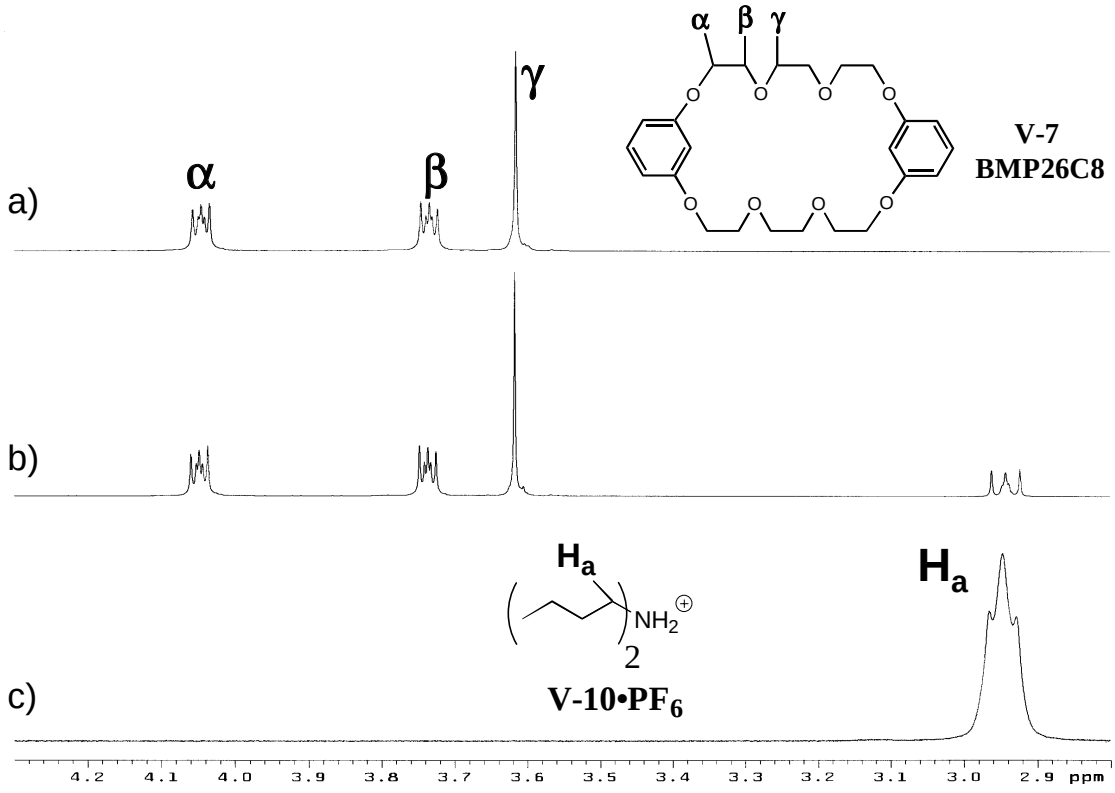

Figure V-15. Stacked ^{1}H NMR plots (400 MHz, CD_3CN, ambient *T*) for a) **BMP26C8**, b) **BMP26C8** + **V-10•PF$_6$** (1:1 stoichiometry, 0.010 M), and c) **V-10•PF$_6$**.

Another indication for the lack of complexation of the ammonium salts **V-8•PF$_6$**, **V-9•PF$_6$**, or **V-10•PF$_6$** by **BMP26C8** was the observation that **V-8•PF$_6$**, **V-9•PF$_6$**, or **V-**

10•PF_6 did not dissolve in the presence of **BMP26C8** in chloroform. Stoddart *et al*. have demonstrated that these chloroform insoluble salts become soluble by complexation in the presence of the bis-*ortho* substituted crown ether **DB24C8**.[51-55] As noted by Pedersen[2] and Izatt *et al*.[32] with the 18-membered bis-*ortho* substituted crown ether **DB18C6**, an unfavorable crown ether conformation may be the reason no detectable complexation of the larger 26-membered bis-*meta* substituted crown ether **BMP26C8** takes place in solution with the above mentioned secondary ammonium ions.

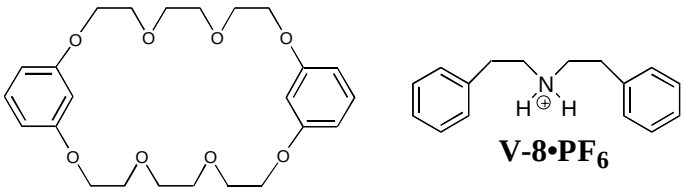

V-8•PF_6

V-7
BMP26C8

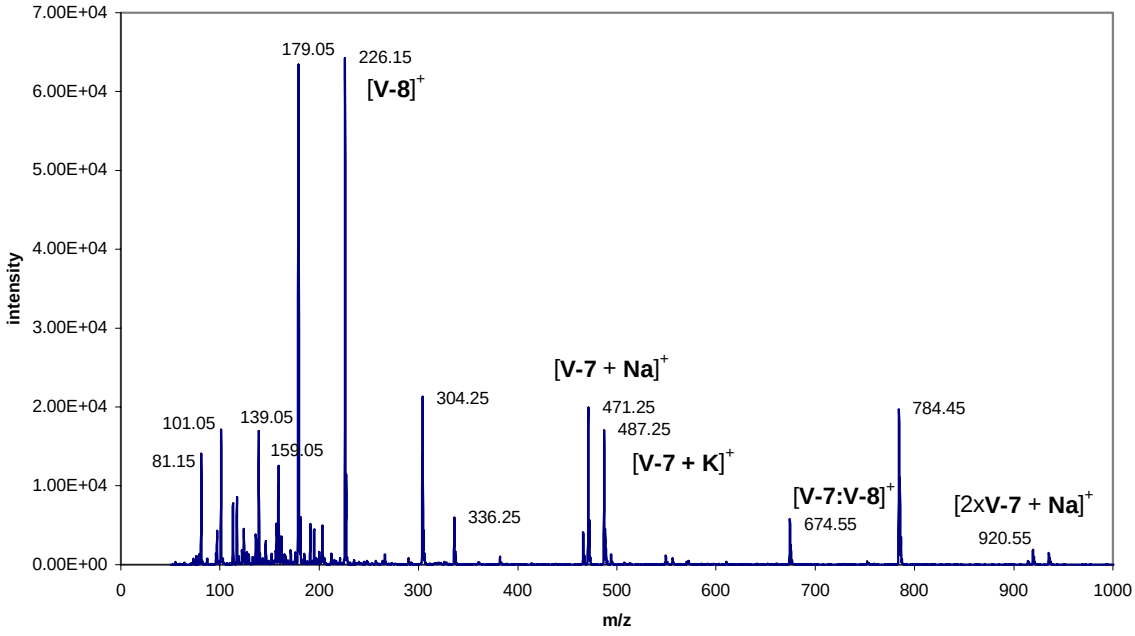

Figure V-16. Positive ion ESI-MS for 1:1 mixture of **BMP26C8** and **V-8•PF_6**.

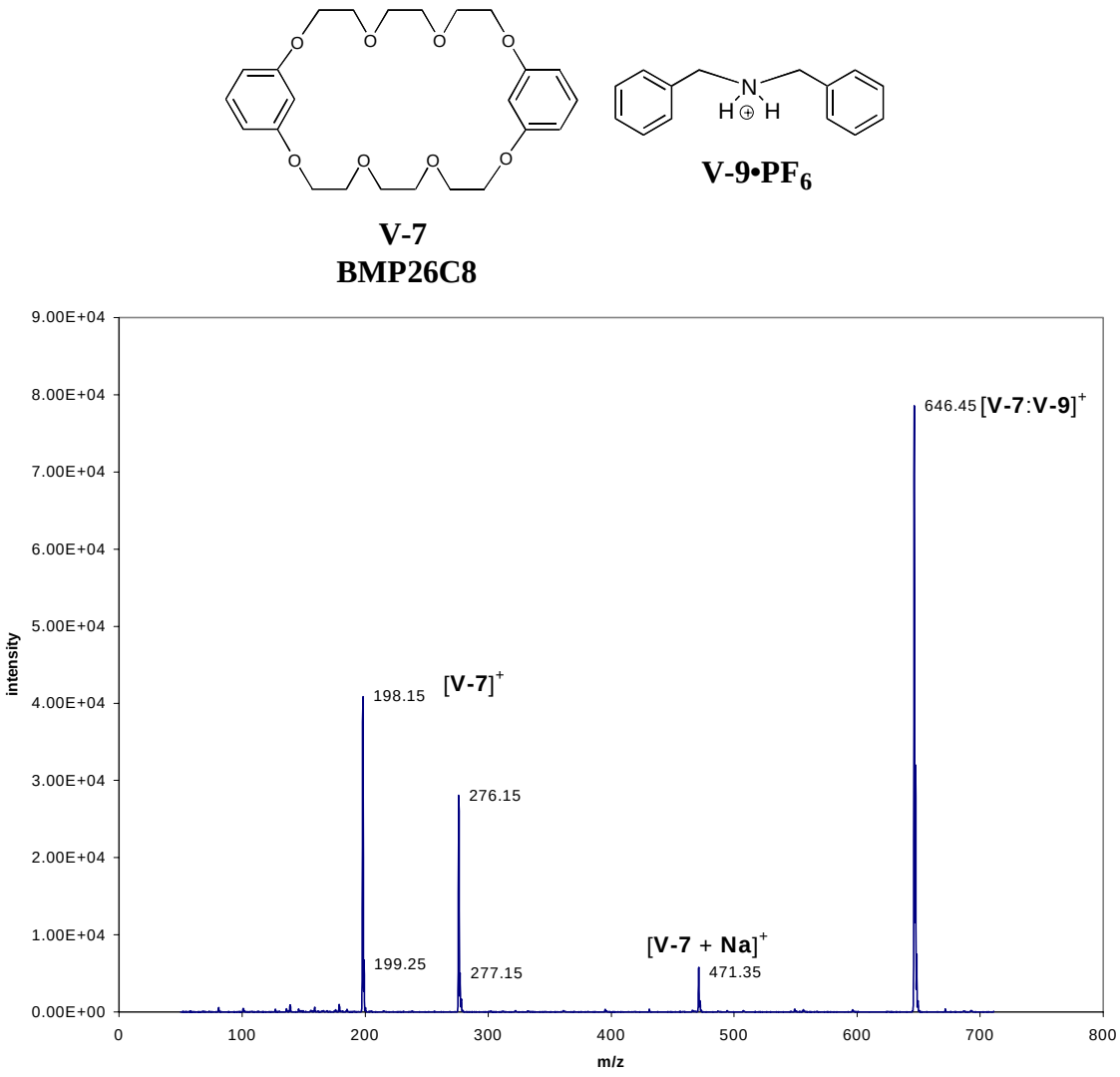

Figure V-17. Positive ion ESI-MS for 1:1 mixture of **BMP26C8** and **V-9•PF$_6$**.

1:1 Complexes, perhaps [1.1]pseudorotaxanes, of **BMP26C8** with the secondary ammonium ions **V-8•PF$_6$**, **V-9•PF$_6$**, or **V-10•PF$_6$** were, however, determined to exist by High Resolution FAB-MS and Electron Spray Ionization-Mass Spectrometry (ESI-MS). Solids, obtained by evaporation of equimolar solutions of the two components, gave peaks at m/z 646.5, 578.5, and 674.6, respectively, corresponding to the 1:1 complex

cations [**BMP26C8:V-8**]$^+$, [**BMP26C8:V-9**]$^+$, or [**BMP26C8:V-10**]$^+$ (**Figures V-16**, **V-17**, and **V-18**) for positive ion ESI-MS. Comparison of the peak intensities of the ammonium salt and the complex in each spectrum gives a relative indication of the strength of the complexation. In **Figure V-16** and **V-17** the peaks for the complexes are at least 2 times as intense as the peaks for the salts, indicating that fairly stable complexes existed. But, in **Figure V-16** the peak for the salt is about six times as intense as the peak for the complex. This result indicated that the complex between **BMP26C8** and the diphenethyl ammonium ion (**V-8•PF_6**) is not as strong as for the complexes with the dibenzyl ammonium ion (**V-9•PF_6**) or the di-*n*-butyl ammonium ion (**V-10•PF_6**). Attempts to grow crystals of these complexes suitable for X-ray crystallography have been so far futile.

The above results indicate that if a complex did exist between **BMP26C8** and one or more of the three secondary ammonium salts **V-8•PF_6**, **V-9•PF_6**, and **V-10•PF_6** in solution the association must be weak and undetectable by the NMR under the experimental conditions. For the mass spectral data the results are actually an analysis of what exists in a matrix mixture, essentially the solid phase. These results are deceiving due to the inexact or often times undeterminable concentration of each component in the matrix. Also, crown ethers are known to adopt a conformation in the gas phase different from the solution phase. It has been suggested that crown ethers are more flexible in the gas phase.[6] Therefore, the pursuit of pseudorotaxane and rotaxane formation using the 25-membered bisphenylene crown ether **BMP26C8** was abandoned.

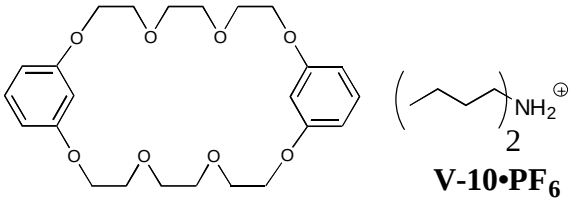

V-7
BMP26C8

V-10•PF_6

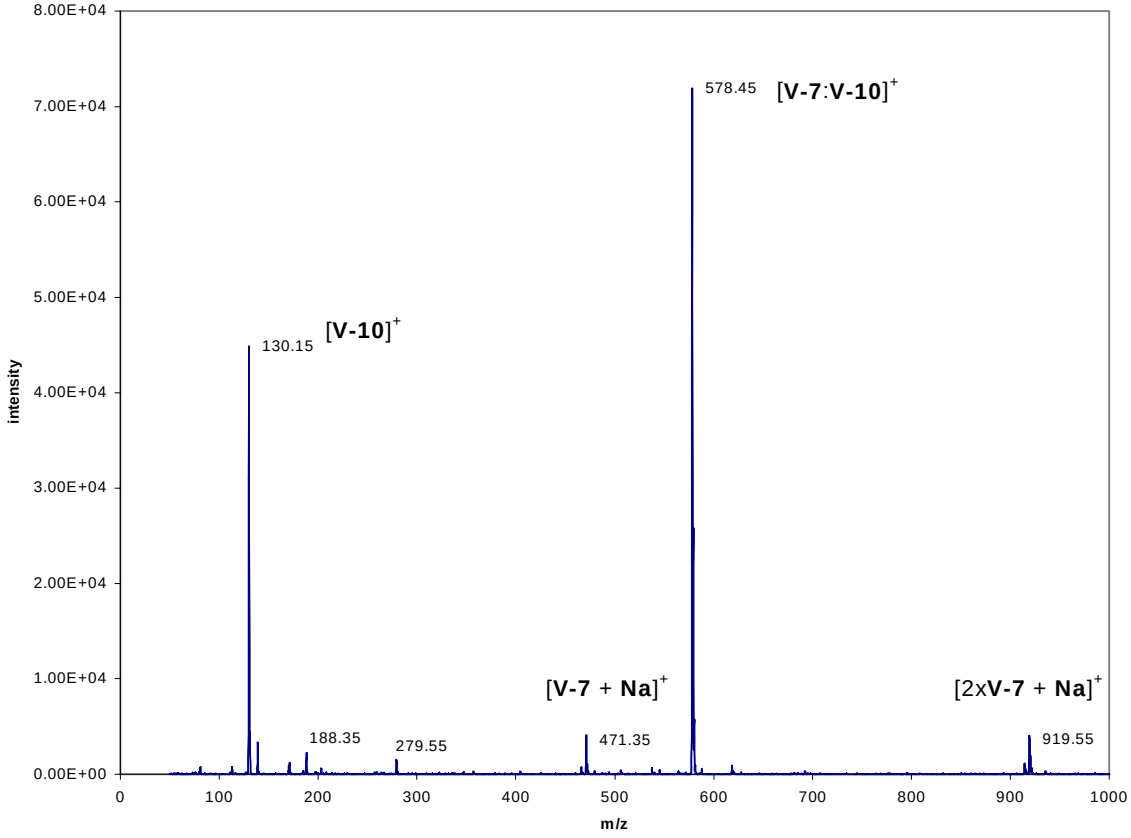

Figure V-18. Positive ion ESI-MS for 1:1 mixture of **BMP26C8** and **V-10•PF_6**.

There may be another reason why the complexation between secondary ammonium ions and **BMP26C8** does not occur in solution. A crystal suitable for X-ray crystallographic analysis was obtained by slow evaporation of an acetone solution containing both **BMP26C8** and the di-*n*-butyl ammonium ion **V-10•PF_6**. The crystals formed were not of the expected complex, but of **BMP26C8** alone (**Figure V-19**). The

structure of the macrocycle differs from that of previously reported phenylene-based macrocycles.[91-94] Instead of the "all-*gauche*" conformation of the polyether bridges adopted by other bisphenylene macrocycles, there exist two *trans* bonds (C5-C6 and C17-C18). The cavity of the macrocycle is collapsed and the overall shape of the macrocycle is reminiscent of **DB24C8**.[91] However, the phenyl rings in **BMP26C8** are almost opposite each other along the short axis (centroid-centroid distance 7.12 Å) rather then the long axis as in **DB24C8**. The phenyl rings also are orientated in an edge-to-edge conformation rather than the more open face-to-face orientation. Therefore, the conformation of the macrocycle in solution may be the same and upon crystallization may exclude the secondary ammonium ion(s) from complexing.

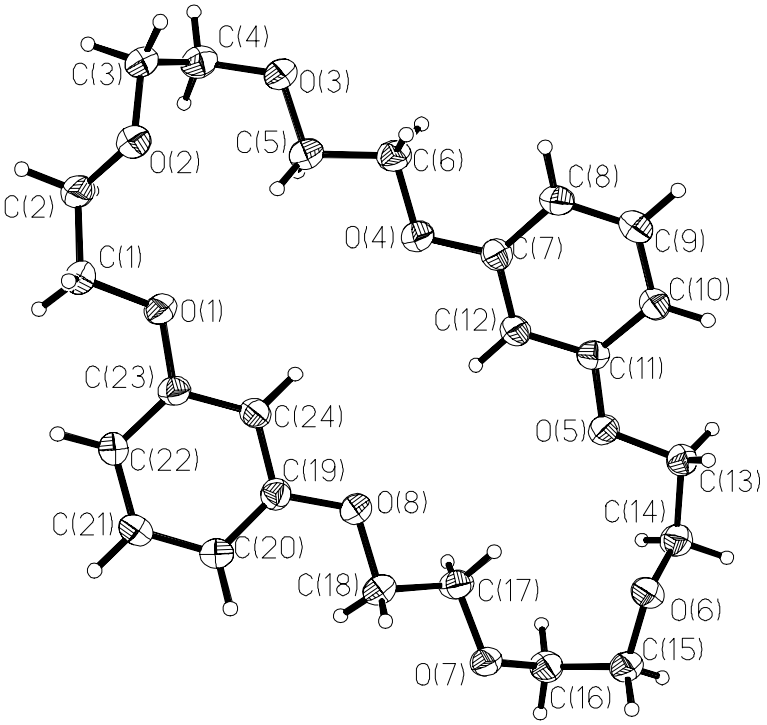

a)

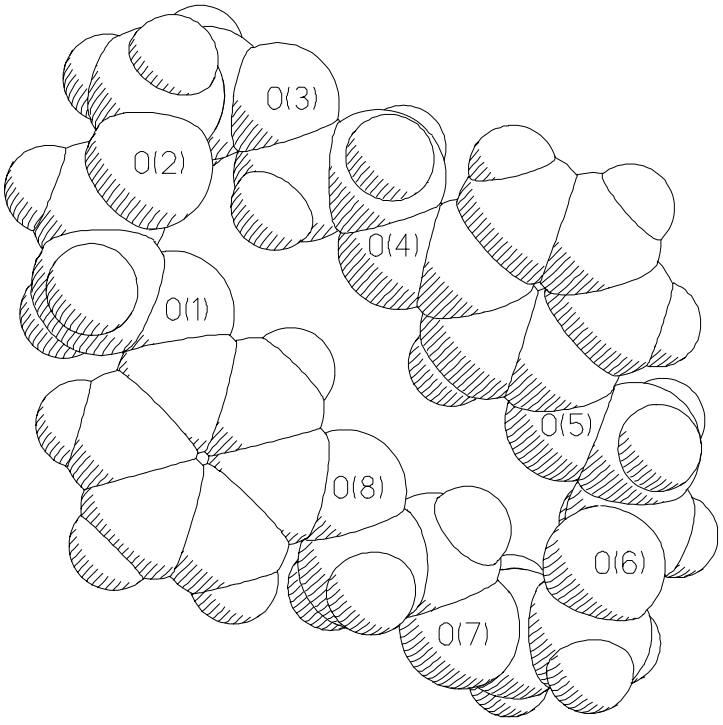

b)

Figure V-19. X-ray structure of 26-membered macrocycle **BMP26C8**: a) ORTEP drawing b) space-filling representation.

V.2.2 Complexation of Bis(*m*-phenylene)-32-crown-10 (V-12) with Secondary Ammonium Ions

V.2.2.1 Bis(*m*-phenylene)-32-crown-10 (V-12) with Diphenethyl- (V-8•PF_6) and Dibenzyl ammonium hexafluorophosphate (V-9•PF_6)

Encouraged by the result that bis(*p*-phenylene)-34-crown-10 (**V-11**) formed a [1.2]pseudorotaxane with dibenzyl ammonium hexafluorophosphate (**V-9•PF_6**) in the solid state,[51-55] we investigated the complexation between bis(*m*-phenylene)-32-crown-10 **(V-12**) and the dibenzyl ammonium salt **V-9•PF_6**. Since the threading and dethreading processes were fast on the NMR time scale, time-averaged signals were observed for the protons of **BMP32C10** and the dibenzyl ammonium salt **V-9•PF_6** in their "complexed" and "uncomplexed" forms (**Figure V-20**). The Low Resolution FAB-MS results corroborated the formation of a 1:2 complex by the presence of a peak at m/z 1077.6, which possibly corresponded to the [1.2]pseudorotaxane [**BMP32C10:(V-9)$_2$•PF_6**]$^+$ (**Figure V-21**). The intensity of the peak assigned to **BMP32C10** alone, relative to that for [**BMP32C10:(V-9)$_2$•PF_6**]$^+$ (541.1 m/z), was ~400:1, however. Also observed was a peak at m/z 734.2 which was possibly the [1.1]pseudorotaxane [**BMP32C10:V-9•PF_6**]$^+$. The intensity of the peak assigned to [**BMP32C10:V-9•PF_6**]$^+$ was approximately 90% as large as that of **BMP32C10** alone. These results indicate that the 1:1 complex is more stable than the 2:1 complex under these conditions. High Resolution FAB-MS for [**BMP32C10:(V-9)$_2$•PF_6**]$^+$ gave a m/z equal to 674.3614 (dev. -11.7 ppm).

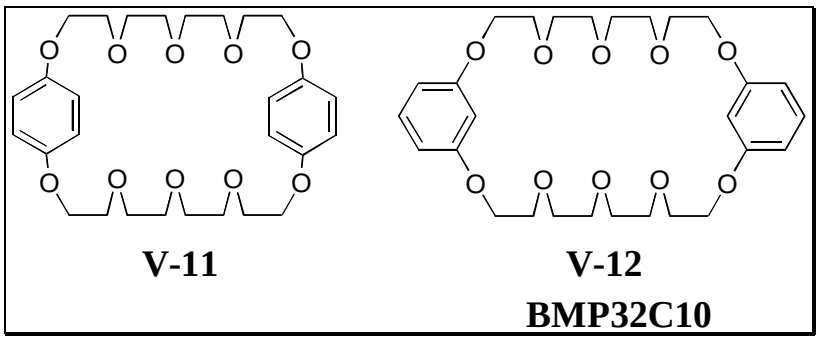

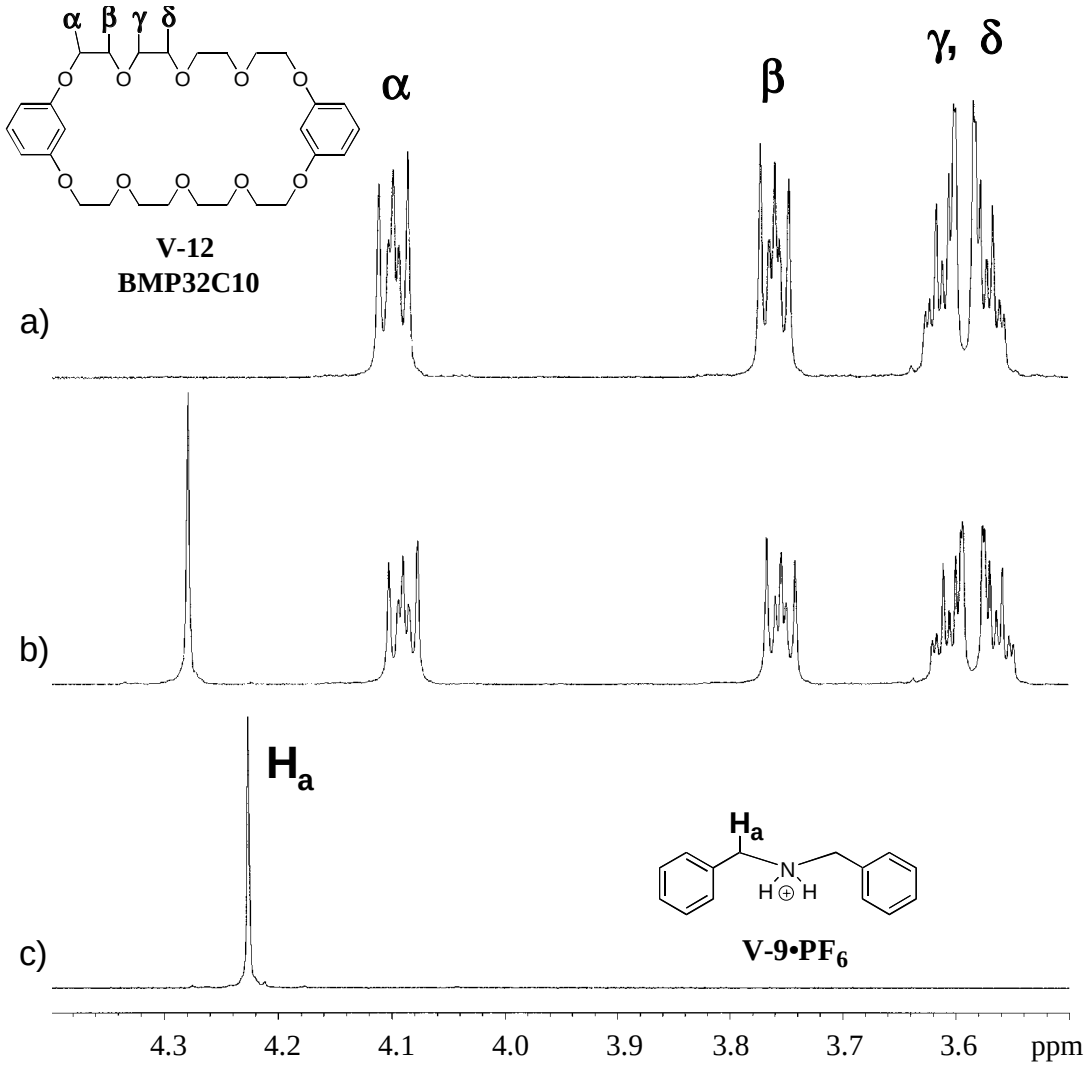

Figure V-20. Stacked ^{1}H NMR plots (400 MHz, CD_3CN, ambient *T*) for a) **BMP32C10**, b) **BMP32C10** + **V-9•PF$_6$** (1:1 stoichiometry, 0.010 M), and c) **V-9•PF$_6$**.

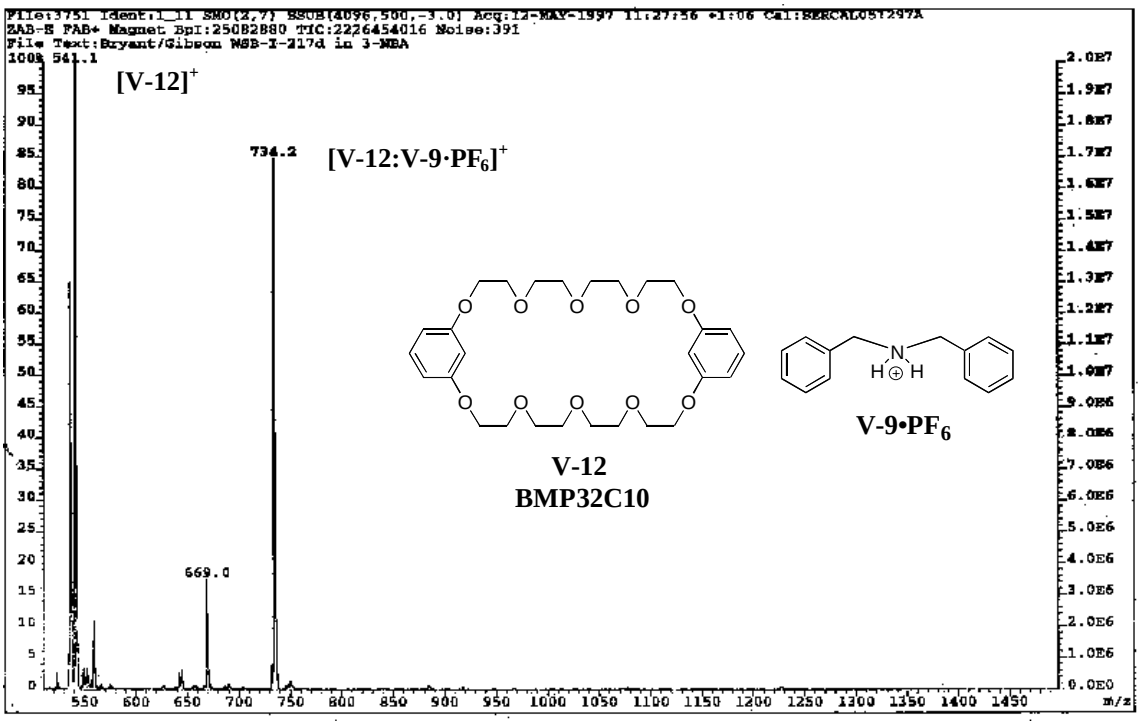

Figure V-21. Low Resolution FAB-MS for **BMP32C10** + **V-9•PF_6**.

X-ray crystallography confirmed the [1.2]pseudorotaxane structure for **BMP32C10:$(V\text{-}9)_2$•2(PF_6)** (**Figure V-22**). The complex resides on an inversion center, with two N-H--O hydrogen bonds per ammonium ion stabilizing the interaction. The hydrogen bonds involve alternate 1,3-ether oxygens [O(2), O(3); O(2a), O(3a)] on the same ethyleneoxy bridge. Further stabilization occurs from two aromatic-aromatic edge-to-face interactions[95-97] between one of the *ortho* aromatic hydrogen atoms of each ammonium ion and a resorcinol ring. There appear to be no strong stabilizing interactions between the complexes in the crystal lattice.

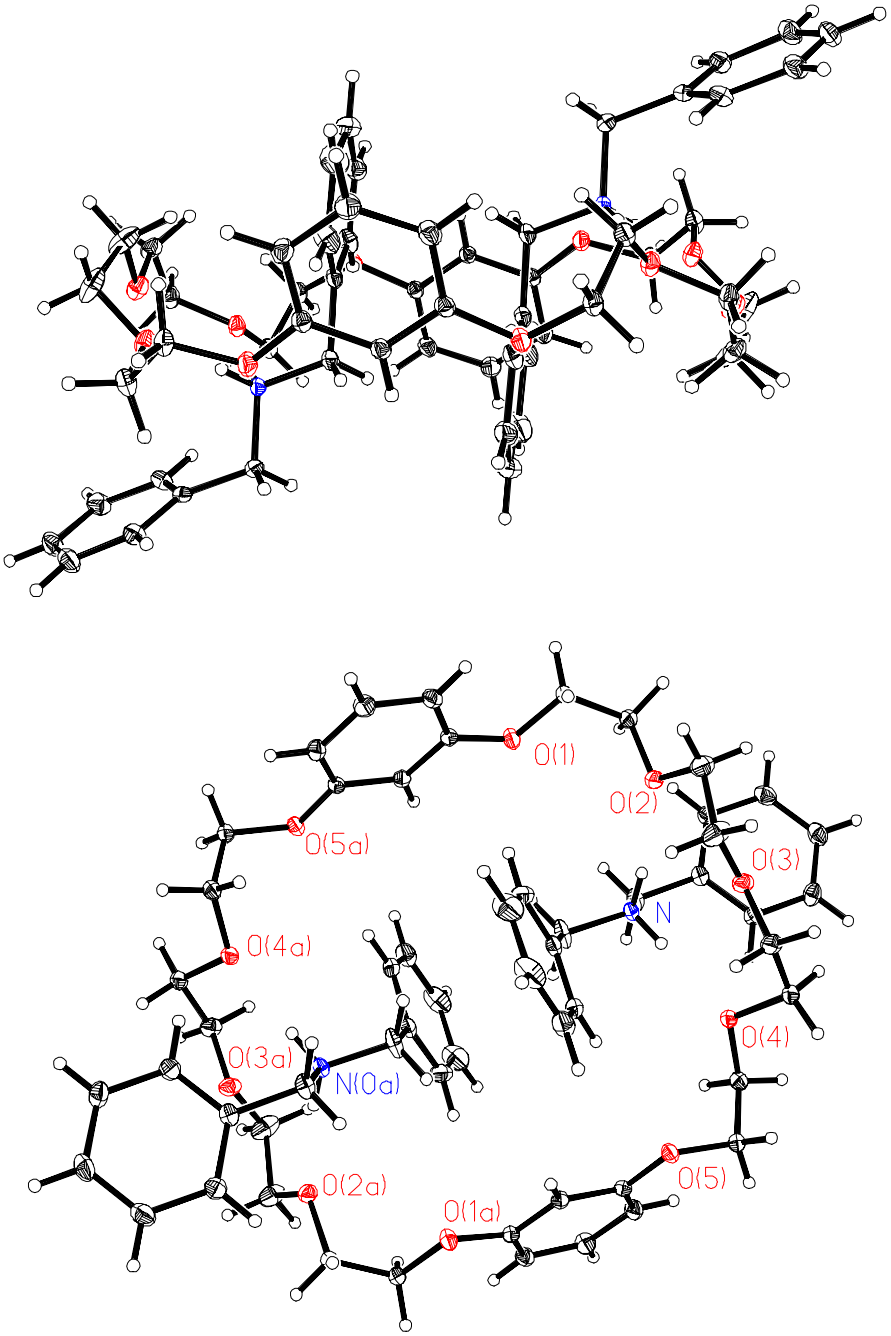

Figure V-22. Side-on and top views of the X-ray structure of the [2.1]pseudorotaxane for **BMP32C10:(V-9)$_2$•2(PF$_6$)** (PF_6 anions have been omitted for clarity). The hydrogen bonds have the following distances and angles: [N--O] 3.02 Å, 2.88 Å; [H--O] 2.12 Å, 1.98 Å; [N-H--O] 176°, 170°. The aromatic-aromatic edge-to-face interactions have the following parameters: centroid-centroid distance, 5.50 Å; C-H--centroid angle, 140°; H--centroid distance, 3.48 Å.

As discussed earlier in this chapter, before the association constant(s) can be determined using NMR, the stoichiometry of the complex(es) must be determined. Determination of the stoichiometry of the complex formed by **BMP32C10** and the dibenzyl ammonium salt **V-9•PF$_6$** was attempted using the mole ratio method. The crown ether **BMP32C10** was added in small increments to a solution of the dibenzyl ammonium salt **V-9•PF$_6$** in acetonitrile-d_3. However, there was no observable break point in the plotted data (**Figure V-23**). When the data obtained from mole ratio experiments is plotted using the Scatchard equation any curvature indicates that more than a 1:1 complex is present. A good fit is an indicator that only a 1:1 complex exists. The data for **BMP32C10** and the dibenzyl ammonium salt **V-9•PF$_6$** was plotted using the Scatchard equation (**Figure V-24**). The fit was good (R^2 = 0.9916) and the complexation was assumed to have a 1:1 stoichiometry in solution. This observation contradicts the observed stoichiometry of the X-ray crystal structure of the [1.2]pseudorotaxane discussed above.

Three graphical methods, Benesi-Hildebrand, Rose-Drago, and Creswell-Allred, were employed to calculate the association constant for the 1:1 complex between **BMP32C10** and the dibenzyl ammonium salt **V-9•PF$_6$**. A new set of experimental data was collected where [**BMP32C10**] (9.65 mM) was held constant and [**V-9•PF$_6$**] was varied from 10.16 mM to 254.02 mM. The observed proton was the H_c proton of **BMP32C10**. The results are listed in **Table V-4**. The error for K_a for the Benesi-Hildebrand was determined for a 95% confidence level using the following equation

$$\Delta K_a = K_a \sqrt{\left(\frac{\Delta b}{b}\right)^2 + \left(\frac{\Delta m}{m}\right)^2} \qquad (\mathbf{24})$$

where, b is the intercept and m is the slope. The initial data obtained for the complexation was amended to meet the requirements of the Weber "probability of binding," **p**, discussed above. As shown in **Table V-5**, for the data obtained for the Creswell-Allred method, the **p** is too low for some of the solutions containing the lower $[\boldsymbol{S}]_o$ values. These

data points were omitted in determining the K_a values in **Table V-4** and the new data set is shown in the last three columns. However, the exclusion of these data points did not change the calculated Δ_o value, except for the last data set at 57 ^oC. The K_a calculated at 57 ^oC changed by 1.1 M^{-1}, from 5.5 to 4.6 M^{-1}. The K_a values at the other temperatures changed from only 0.1 to 0.6 M^{-1}.

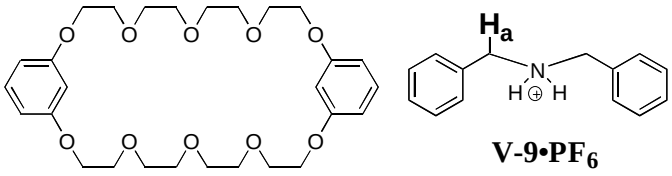

V-12
BMP32C10

V-9•PF$_6$

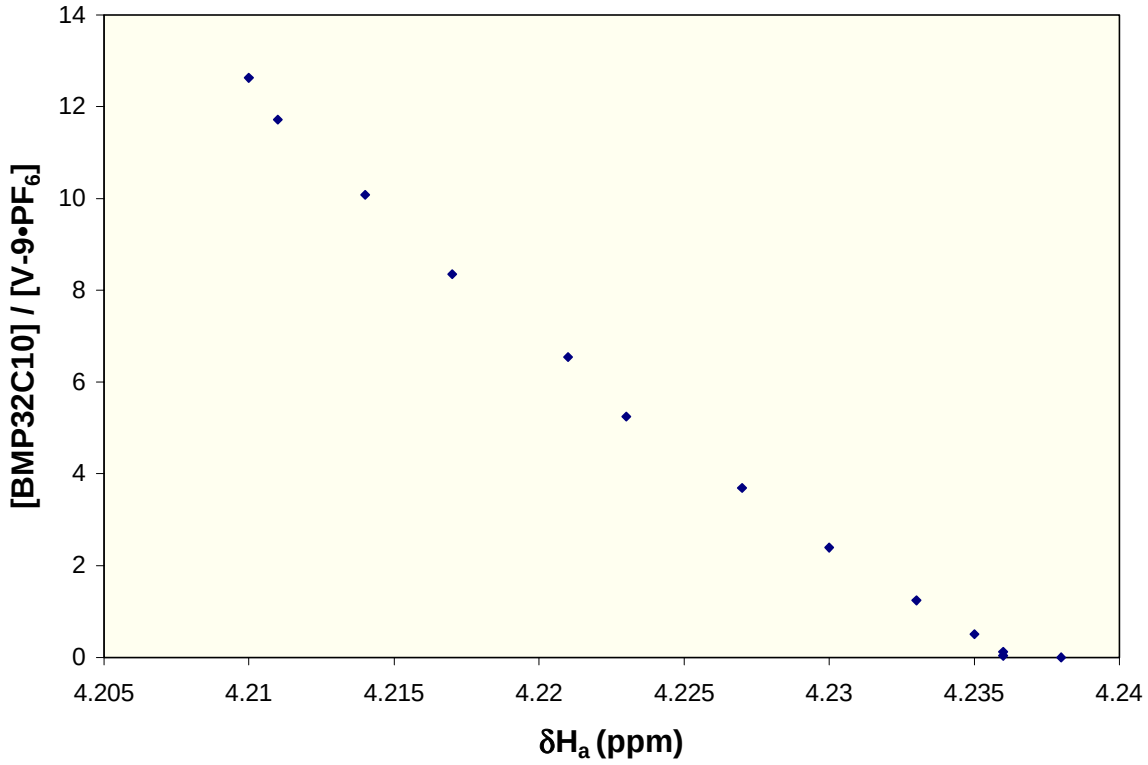

Figure V-23. Mole ratio plot for **BMP32C10** + **V-9•PF$_6$** in acetonitrile-d_3 ([**V-9•PF$_6$**] = 0.010 M).

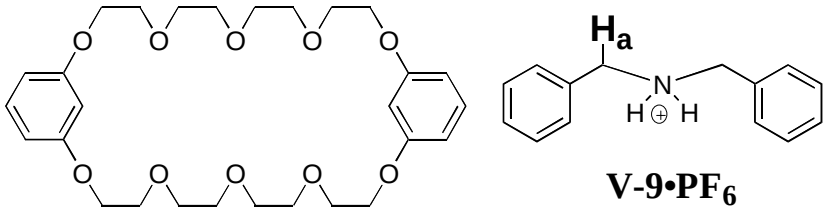

V-12
BMP32C10

V-9•PF_6

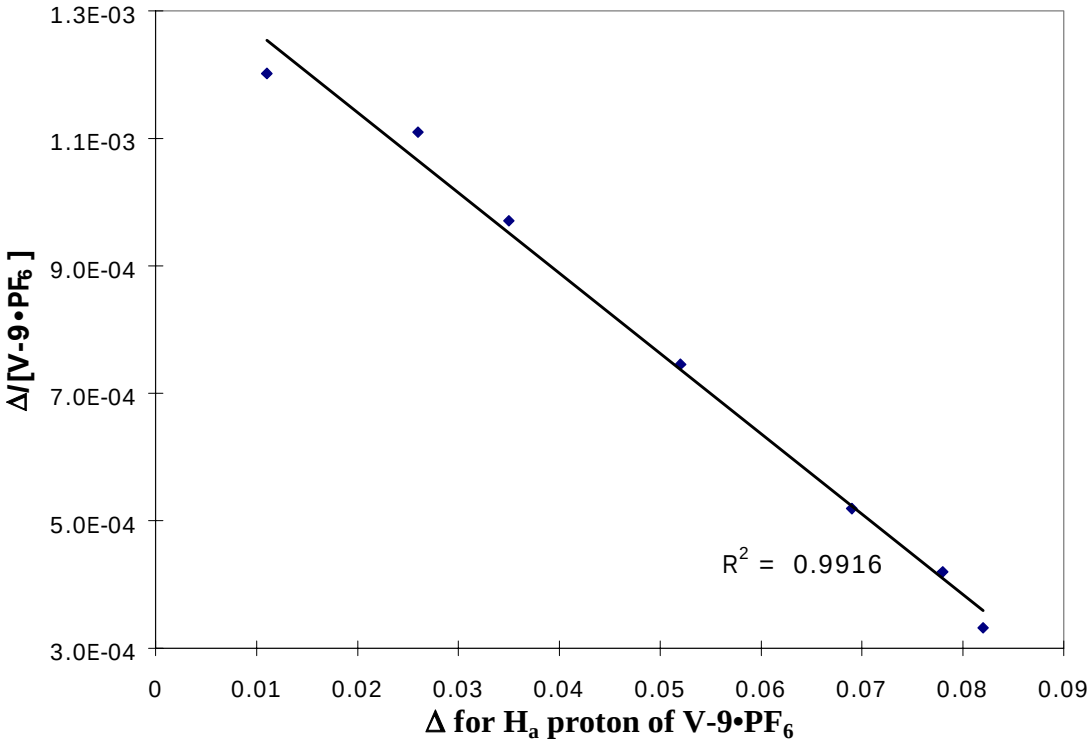

Figure V-24. Scatchard plot for **BMP32C10** + **V-9•PF_6**.

Table V-4. Results from the graphical methods used to determine the 1:1 association constants for the complex between **BMP32C10** the dibenzyl ammonium salt the dibenzyl ammonium salt **V-9•PF_6** using the H_c proton of **BMP32C10** in acetonitrile-d_3.

T (^oC)	K_a (M^{-1})			Avg. ΔG (kJ/mole)
	Benesi-Hildebrand (R^2)	**Rose-Drago**	**Creswell-Allred** (R^2)	
25.0	13.7 ± 0.2 (1.000)	14.0 ± 1.4	13.5 ± 0.3 (0.999)	-6.5
33.0	10.5 + 0.1 (1.000)	10.2 ± 0.2	10.5 ± 0.1 (1.000)	-5.9
41.0	9.3 + 0.3 (0.999)	8.7 ± 1.3	8.8 ± 0.4 (0.996)	-5.7
49.0	6.5 + 0.3 (0.999)	6.2 ± 0.5	6.2 ± 0.1 (1.000)	-4.9
57.0	4.6 + 0.1 (1.000)	4.5 ± 0.1	4.6 ± 0.1 (1.000)	-4.2

The last column of **Table V-4** lists the ΔG values at each temperature. As expected the ΔG values decreased with increasing temperature. Van't Hoff plots were created for all three methods to determine the ΔH and ΔS values for **BMP32C10**:**V-9•PF_6** (**Table V-6**). The average ΔH and ΔS values were –27.6 kJ/mol and –70.4 J/mol·K, respectively. As a comparison, the binding of 18-crown-6 with Me-$NH_3^+I^-$ had a ΔH value of -10.71.[98]

The complex between **BMP32C10** and the dibenzyl ammonium salt **V-9•PF_6** is a prime example of the common mistake made by assuming that the stoichiometry of the complex in the solid state is the same as in the solution state. Here the X-ray crystal structure was shown to be the [1.2]pseudorotaxane **BMP32C10**:(**V-9**)$_2$•**2(PF_6)** and the mass spectrometry results confirmed a 1:2 complex, whereas, the solution stoichiometry was determined to be only 1:1. Therefore, caution should be used in determining the

stoichiometry of complexation by NMR and the data should be carefully examined before K_a values can be calculated.

The formation of the complex between **BMP32C10** and the diphenethyl ammonium salt **V-8•PF$_6$** caused a small change in the chemical shifts for the time-averaged proton signals of both species (**Figure V-25**). Low Resolution FAB-MS detected only a 1:1 complex, as evidenced by a peak at m/z 762.2, which may correspond to the [1.1]pseudorotaxane complex **BMP32C10:V-8 (Figure V-26)**. The intensity of the peak assigned as [**BMP32C10:V-8**]$^+$ was approximately 55% as large as that of **BMP32C10** alone. There was no observed peak for the 2:1 complex [**BMP32C10:(V-8)$_2$•PF$_6$**]$^+$. These observations suggest a lower association constant for this system as compared to the complex between **BMP32C10** and the dibenzyl ammonium salt **V-9•PF$_6$**. The lower association constant is probably due to the decreased acidity of the benzylic methylene protons and the ammonium center. Since there is no longer an sp^2 carbon beta to the ammonium center the through-bond effects that increase the acidity of the ammonium center in the dibenzyl ammonium salt **V-9•PF$_6$** are not as profound in the diphenethyl ammonium salt **V-8•PF$_6$**.

X-ray crystallography did confirm the structure of a [1.2]pseudorotaxane **BMP32C10:(V-8)$_2$•2(PF$_6$)** (**Figure V-27**). The complex is stabilized by two N-H--O hydrogen bonds per ammonium salt involving alternate 1,3-ether oxygens [O(2), O(3); O(2a), O(3a)] on the same ethyleneoxy bridge. There is also further stabilization by two aromatic-aromatic edge-to-face interactions. However, in this case the interactions occur between the aromatic rings of the two ammonium ions and not the benzyl groups with the resorcinol rings of the macrocycle as was observed in the [1.2]pseudorotaxane **BMP32C10:(V-9)$_2$•2(PF$_6$)**. There appear to be no strong stabilizing interactions between the complexes in the crystal lattice.

Table V-5. Data for determination of K_a from Creswell-Allred graphical method for complex of **BMP32C10** (**R**) and **V-9•PF$_6$** (**S**) in acetonitrile-d$_3$. (**p** = Δ/Δ_o)

Temp (°C)	$[R]_o$ (mM)	$[S]_o$ (mM)	δ_{obs} (ppm)	δ_R (ppm)	Δ (ppm)	initial			new		
						Δ_o (ppm)	p	[*RS*] (mM)	Δ_o (ppm)	p	[*RS*] (mM)
25.0	9.65	10	6.447	6.458	0.011	0.1091	0.10	0.97			
		26	6.432		0.026		0.24	2.3	0.1075	0.24	2.3
		39.1	6.423		0.035		0.32	3.10		0.33	3.14
		74.3	6.406		0.052		0.48	4.60		0.48	4.67
		139	6.389		0.069		0.63	6.10		0.64	6.19
		193	6.380		0.078		0.71	6.90		0.73	7.00
		254	6.376		0.082		0.75	7.25		0.76	7.36
33.0	9.65	10.2	6.450	6.461	0.011	0.1260	0.09	0.84			
		26	6.436		0.025		0.20	1.9	0.1257	0.20	1.9
		39.1	6.426		0.035		0.28	2.68		0.28	2.69
		74.3	6.408		0.053		0.42	4.06		0.42	4.07
		139	6.388		0.073		0.58	5.59		0.58	5.60
		193	6.378		0.083		0.66	6.36		0.66	6.37
		254	6.370		0.091		0.72	6.97		0.72	6.98
41.0	9.65	10	6.453	6.463	0.010	0.1382	0.07	0.70			
		26	6.439		0.024		0.17	1.7			
		39.1	6.429		0.034		0.25	2.37	0.1375	0.25	2.39
		74.3	6.411		0.052		0.38	3.63		0.38	3.65
		139	6.389		0.074		0.54	5.17		0.54	5.19
		193	6.380		0.083		0.60	5.80		0.60	5.82
		254	6.367		0.096		0.69	6.71		0.70	6.74
49.0	9.65	10	6.457	6.466	0.009	0.1618	0.06	0.54			
		26	6.444		0.022		0.14	1.3			
		39.1	6.435		0.031		0.19	1.85	0.1631	0.19	1.83
		74.3	6.417		0.049		0.30	2.92		0.30	2.90
		139	6.392		0.074		0.46	4.41		0.45	4.38
		193	6.379		0.087		0.54	5.19		0.53	5.15
		254	6.367		0.099		0.61	5.90		0.61	5.86
57.0	9.65	10	6.460	6.469	0.009	0.1691	0.05	0.51			
		26	6.448		0.021		0.12	1.2			
		39.1	6.440		0.029		0.17	1.65			
		74.3	6.423		0.046		0.27	2.62	0.1861	0.25	2.38
		139	6.398		0.071		0.42	4.05		0.38	3.68
		193	6.383		0.086		0.51	4.91		0.46	4.46
		254	6.370		0.099		0.59	5.65		0.53	5.13

Table V-6. ΔH and ΔS obtained from van't Hoff plots for different graphical methods for **BMP32C10**:**V-9•PF_6** in acetonitrile-d_3.

Graphical Method	ΔH (kJ/mol)	ΔS (J/mol·K)	R^2
Benesi-Hildebrand	-27.1	-68.8	0.966
Rose-Drago	-28.3	-72.7	0.985
Creswell-Allred	-27.3	-69.7	0.983
Average	-27.6	-70.4	

The ability of **BMP32C10** to adapt its conformation to include different ammonium ions is evident by comparing the crystal parameters of the pure macrocycle[92] to that of the macrocycle in the [1.2]pseudorotaxanes **BMP32C10:(V-8)$_2$•2(PF_6)** and **BMP32C10:(V-9)$_2$•2(PF_6)** (**Table V-7**). The "all-*gauche*" conformation of the ethyleneoxy bridges is maintained in both complexes. Although there appears to be little change in the distances between the -NH_2- centers, the dimensions of the macrocyclic cavity change substantially. The macrocycle in **BMP32C10:(V-9)$_2$•2(PF_6)** expands in both dimensions relative to **BMP32C10** alone, whereas in **BMP32C10:(V-8)$_2$•2(PF_6)** it expands along one axis but shrinks along the other. Also, the centroid-centroid distances of the aromatic rings of the macrocycle increased in **BMP32C10:(V-8)$_2$•2(PF_6)**, but decreased in **BMP32C10:(V-9)$_2$•2(PF_6)** relative to pure **BMP32C10**.

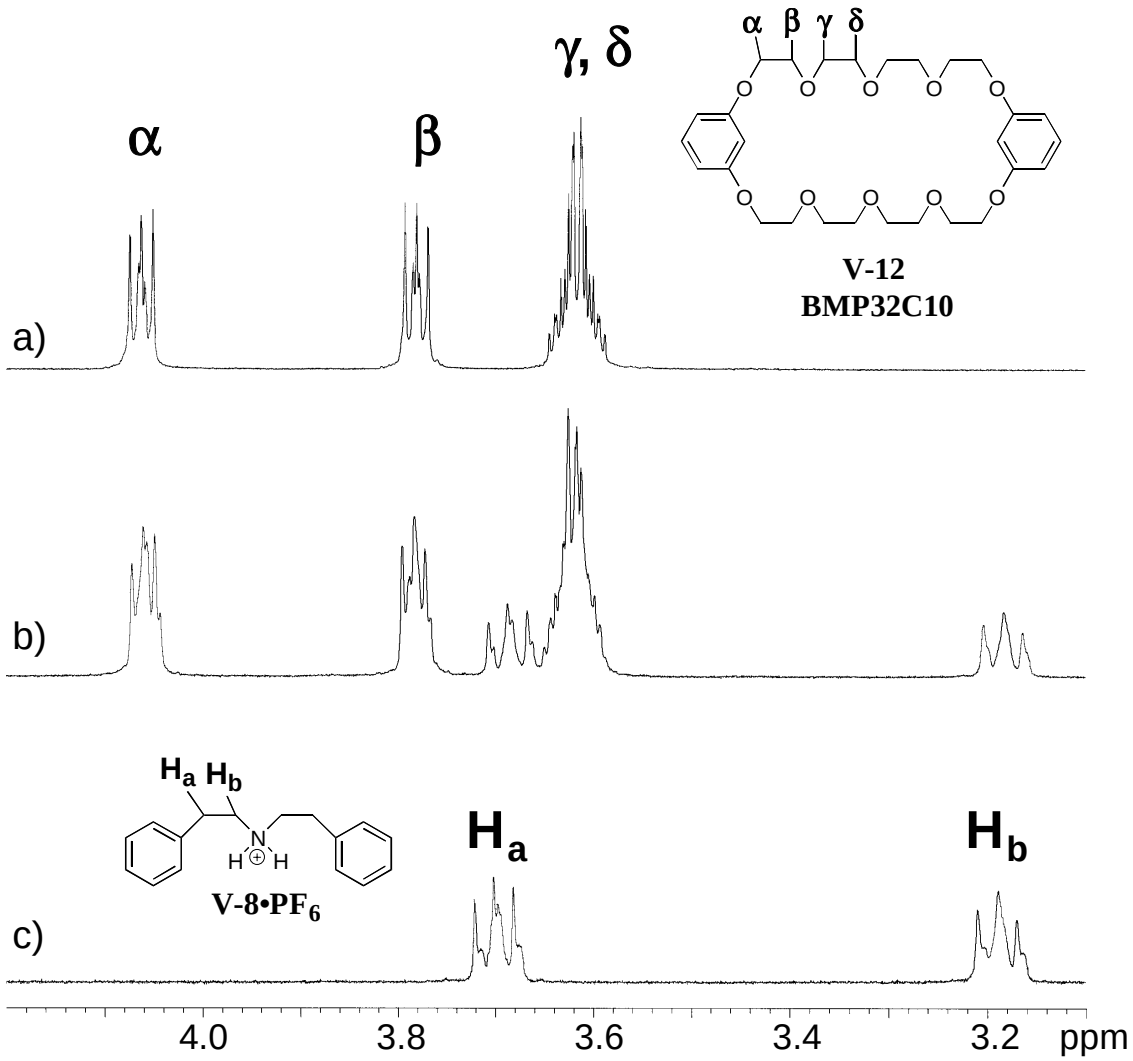

Figure V-25. Stacked ^{1}H NMR plots (400 MHz, acetone-d_6, ambient *T*) for a) **BMP32C10**, b) **BMP32C10** + **V-8•PF$_6$** (1:1 stoichiometry, 0.010 M), and c) **V-8•PF$_6$**.

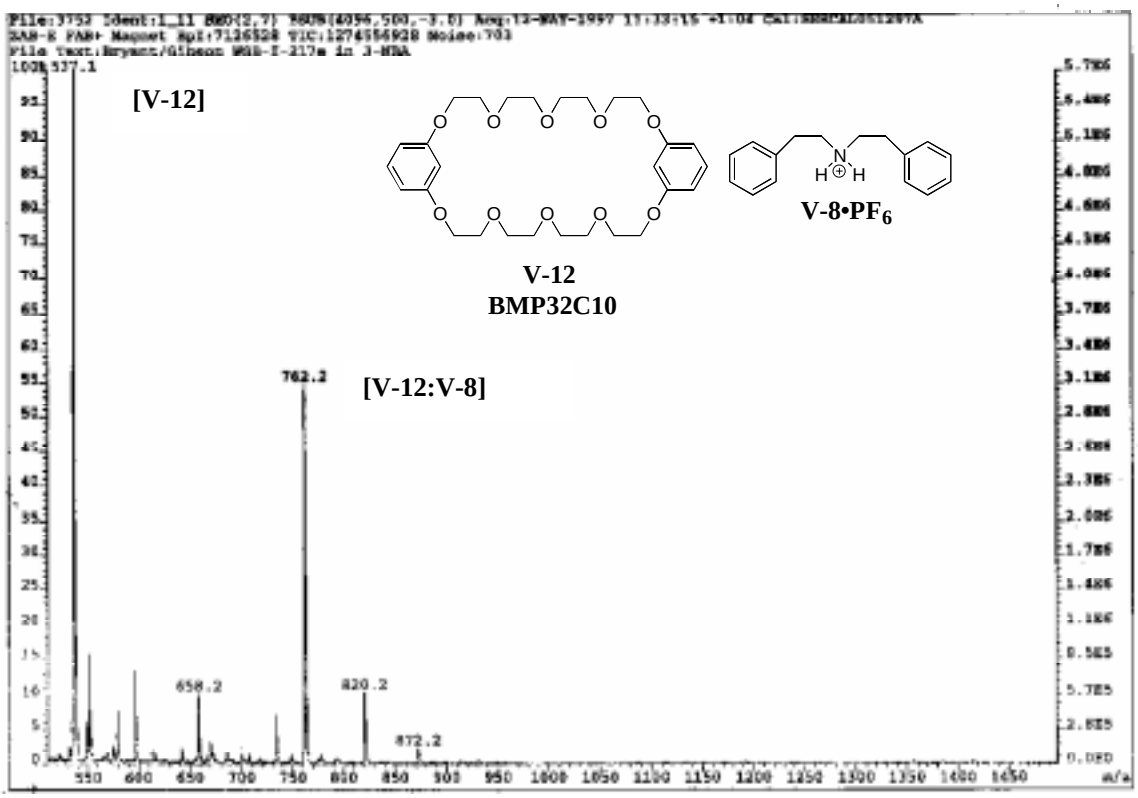

Figure V-26. LRFAB-MS for **BMP32C10** + **$(V\text{-}8)_2$•2(PF_6)**.

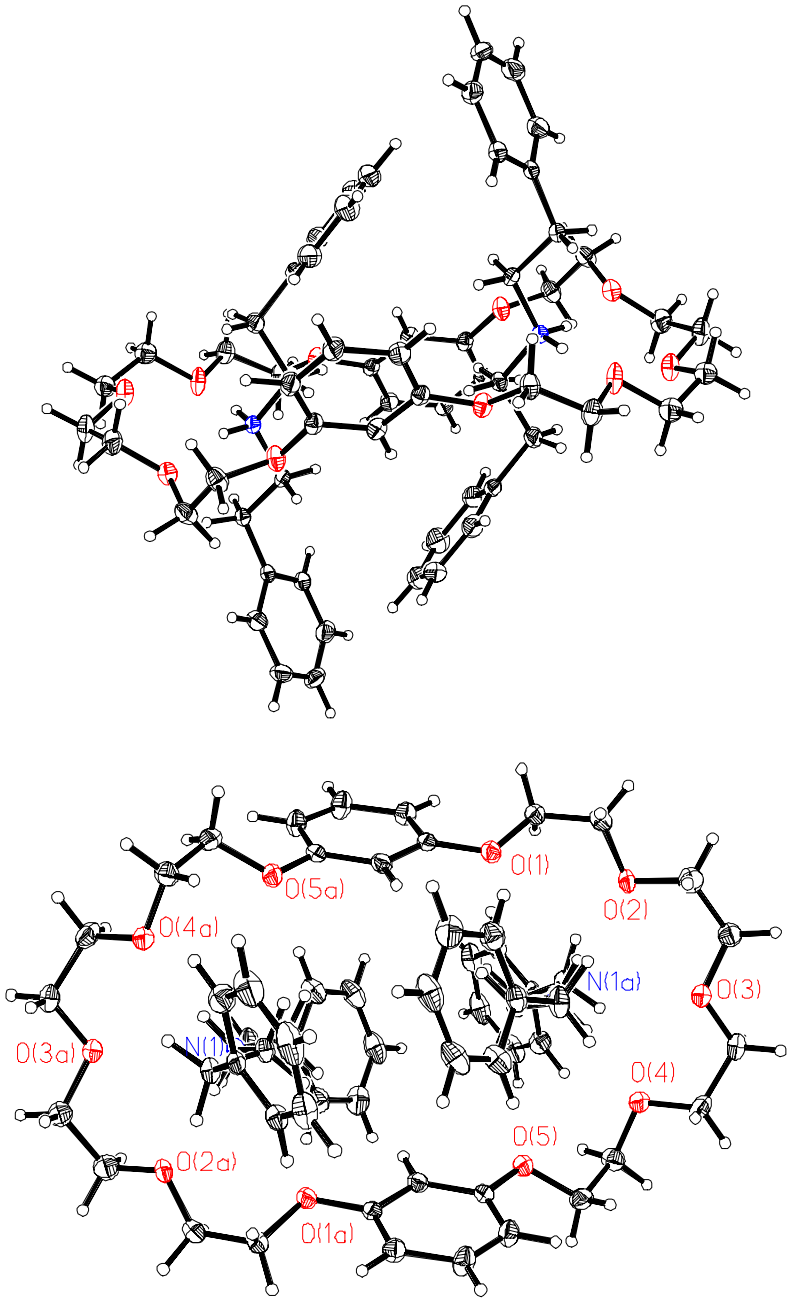

Figure V-27. Side-on and top views of the X-ray structure of the pseudorotaxane pseudorotaxane **BMP32C10:(V-8)$_2$•2(PF$_6$)** (PF_6 anions have been omitted for clarity). The hydrogen bonds have the following distances and angles: [N--O] 2.85 Å, 2.84 Å; [H--O] 1.96 Å, 1.93 Å; [N-H--O] 165°, 175°. The aromatic-aromatic edge-to-face interactions have the following parameters: centroid-centroid distance, 4.83 Å; C-H--centroid angle, 142°; H--centroid distance, 2.80 Å.

Table V-7. Comparison of crystal parameters (Å).

Compound or Complex	**BMP32C10**[91]	**BMP32C10: (V-8)$_2$•2(PF$_6$)**	**BMP32C10: (V-9)$_2$•2(PF$_6$)**
Cavity size	7.8 x 4.9	8.6 x 4.1	8.2 x 6.7
Centroid-centroid distance of aromatic rings in macrocycle	8.8	8.3	10.3
Mean plane separation between aromatic rings of macrocycle	7.0	5.6	8.2
Distance between the two -NH_2- centers	N/A	7.0	7.2

V.2.2.2 Bis(*m*-phenylene)-32-crown-10 (BMP32C10) with N,N'-Dibenzyl-*m*-xylylenediammonium Bishexafluorophosphate (V-13•2(PF$_6$))

The X-ray crystal structure of the complex between **BMP32C10** and N,N'-dibenzyl-*p*-xylylenediammonium bishexafluorophosphate (**V-13•2(PF$_6$)**) reported by Stoddart *et al*. revealed a [2.2]pseudorotaxane.[51] To determine if the stoichiometry and association constant(s) were affected by the substitution on the internal aromatic ring of the diammonium salt, the complexation between **BMP32C10** and N,N'-dibenzyl-*m*-xylylenediammonium bishexafluorophosphate (**V-14•2(PF$_6$)**) was investigated by ^{1}H NMR (**Figure V-28**). The complexation was fast on the NMR time-scale; therefore, several NMR experiments were needed to determine the stoichiometry and association constant(s). Again, the stoichiometry of the complex was determined using the mole ratio method in acetone-d$_6$. The *m*-substituted diammonium salt **V-14•2(PF$_6$)** was added to a solution of **BMP32C10** and the break point in the plot suggested a 1:1 ratio (**Figure V-29**); however, the same result would occur if the stoichiometry was a 2:2 or 3:3 complex. Therefore, the mole ratio plot only gives a "reduced" stoichiometry. The result does

eliminate the possibility of an uneven complex stoichiometry (e.g. 1:2, 2:3, etc..), however.

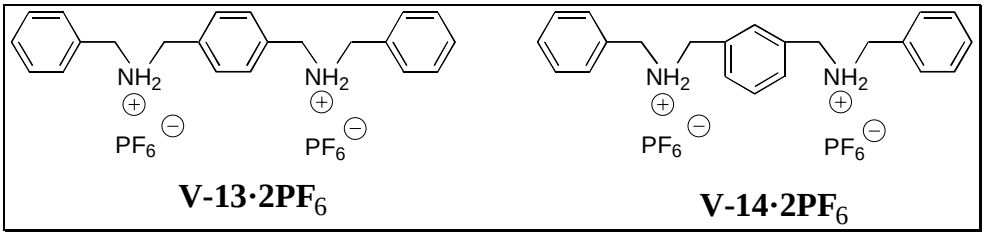

V-13·2PF$_6$ **V-14·2PF$_6$**

The data obtained from the mole ratio method was used to determine the association constant for the complexation of **BMP32C10** and the *m*-substituted diammonium salt **V-14•2(PF$_6$)** at 23.0 ^{o}C. Again, the experimental data were used to solve the equations for the three graphical methods, the Benesi-Hildebrand, Rose-Drago, and Creswell-Allred methods, to arrive at an average K_a value. First, it was determined if the experimental data represented a suitable concentration range based on the Weber "probability of binding" explained above. **Table V-8** demonstrates that the last data points were not within the constraints of **p**. The values for the K_a changed significantly when the data not within the Weber “probability of binding” were not used. The results are compared in **Table V-9** for each graphical method. It is interesting to note that the error in the Benesi-Hildebrand method was reduced significantly using the data that met the **p** constraint. This demonstrates the importance of adhering to the Weber "probability of binding."

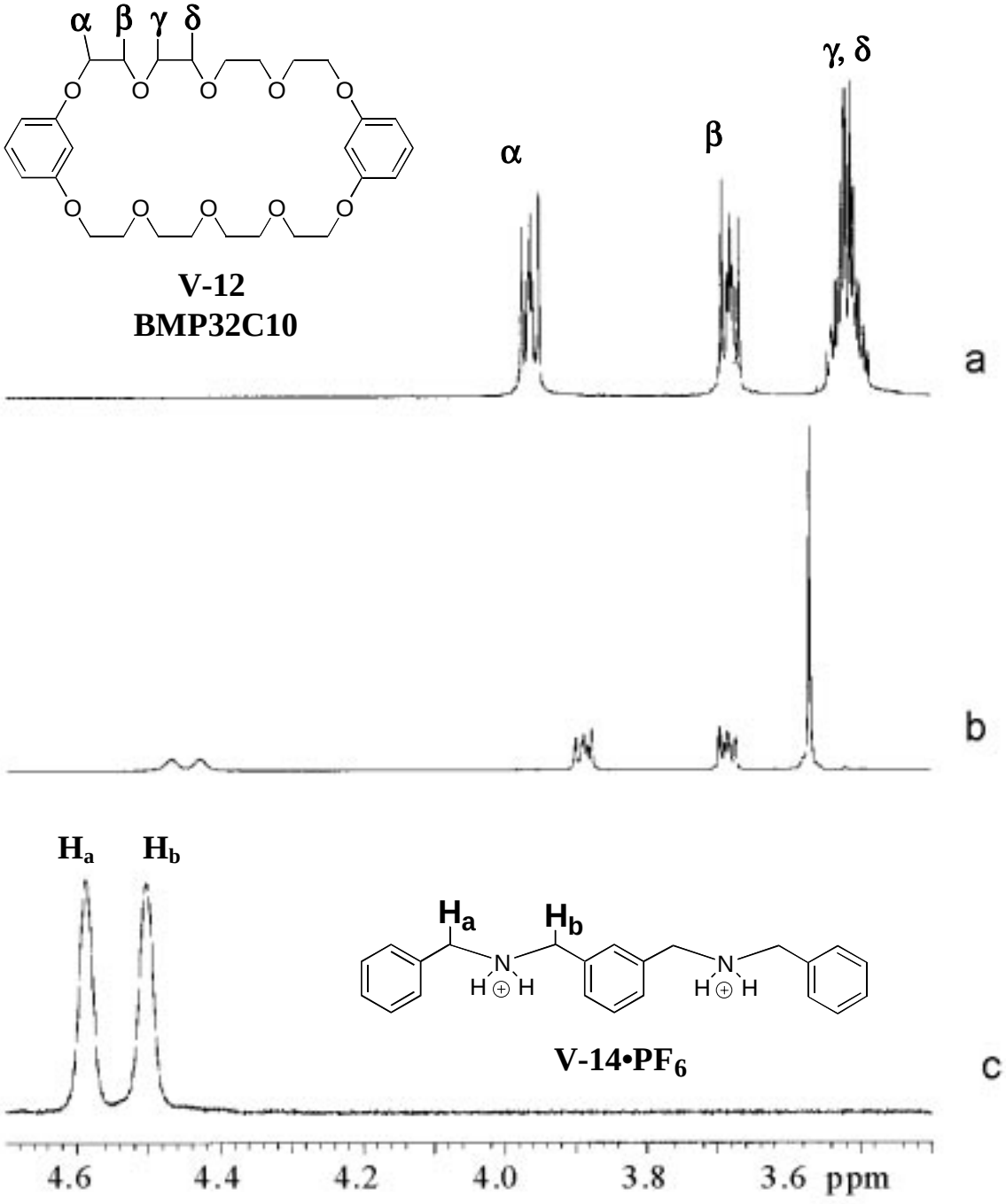

Figure V-28. Stacked ^{1}H NMR (400 MHz, acetone-d_6) spectra of a) **BMP32C10** (0.010 M), b) 1:1 solution of **BMP32C10** and **V-14•2(PF$_6$)** (0.010 M), and c) **V-14•2(PF$_6$)** (0.010 M).

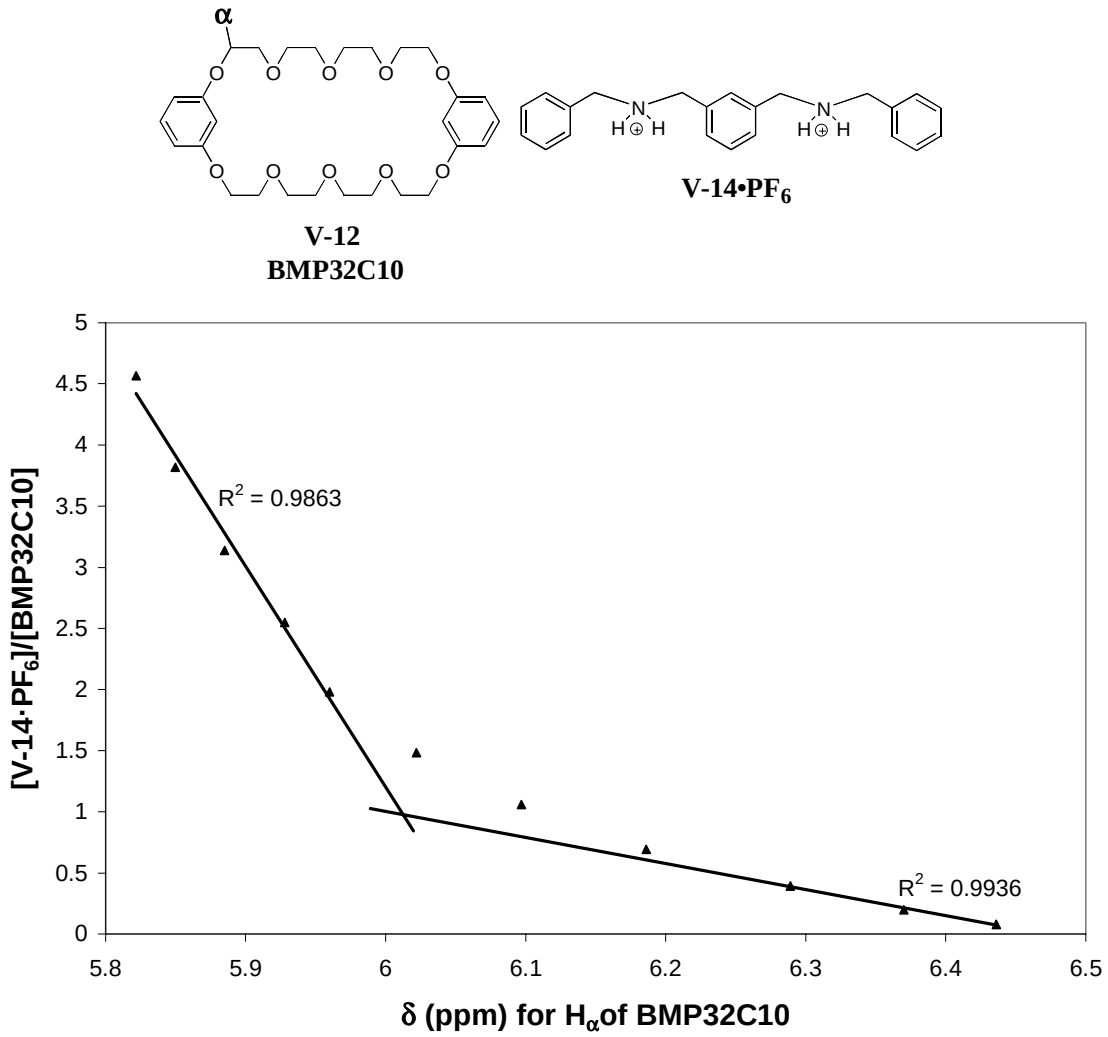

Figure V-29. Mole ratio plot for complex between **BMP32C10** and **V-14•2(PF_6)** in acetone-d_6.

Table V-8. Data for determination of K_a from Creswell-Allred graphical method for complex of **BMP32C10** (***R***) and **V-14•2(PF$_6$)** (***S***) in acetone-d$_6$. (**p** = Δ/Δ_o), $[\boldsymbol{R}]_o$ (mM) 10.0, δ_R (ppm) = 6.473, Temp(^{o}C) = 23.0.

			initial			new		
$[S]_o$ (mM)	δ_{obs} (ppm)	Δ (ppm)	Δ_o (ppm	p	[*RS*] (mM)	Δ_o (ppm)	p	[*RS*] (mM)
10.6	6.097	0.376	0.734	0.51	5.12	0.672	0.56	5.60
14.8	6.022	0.451		0.61	6.15		0.67	6.71
19.8	5.960	0.513		0.70	6.99		0.76	7.64
25.5	5.928	0.545		0.74	7.43		0.81	8.11
31.3	5.885	0.588		0.80	8.01			
38.2	5.850	0.623		0.85	8.49			
45.7	5.822	0.651		0.89	8.87			

Table V-9. Results from the graphical methods used to determine the 1:1 association constants for **BMP32C10:V-14•2(PF$_6$)** using the H$_a$ proton of **BMP32C10** in acetone-d$_6$ (Temp = 23.0 ^{o}C).

Graphical Method	K initial (M^{-1}) (R^2)	K new (M^{-1}) (R^2)	ΔG (kJ/mole)
Benesi-Hildebrand	202 $\pm$ 202 (0.998)	251 $\pm$ 7 (0.994)	-13.6
Rose-Drago	193 $\pm$ 26	264 $\pm$ 33	-13.7
Creswell-Allred	185 $\pm$ 12 (0.991)	255 $\pm$ 8 (0.998)	-13.6

Crystals suitable for X-ray analysis were grown by vapor diffusion of *n*-pentane into an equimolar solution of **BMP32C10** and the *m*-substituted diammonium salt **V-14•2(PF$_6$)** in acetone. The resulting X-ray structure was not the expected pseudorotaxane structure, but rather a 1:1 "*exo*" complex **BMP32C10:V-14•2(PF$_6$)** (**Figure V-30**). The complex resembles a "cradled barbell" where the *m*-substituted diammonium salt **V-14•2(PF$_6$)**, the “barbell”, is surrounded by the “cradle” of the crown ether **BMP32C10**. The conformation of the crown ether is reminiscent of the 'seam of a tennis ball' previously observed for dibenzo-30-crown-10 in its complex with one potassium ion from the early work of Truter *et al.*[99] Stoddart *et al.* have also shown that both a

pseudorotaxane and an "exo," "hot dog," complex can form independently under different crystallization conditions for 1,5-bis(3,5-di-tert-butylbenzylammonium)pentane bis(hexaflurorophosphate) and **BMP32C10**.[100] Attempts to grow crystals of a pseudorotaxane complex with **BMP32C10** and the *m*-substituted diammonium salt **V-14•2(PF$_6$)** have thus far been futile.

The primary stabilizing interaction between the components in the "cradled barbell" complex **BMP32C10:V-14•2(PF$_6$)** is hydrogen bonding. All four ammonium hydrogens are bonded to ether oxygens (one is hydrogen bonded to two ether oxygens giving a total of five N-H---O hydrogen bonds). One of the four ammonium hydrogens is bonded to a phenolic oxygen. There is no carbon-hydrogen-oxygen hydrogen bonding. Further stabilization occurs via two types of π-π stacking interactions. One of the terminal phenyl rings of **V-14** is aligned perpendicularly to one of the resorcinol rings of **BMP32C10**; this results in a favorable edge-to-face π interaction. The concave shape of **BMP32C10** allows the central phenylene ring of the *m*-substituted diammonium ion **V-14** to be "cradled" between the two resorcinol rings of **5**, resulting in face-to-face π–stacking. This alignment is repeated in the packing diagram (**Figure V-31**) as an extended π-stacking column.

Low Resolution Fast-Atom Bombardment Mass Spectroscopy (LRFAB-MS, matrix: 3-NBA/Gly) was done on the crystals. Two peaks were observed that gave direct evidence for the 1:1 complex **BMP32C10:V-14** at 853.5 (**BMP32C10** + **V-14** - H) and 999.5 m/z (**BMP32C10:V-14•(PF$_6$)$^+$**). High Resolution FAB-MS gave 999.4364 m/z (deviation 0.6 ppm). The highest mass peak was 1607.9 m/z which corresponds to the 2:1 complex **BMP32C10:(V-14)$_2$•2(PF$_6$)** minus one PF_6 counterion. The observance of these peaks does not, however, prove that 1:1 or 2:1 pseudorotaxane structures exist, but it does suggest that they might exist.

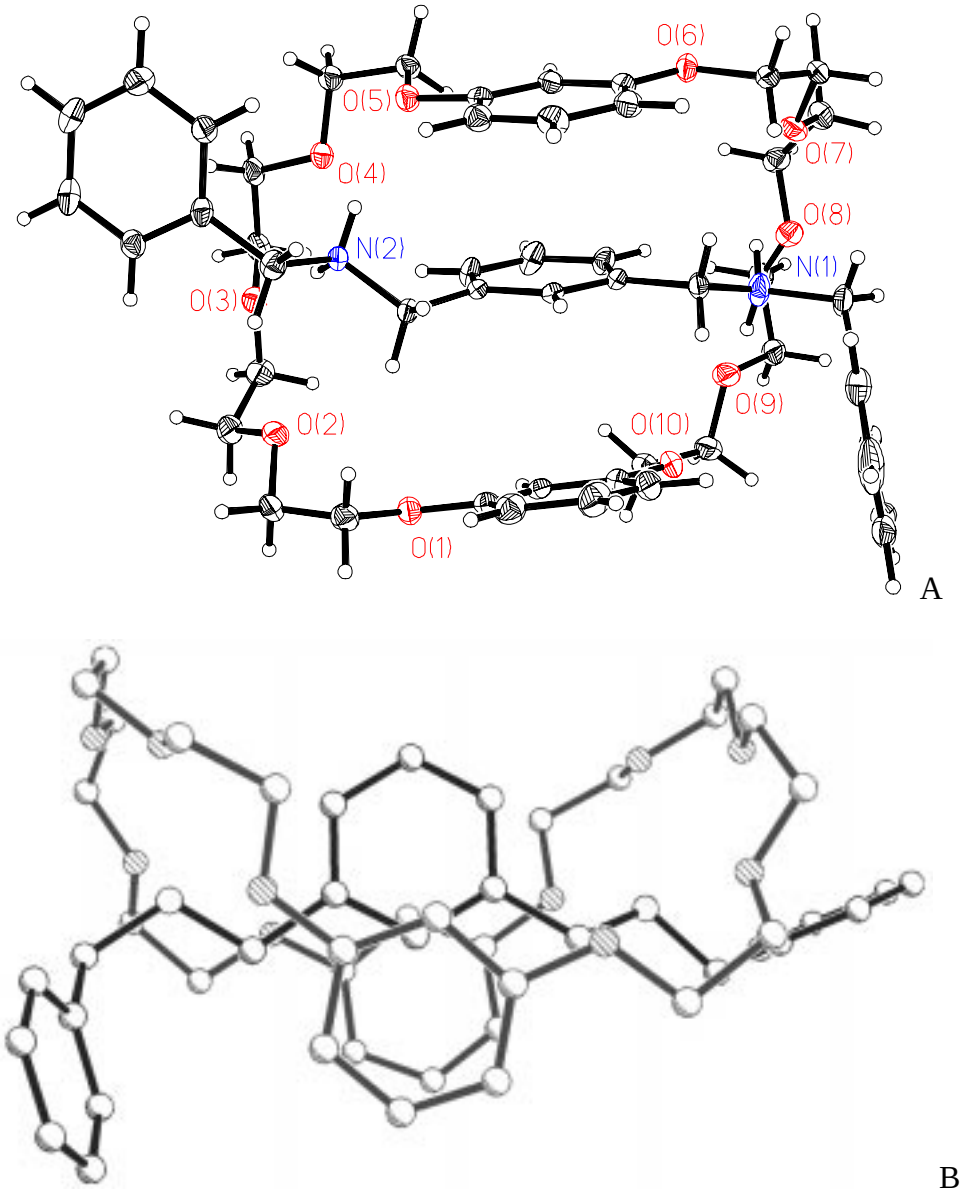

Figure V-30. Crystal structure of "cradled barbell" complex between **BMP32C10** and **V-14•2(PF$_6$)**. A) Ortep representation. Oxygens are red, nitrogens are blue. Hydrogen bond parameters are: [H---O] distances (Å) 2.18, 2.24, 2.01, 2.02, 2.07; [N---O] distances (Å) 2.95, 2.89, 2.87, 2.92, 2.98; [N-H---O] angles (^{o}) 142.3, 126.9, 155.8, 168.7, 170.9. π-π Edge-to-face parameters: centroid/centroid distance 4.91 Å; [H-centroid] distance 2.78 Å; [C-centroid] distance 3.70 Å; [C-H—centroid] angle 164.2^o. π-π Face-to-face parameters for the "sandwich": centroid/centroid distances (Å) 4.22 and 3.98; ring plane/ring plane inclinations (^{o}) 13.1 (top-middle), 4.9 (middle-bottom), 16.7 (top-bottom). B) Orthogonal view. **V-14•2(PF$_6$)** is blue and **BMP32C10** is red. Counterions, hydrogens and solvent molecules have been omitted for clarity.

The above experimental observations demonstrate that it is generally difficult, if not impossible, to determine precisely what type of complexation is occurring in the solution and "gas" phases. The possibility of both "*endo*" and "*exo*" complexation complicates the interpretation of the experimental results. Although in the present case a 1:1 "*exo*" complex was observed in the solid state, one cannot assume that the same complex exists exclusively in solution. Taken together, our results dictate that great caution be used in interpreting solution and "gas" phase data for such complexes on the basis of X-ray crystal structures.

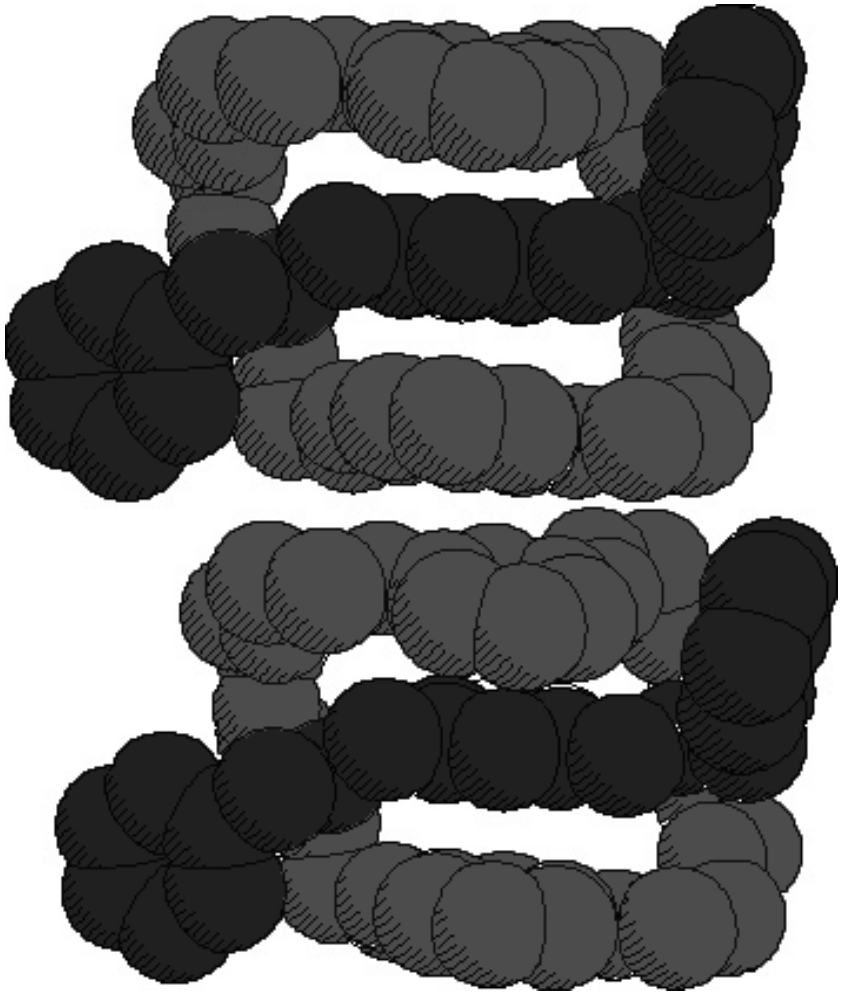

Figure V-31. Packing diagram illustrating the π-stacking between the aromatic rings of **BMP32C10** (blue) and **V-14•2(PF$_6$)** (red). Counterions, solvent molecules, and hydrogens have been omitted for clarity.

V.2.3 Complexation of Dibenzo-24-crown-8 (V-3) with Secondary Ammonium Ions

V.2.3.1 Dibenzo-24-crown-8 (V-3) with Diphenethyl ammonium Hexafluorophosphate (V-8•PF_6)

Stoddart *et al*. have demonstrated that face-to-face π-stacking further stabilizes the complexation of some of the crown ether/ammonium salt pseudorotaxanes.[51-55] It must be noted, however, that the interaction is a secondary stabilization interaction and that hydrogen bonding is the much stronger, primary stabilizing parameter in these systems. Using Corey-Pauling-Koltun (CPK) models it was found that if one adds two extra methylene units to the dibenzyl ammonium salt **V-9•PF_6**, to give the diphenethyl **V-8•PF_6**, it might be possible to increase the face-to-face π-stacking affinity and thus increase the contribution of the secondary stabilizing interaction.

The two components, the diphenethyl ammonium salt **V-8•PF_6** and **DB24C8**, were stirred in a deuterated solvent and analyzed by ^{1}H NMR. An example of an expanded NMR spectrum for the complex in acetonitrile-d_3 is shown in **Figure V-32a**. Comparison of **Figure V-32c** with the diphenethyl ammonium salt **V-8•PF_6** (**Figure V-32b**) and **DB24C8** (**Figure V-32c**) revealed that the labeled peaks in **Figure V-32a** were new peaks. These new peaks were assigned as "complexed" peaks of **DB24C8** and the diphenethyl ammonium salt **V-8•PF_6** in the complex **DB24C8**:**V-8•PF_6** and are a result of the slow-exchange complexation process on the NMR timescale. The same slow-exchange process was observed for the complex between **DB24C8** and the dibenzyl ammonium salt **V-9•PF_6**.[51] The observed slow-exchange process is due presumably to the threading of the ammonium ion through the cavity of **DB24C8**. As mentioned in **Chapter I**, the smallest number of carbon, nitrogen, and/or oxygen atoms required to allow the terminal methyl group of a hydrocarbon chain to thread a macrocycle is 22. Since the end unit of both the diphenethyl ammonium salt **V-8•PF_6** and the dibenzyl ammonium salt **V-9•PF_6** is an aromatic group, a larger ring size would be required for the threading by either molecule. The 24 atoms in **DB24C8** may be the limiting case for the threading of guest having an aromatic end-group.

Comparison of the calculated values for the association constants in different solvents for **DB24C8**:**V-8•PF_6** revealed that increasing the polarity of the solvent decreased the association constant (**Table V-10**). For crown ether complexes, in general, the equilibrium shifts to the complexed side of the equilibrium equation as solvent polarity decreases.[31] This is mainly due to hydrogen bonding. As the solvent polarity increases the solvation of the components becomes increasingly stronger thus preventing the hydrogen bonding from occurring. Therefore, there is less of the complex **DB24C8**:**V-8•PF_6** as the polarity of the solvent increases.

A comparison of the calculated values of K_a for **DB24C8**:**V-8•PF_6** and **DB24C8**:**V-9•PF_6** reveals that the desired increase in the association constant was not achieved (**Table V-10**). The lower association constant is probably due to the decreased acidity of the benzylic methylene groups and the ammonium center of the diphenethyl ammonium salt **V-8•PF_6**. Since there is no longer an sp^2 carbon beta to the ammonium center the through-bond effects that increase the acidity of the ammonium center in of the dibenzyl ammonium salt **V-9•PF_6** are not as profound in of the diphenethyl ammonium salt **V-8•PF_6**. The extra methylene group also increases the conformational freedom of the substrate **V-8•PF_6** making it more difficult to achieve a suitable binding conformation.

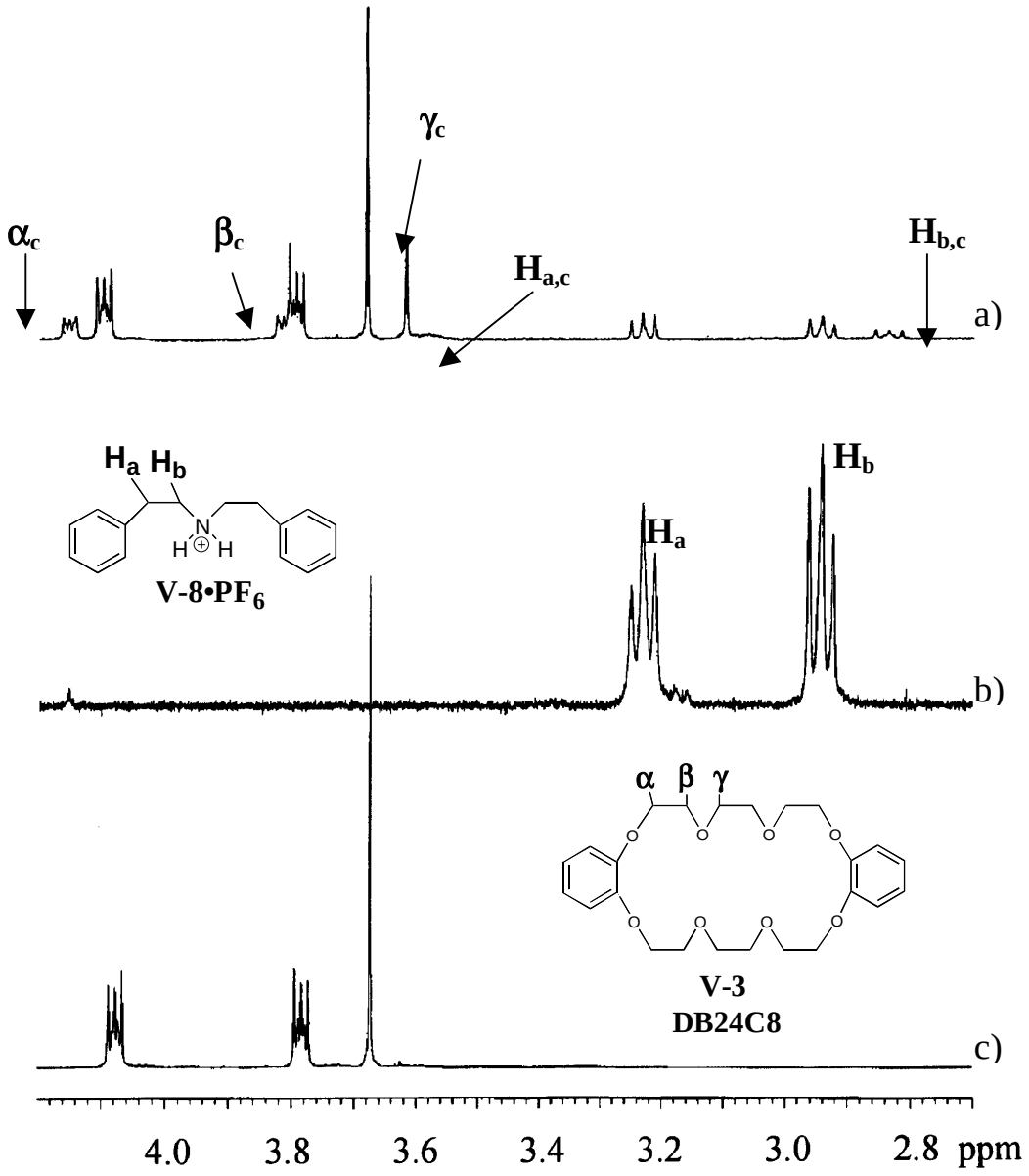

Figure V-32. Stacked ^{1}H NMR plots (400 MHz, CD_3CN, ambient *T*) for a) **DB24C8** + **V-8•PF$_6$** (1:1 stoichiometry, 0.010 M), b) **V-8•PF$_6$**, and c) **DB24C8**. Subscripts c = "complexed" in c).

Table V-10. Association constants (M^{-1}) for **DB24C8**:**V-8•PF_6** and **DB24C8**:**V-9•PF_6**[51] in various solvents.

Solvent	Dielectric Constant[a]	DB24C8:V-8•PF_6	DB24C8:V-9•PF_6
CD_3SOCD_3	46.5	0	0
CD_3CN	35.9	71	4.2×10^2
CD_3COCD_3	20.6	90	3.6×10^2
$CDCl_3$	4.81	4.6×10^2	2.7×10^4

[a]Dielectric constants were obtained from reference 101.

V.2.3.2 Dibenzo-24-crown-8 (V-3) with Di-*n*-butyl ammonium Hexafluorophosphate (V-10•PF_6)

The reported association constant for the complex between **DB24C8** and the di-*n*-butyl ammonium salt **V-10•PF_6** in acetonitrile-d_3 was 70 M^{-1}.[52] The threading was fast on the NMR time scale and K_a was calculated using several NMR experiments. The X-ray crystal structure revealed a [1.1]pseudorotaxane and a 1:1 complex was also observed by FAB-MS. However, the stoichiometry was not determined in solution. Although highly unlikely, it is possible that a 1:1 or 1:2 (**DB24C8:(V-10)$_2$•2(PF_6)**) face-to-face complex might exist. Therefore, to determine the stoichiometry of the complex in solution the mole ratio method was (**Figure V-33**). In this case the di-*n*-butyl ammonium salt, **V-10•PF_6**, was added in measured amounts to a solution of **DB24C8** in acetone-d_6 and the α proton of **DB24C8** was observed. The break point was slightly higher than a 1:1 stoichiometry (actually 1.3:1). As shown in **Figure 33** the plot is rather curved which indicates a low association constant.[77] This may be the reason the stoichiometry is not exact. However, the stoichiometry was assumed to be 1:1. The data were also plotted using the Scatchard equation (**Figure V-34**) and the good fit confirmed the 1:1 stoichiometry. The association constant was calculated using the three graphical methods discussed above (**Table V-11**).

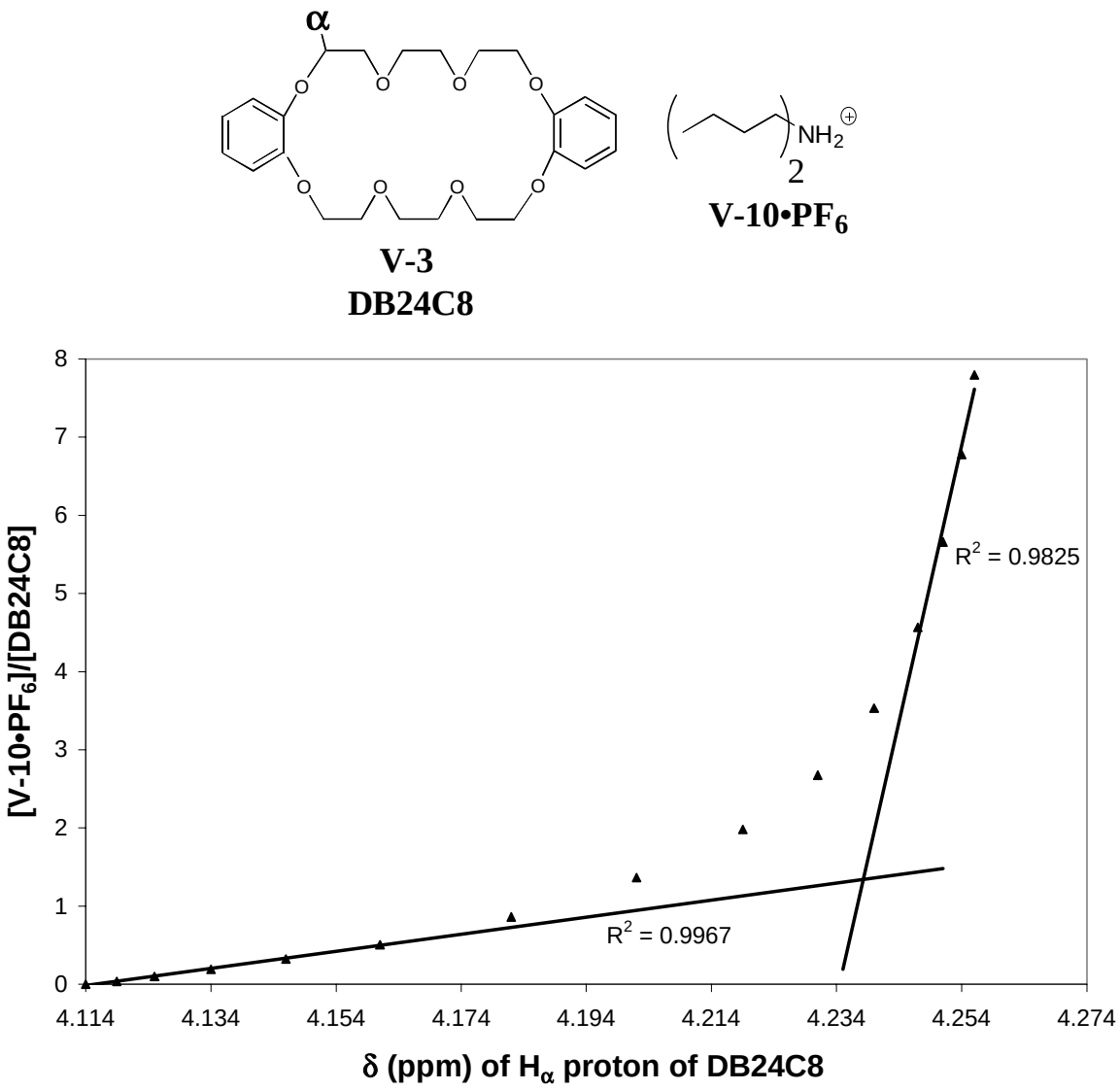

Figure V-33. Mole ratio plot for complex between **DB24C8** and **V-10•PF_6** in acetonitile-d_3.

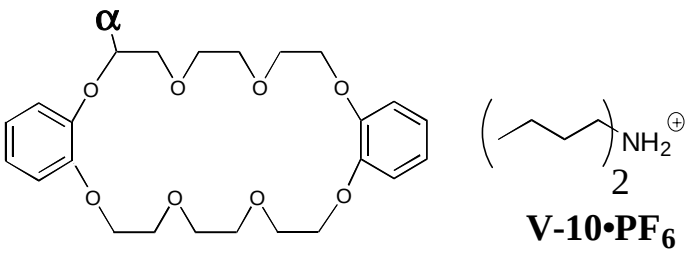

V-3
DB24C8

V-10•PF$_6$

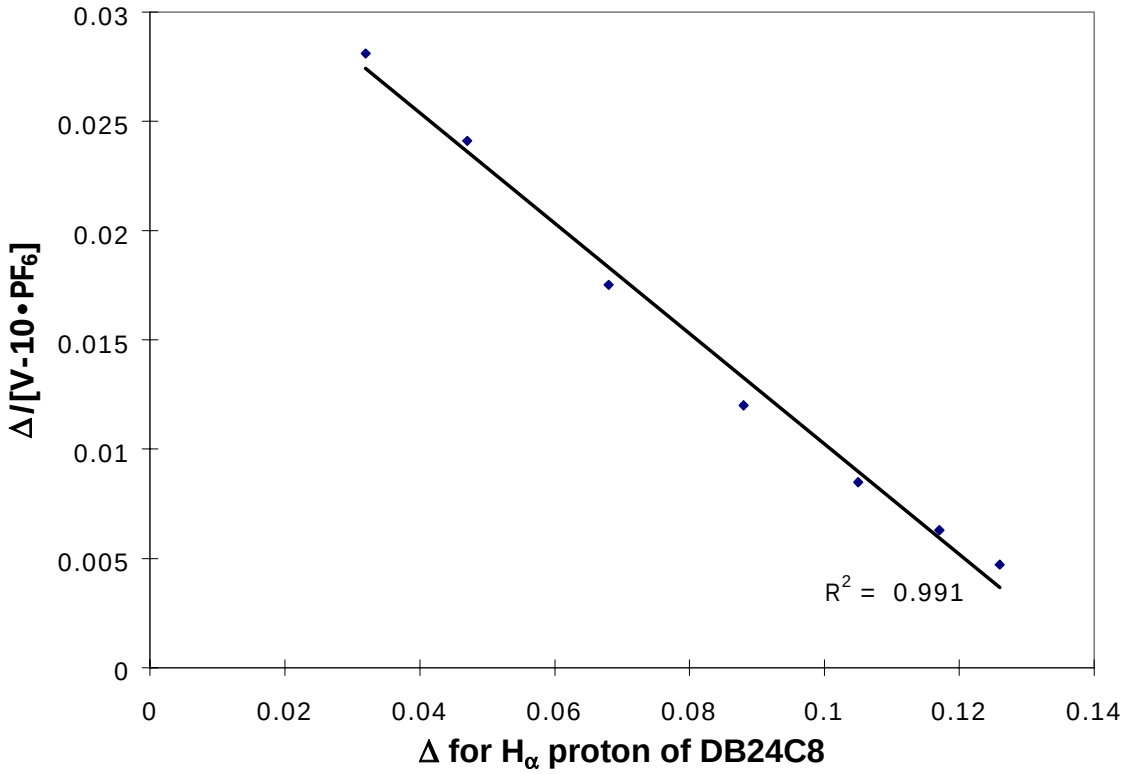

Figure V-34. Scatchard plot for **DB24C8** + **V-10•PF$_6$**.

A comparison of the average K_a (165 M^{-1}) of the complex **DB24C8:V-10•PF$_6$** to that of the complex **DB24C8**:**V-9•PF$_6$** (360 M^{-1}) reveals that almost a two-fold increase in the K_a is achieved with the dibenzyl ammonium salt **V-9•PF$_6$** as the substrate. This is probably due to several factors: 1) the di-*n*-butyl ammonium salt **V-10•PF$_6$** has more conformational freedom than the dienzyl ammonium salt **V-9•PF$_6$,** 2) there is no π–π

stabilizing interaction between **DB24C8** and the di-*n*-butyl ammonium salt **V-10•PF_6**, and 3) there is no longer an sp^2 carbon beta to the ammonium center in the di-*n*-butyl ammonium salt **V-10•PF_6** whose through-bond effects would increase the acidity of the ammonium center, thus increasing the hydrogen bonding. Another factor may be that the hydrogens alpha to the ammonium center in the di-*n*-butyl ammonium salt**V-10•PF_6** are not as acidic as in the dibenzyl ammonium salt **V-9•PF_6**. Those hydrogens have been shown to contribute to the stabilizing of the complex **DB24C8**:**V-9•PF_6** in the X-ray crystal structure by hydrogen bonding to the ether oxygens of **DB24C8**.[51]

Table V-11. Results from the graphical methods used to determine the 1:1 association constants for **DB24C8:V-10•PF_6** using the H_a proton of **DB24C8** in acetone-d_6 (Temp = 23.0 ^oC).

Graphical Method	**K (M^{-1})** (R^2)	**ΔG (kJ/mole)**
Benesi-Hildebrand	166 ± 1 (0.996)	-12.6
Rose-Drago	186 ± 15	-12.9
Creswell-Allred	143 ± 42 (1.000)	-12.2
Average	165	

V.2.3.3 Dibenzo-24-crown-8 (V-3) with N,N'-Dibenzyl-*p*- (V-13•2(PF_6)) and N,N'-Dibenzyl-*m*-xylylene diammonium (V-14•2(PF_6)) Ions

The complexation between **DB24C8** and the *p*-substituted diammonium salt **V-13•2(PF_6)** has been reported and was evident by ^1H NMR, FAB-MS and X-ray crystallography.[54] The X-ray crystal structure revealed a [2.1]pseudorotaxane having two crown ethers per bisammonium salt. However, the association constants of the complex had not been investigated in solution. Also, the peaks for the benzylic protons were not properly assigned. Whereas *para*-substituted dibenzylammonium ions, such as the *p*-substituted diammonium salt **V-13•2(PF_6)**, and their azomethine precursors,

because of their linearity, can lead to insoluble polymers, the *meta*-substituted analogs, such as **V-14•2(PF$_6$)**, are expected to be soluble, making possible simplified synthesis and characterization of polyrotaxanes. Determination of the stoichiometries and association constants for the monomeric complexes will allow us to determine if the complexation is structure dependent. Thus, the complexations between **DB24C8** and both the *p*-substituted diammonium salt **V-13•2(PF$_6$)** and the *m*-substituted diammonium salt **V-14•2(PF$_6$)** were investigated to determine the extent of complexation under identical conditions. The comparison of the association constants then can give insight into how a polymeric systems might be designed.

When **DB24C8** was mixed with either the *p*-substituted diammonium salt **V-13•2(PF$_6$)** or the *m*-substituted diammonium salt **V-14•2(PF$_6$)** the complexation exhibited slow-exchange on the ^{1}H NMR timescale. However, the peak assigments could not be made based on one ^{1}H NMR spectrum alone. This was mainly due to the fact that the stoichiometry of both complexes was 2:1 (crown:salt). Also, since the complexation was under slow-exchange two sets of peaks were observed for all of the protons of both **DB24C8** and the salt of interest. Focusing only on the benzylic methylene protons of the salt there are possibly eight different resonances that can be observed for protons **H$_a$** through **H$_h$** (assuming they are all inequivalent) in the presence of **DB24C8** (see **Figure V-35** for proton labels). These signals can be integrated and the association constants can be calculated according to equations **25** and **26** using the initial concentrations of **DB24C8** and the salt of interest.

$$K_1 = \frac{[RS]}{[R][S]} \qquad (\mathbf{25})$$

$$K_2 = \frac{[R_2S]}{[R][RS]} \qquad (\mathbf{26})$$

where ***R*** = **DB24C8** and ***S*** = **V-13•2(PF$_6$)** or **V-14•2(PF$_6$)**.

However, the peaks were not well resolved in the ^{1}H NMR spectra and those peaks that were resolved were difficult to assign. Several NMR experiments were needed

to elucidate the peak assignments. The partially deuterated analogs of the *p*-substituted diammonium salt **V-13•2(PF$_6$)** and the *m*-substituted diammonium salt **V-14•2(PF$_6$)**, **V-15•2(PF$_6$)** and **V-16•2(PF$_6$)**, respectively, were synthesized also to aid in making the peak assignments.

Figures V-36, **V-37**, **V-38**, and **V-39** show several stacked ^{1}H NMRs comparing the benzylic methylene regions. The peak assignments were made based on the following arguments. In **Figure V-36d** the peaks for **H$_a$** and **H$_b$** are at 4.23 and 4.24 ppm, respectively. In spectrum **c** of **Figure V-36** several new peaks are observed downfield from **H$_a$** and **H$_b$**. By intergration the tentative peak assignments are made as shown in **Figure V-36c**. The peaks for the 2:1 complex are determined by comparing the spectrum in **Figure V-36b** with that of **Figure V-36c**. In **Figure V-36b** a 10-fold excess of **DB24C8** was used to force the equilibrium to form exclusively the 2:1 complex. Direct assignment of which peaks are from the 1:1 complex and which are for the 2:1 complex were made from comparing **Figures V-36b** and **c**. Unfortunately, using the fully protonated *p*-substituted diammonium salt **V-13•2PF$_6$** the exact proton assignments could not be made. However, using the partially deuterated *p*-substituted diammonium salt **V-15•2PF$_6$** the exact assignments were made. **Figure V-37a** (an equimolar solution of **DB24C8** and **V-15•2PF$_6$**) shows two peaks with integral values that when added together totaled half that of the central peak's integral value. These peaks can only be from protons **H$_h$** for the upfield peak and **H$_d$** for the downfield peak. This is inferred from **Figure V-36b**. **Figure V-36b** and **V-37b** are the same spectrum. Therefore, by process of elimination the central peak is assigned as **H$_c$** and **H$_g$**.

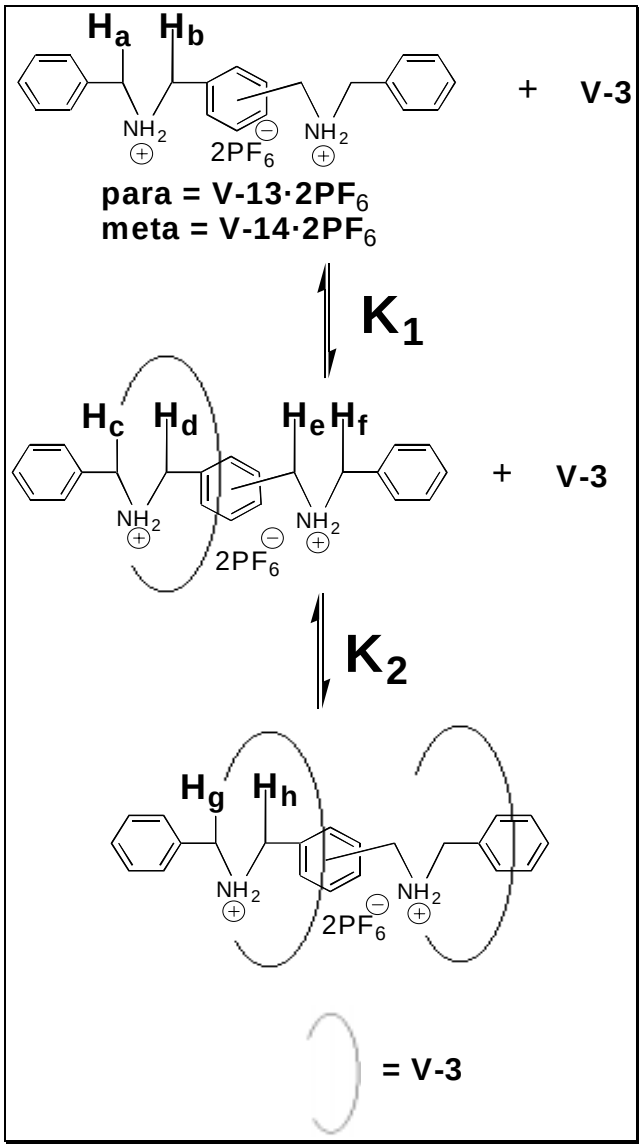

Figure V-35. Equilibrium equations for the complexation of secondary diammonium salts the *p*-substituted diammonium salt **V-13•2(PF$_6$)** and the *m*-substituted diammonium salt **V-14•2(PF$_6$)** with **DB24C8**.

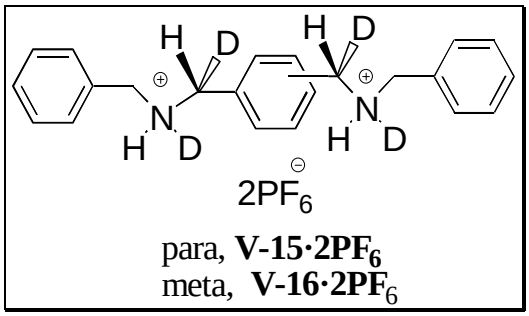

para, **V-15·2PF$_6$**
meta, **V-16·2PF$_6$**

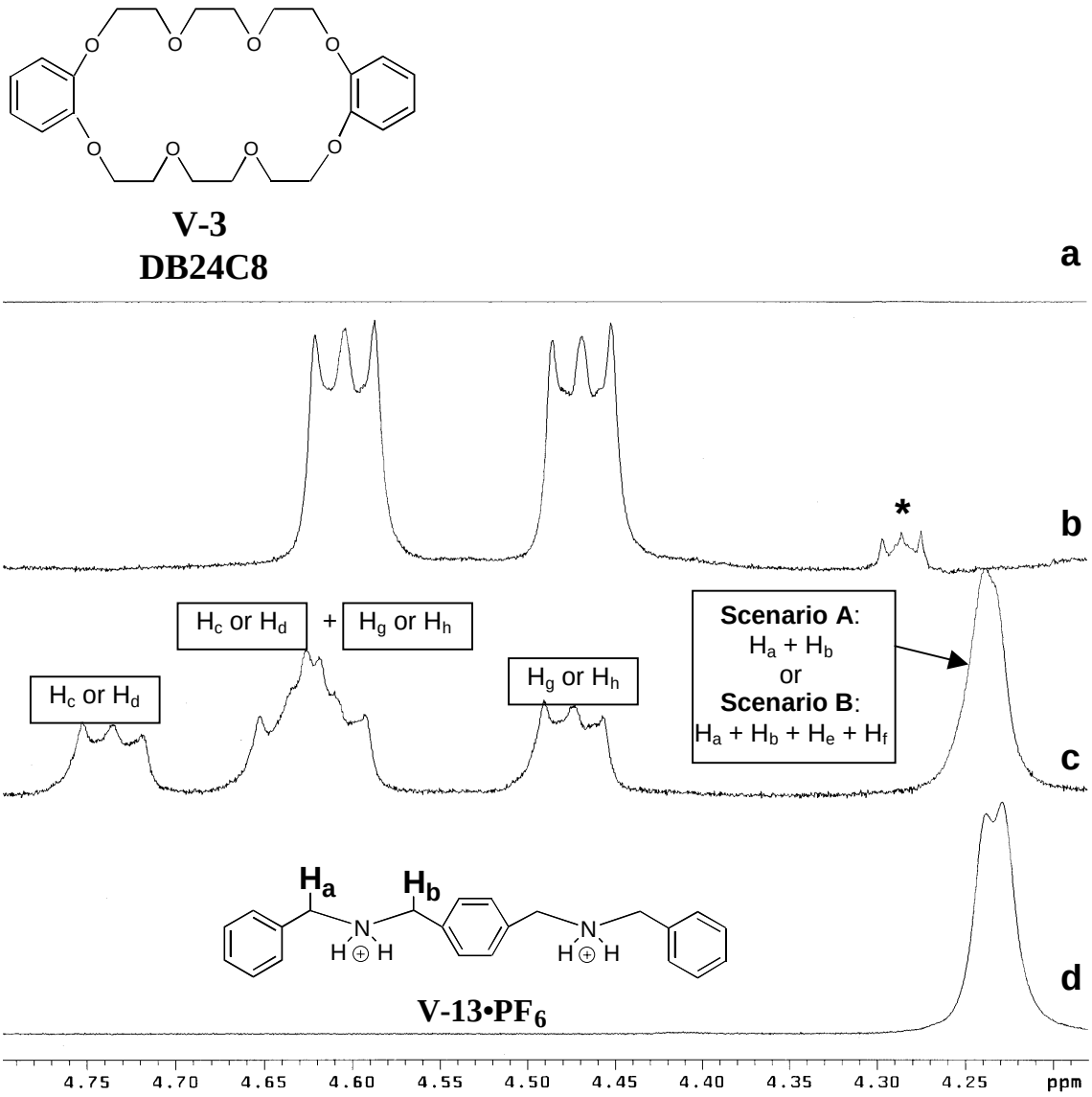

Figure V-36. Stacked ^{1}H NMR (400 MHz, $CDCl_3$:CD_3CN, 1:1, v:v) spectra of a) **DB24C8** (0.010 M), b) **DB24C8** (0.100 M) + **V-13•2PF$_6$** (0.010 M) c) **DB24C8** (0.010 M) + **V-13•2PF$_6$** (0.010 M), and d) **V-13•2PF$_6$** (0.010 M). The peak labeled with a ***** in b is a ^{13}C satellite from the upfield signal from **V-13**.

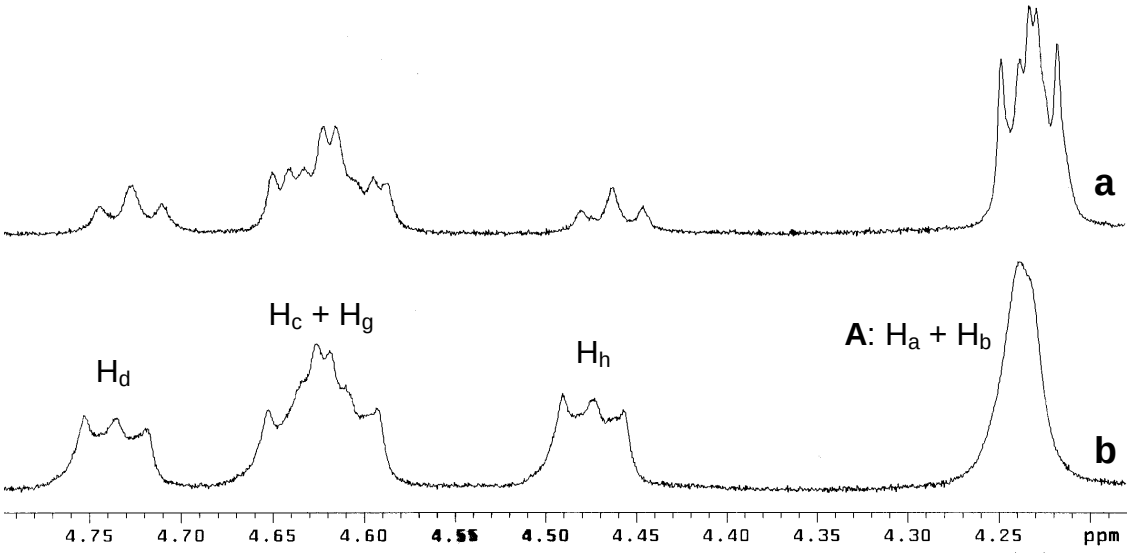

Figure V-37. Stacked ^{1}H NMR (400 MHz, $CDCl_3$:CD_3CN, 1:1, v:v) spectra of a) **DB24C8** (0.010 M) + **V-15•2PF$_6$** (0.010 M) and b) **V-23** (0.010 M) + **V-13•2PF$_6$** (0.010 M).

The question of whether the peak at 4.24 ppm in **Figure V-36c** can be assigned to protons $\mathbf{H_a}$ + $\mathbf{H_b}$ (**Scenario A**) or $\mathbf{H_a}$ + $\mathbf{H_b}$ + $\mathbf{H_e}$ + $\mathbf{H_f}$ (**Scenario B**) still remained. In other words, did the peak integral value represent 8 or 12 protons. The two scenarios were labeled as **Scenario A** and **Scenario B** in **Figure V-36c**. To determine the association constants for the complexes this question had to be answered. It was answered by comparing the intergral values of $\mathbf{H_d}$ with that of the intergral values of the peak in question. For the partially deuterated *p*-substituted diammonium salt **V-15•2PF$_6$** the ratio of $\mathbf{H_d}$ to $\mathbf{H_a}$ + $\mathbf{H_b}$ should be 1/8 (0.125) and for $\mathbf{H_d}$ to $\mathbf{H_a}$ + $\mathbf{H_b}$ + $\mathbf{H_e}$ + $\mathbf{H_f}$ should be 1/11 (0.0909). Using the integral values from **Figure V-37a** the ratio was 1.38 $\pm$ 0.05/6.97 $\pm$ 0.05 (0.198 $\pm$ 0.006). Again this value was close to **Scenario A**. For the undeuterated *p*-substituted diammonium salt **V-13•2PF$_6$** the ratio of $\mathbf{H_d}$ to $\mathbf{H_a}$ + $\mathbf{H_b}$ should be 4/8 (0.500) and for $\mathbf{H_d}$ to $\mathbf{H_a}$ + $\mathbf{H_b}$ + $\mathbf{H_e}$ + $\mathbf{H_f}$ should be 4/12 (0.333). Using the integral values from **Figure V-37b** the ratio was 2.75 $\pm$ 0.05/5.77 $\pm$ 0.05 (0.477 $\pm$ 0.004). Again, this value was close to **Scenario A**. Therefore, it was believed that the peak at 4.24 ppm should be assigned as $\mathbf{H_a}$ + $\mathbf{H_b}$ alone as shown in **Figure V-37b**. The whereabouts of the peaks for

$\mathbf{H_e}$ and $\mathbf{H_f}$ are unknown, but could possibly be in the upfield region hidden by the peaks of the crown ether.

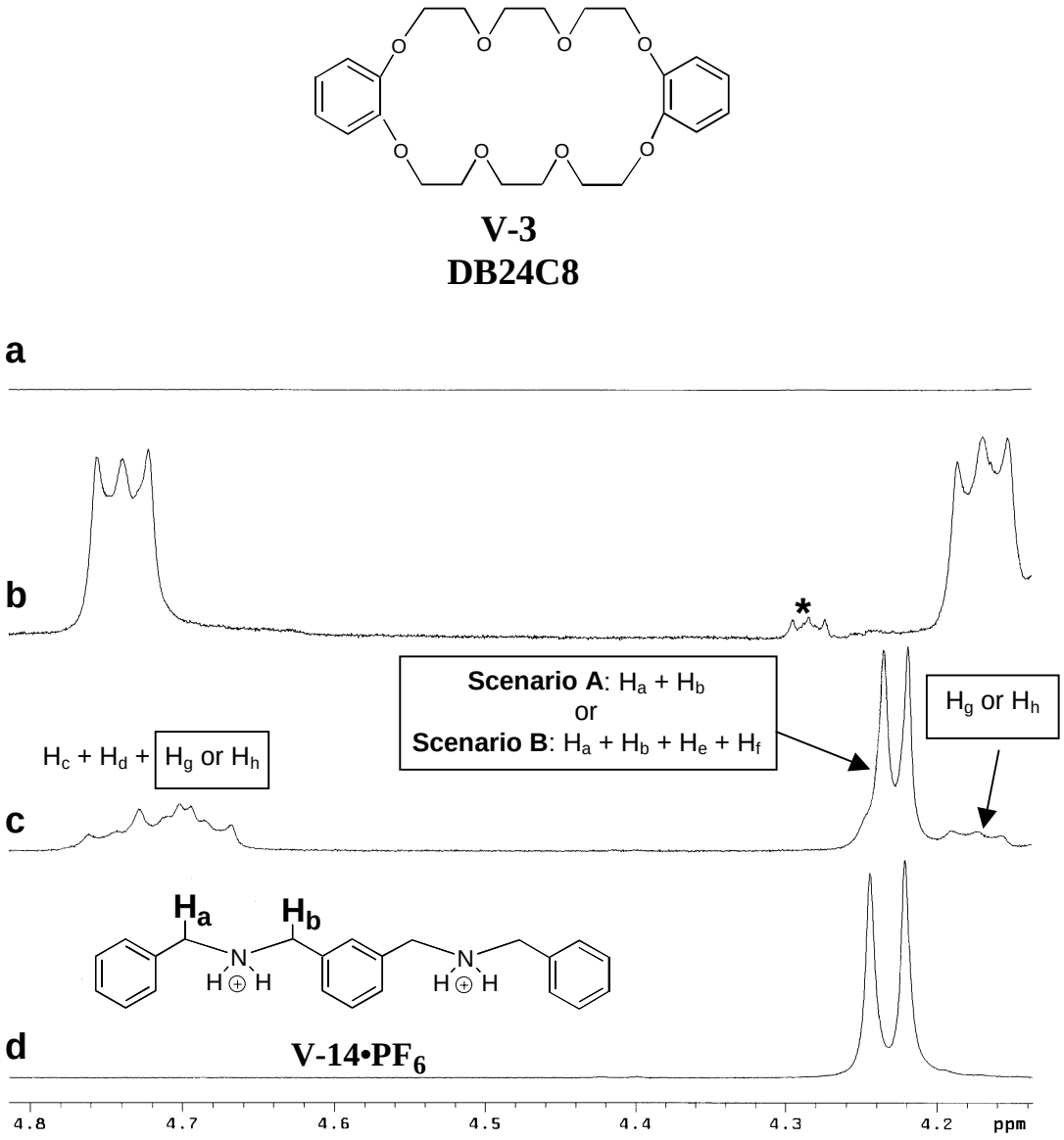

Figure V-38. Stacked ^{1}H NMR (400 MHz, $CDCl_3$:CD_3CN, 1:1, v:v) spectra of a) **DB24C8** (0.010 M), b) **DB24C8** (0.100 M) + **V-14•2PF$_6$** (0.010 M) c) **DB24C8** (0.010 M) + **V-14•2PF$_6$** (0.010 M), and d) **V-14•2PF$_6$** (0.010 M). The peak labeled with a ***** in b is a ^{13}C satellite from the upfield signal from **V-13**.

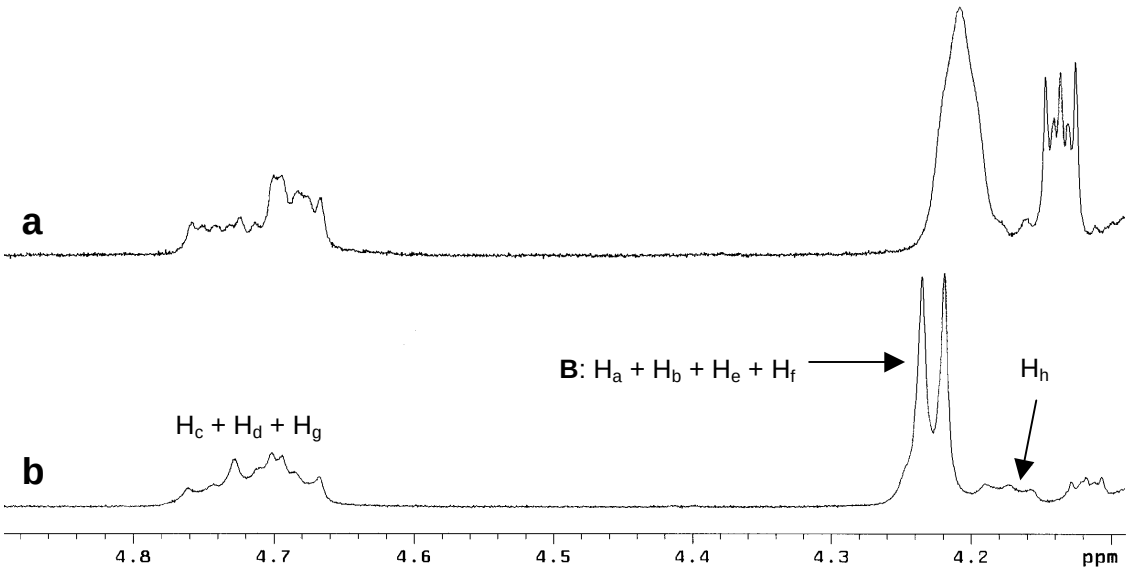

Figure V-39. Stacked ^{1}H NMR (400 MHz, $CDCl_3$:CD_3CN, 1:1, v:v) spectra of a) **DB24C8**(0.010 M) + **V-16•2PF$_6$** (0.010 M) and b) **DB24C8** (0.010 M) + **V-14•2PF$_6$** (0.010 M).

Very similar arguments were made in assigning the peaks in **Figures V-38** and **V-38**, although the spectra appeared to be more complicated. Notice that **Scenario B** is believed to be the assignment for the peaks at 4.22 and 4.24 ppm. This was because the ratio of (**H$_c$** + **H$_d$** + **H$_g$**) to **H$_a$** + **H$_b$** should be 7/8 (0.875) and for (**H$_c$** + **H$_d$** + **H$_g$**) to **H$_a$** + **H$_b$** + **H$_e$** + **H$_f$** should be 7/11 (0.636) for the partially deuterated *m*-substituted diammonium salt **V-16•2PF$_6$**. Experimentally the value is 0.563 $\pm$ 0.006 from **Figure V-39a**. For the undeuterated *m*-substituted diammonioum salt **V-14•2PF$_6$** the calculated value for **Scenario A** is 1.00 and for **Scenario B** is 0.667 and the experimental values is 0.703 $\pm$ 0.006 from **Figure V-39b**. For this system both results indicate that scenario **B** is the most likely case.

Having determined the peak assignments, the calculations of the association constants for the complexes formed between the *p*-substituted diammonium salt **V-13•2PF$_6$** and **DB24C8** and the *m*-substituted diammonium salt **V-14•2PF$_6$** and **DB24C8** were made. The thermodynamic equations for the equilibrium reactions are as follows:
Since [***R***] = [***S***], **Equation 25** can be written as

$$K_{a1} = \frac{[RS]}{[S]^2} \quad (\mathbf{27})$$

The following equations can then be written

$$[S]_o = [S] + [RS] + [R_2S] \quad (\mathbf{28})$$

$$[R]_o = [R] + [RS] + [R_2S] \quad (\mathbf{29})$$

where "*o*" denotes the initial concentrations of ***R*** and ***S*** as before. If $[\boldsymbol{R}]_o = [\boldsymbol{S}]_o$ then **Equation 28** equals **Equation 29**. Therefore, to calculate K_{a1} and K_{a2} the values of [***R***], [***RS***], and [$\boldsymbol{R}_2\boldsymbol{S}$] need to be determined. All of the concentrations can be substituted for integral values per proton for the desired species. These values will be denoted by using the brackets, e.g. {***RS***} for the intergral value per proton for the 1:1 complex ***RS***.

For the *p*-substituted diammonium salt **V-13•2PF$_6$** and **DB24C8** the integral values were obtained from **Figure V-37b**. The values for {***S***}, {***RS***}, and {$\boldsymbol{R}_2\boldsymbol{S}$} were obtained from peaks labeled $\mathbf{H_a}$ + $\mathbf{H_b}$, $\mathbf{H_d}$, and $\mathbf{H_h}$, respectively, and were 0.72, 1.38, and 0.86, respectively (error = $\pm$ 0.05). From **Equation 28**

$$\{S\}_o = \{S\} + \{RS\} + \{R_2S\} \quad (\mathbf{30})$$

Therefore, $\{\boldsymbol{S}\}_o$ = 2.96 $\pm$ 0.05. Using the following equations

$$[S] = \frac{\{S\}}{\{S\}_o} \times [S]_o = \frac{0.72}{2.96} \times 0.010\ M = 0.0024 \pm 0.0002\ M$$

$$[RS] = \frac{\{RS\}}{\{S\}_o} \times [S]_o = \frac{1.38}{2.96} \times 0.010\ M = 0.0047 \pm 0.0002\ M$$

$$[R_2S] = \frac{\{R_2S\}}{\{S\}_o} \times [S]_o = \frac{0.86}{2.96} \times 0.010\ M = 0.0029 \pm 0.0002\ M$$

Since [***S***] = [***R***], then [***R***] = 0.0024 M. Substitution of the values into **Equations 26** and **27**, gave K_{a1} and K_{a2} as 8.2 x 10^2 $\pm$ 1.1 x 10^2 M^{-1} and 2.6 x 10^2 $\pm$ 0.2 x 10^2 M^{-1}, respectively, and the overall association constant ($K_{a1}K_{a2}$) was 2.1 x 10^5 $\pm$ 0.5 x 10^5 M^{-2}.

For the *m*-substituted diammonium salt **V-14•2PF$_6$** and **DB24C8** the values were obtained from **Figure V-39b**. The values for {***S***} and {***R***$_2$***S***} were obtained from the peaks labeled **H$_a$** + **H$_b$** + **H$_e$** + **H$_f$** and **H$_h$**, respectively and are 0.97 $\pm$ 0.05 and 0.57 $\pm$ 0.05, respectively. Determining the value for {***RS***} was a little more difficult since both **H$_c$** and **H$_d$** were grouped together. Since {**H$_h$**} = {**H$_g$**}, {**H$_g$**} + {**H$_c$**} + {**H$_d$**} = 1.02 $\pm$ 0.05 and {**H$_c$**} = {**H$_d$**} we can write

$$1.02 = 0.57 + 2\{H_c\}$$
$$\{H_c\} = 0.22 \pm 0.05$$

which was the value for {***RS***}. From **Equation 30** $\{S\}_o$ = 1.76 $\pm$ 0.05. Using the following equations

$$[S] = \frac{\{S\}}{\{S\}_o} \times [S]_o = \frac{0.97}{1.76} \times 0.01\,M = 0.0055 \pm 0.0001\,M$$
$$[RS] = \frac{\{RS\}}{\{S\}_o} \times [S]_o = \frac{0.22}{1.76} \times 0.01\,M = 0.0013 \pm 0.0003\,M$$
$$[R_2S] = \frac{\{R_2S\}}{\{S\}_o} \times [S]_o = \frac{0.57}{1.76} \times 0.01\,M = 0.0033 \pm 0.0002\,M$$

Since [***S***] = [***R***], then [***R***] = 0.0055 $\pm$ 0.0001 M. Substituting the values into **Equations 26** and **27**, gave K_{a1} and K_{a2} as 43 $\pm$ 9 M^{-1} and 4.6 x 10^2 $\pm$ 0.9 x 10^2 M^{-1}, respectively, and the overall association constant ($K_{a1}K_{a2}$) was 2.0 x 10^4 $\pm$ 1.8 x 10^4 M^{-2}.

It is not completely clear why K_{a2} was larger than K_{a1} for (**DB24C8)$_2$:V-14•2PF$_6$**. There is obviously a cooperative effect for the binding of the second macrocycle with the *m*-substituted diammonium salt **V-14•2PF$_6$**. The difference may be due to steric effects. The two ammonium centers are possibly closer together in the *m*-substituted diammonium salt **V-14•2PF$_6$** than in the *p*-substituted diammonium salt **V-13•2PF$_6$**.

Therefore, it may be more difficult for the first macrocycle to thread the *m*-substituted diammonium salt **V-14•2PF$_6$** than the *p*-substituted diammonium salt **V-13•2PF$_6$.** Once the second macrocycle complexes the neighboring ammonium-crown steric interaction is not as prominent and the second equilibrium constant is similar to that of K_{a2} of the crown with salt the *p*-substituted diammonium salt **V-13•2PF$_6$**. Whatever the reason it appears that the *p*-substituted diammonium salt **V-13•2PF$_6$** is the better complexing salt by an order of magnitude for the overall association constant.

V.2.4 Complexation of 30-Crown-10 (V-17) with Secondary Ammonium Ions

The complexation of the aliphatic crown ether 30-crown-10, **V-17**, **30C10**, with diphenethyl and dibenzyl secondary ammonium ions **V-8•PF$_6$** and **V-9•PF$_6$** was investigated to determine if the binding was stronger than for the bisphenylene crown ethers **DB24C8** and **BMP32C10**. By ^{1}H NMR both salts, when present in equimolar amounts to **30C10** (0.010 M), caused a change in the chemical shift of the protons of both components in acetone-d_6. The complexation was fast on the NMR time scale; no "new" peaks were observed in either solution. ESI-MS was conducted on both mixtures of the diphenethyl ammonium salt **V-8•PF$_6$** with **30C10** (**Figure V-40**) and the dibenzyl ammonium salt **V-9•PF$_6$** and **30C10** (**Figure V-41**). Direct evidence for the formation of the 1:1 complexes was obtained by the observation of the peaks for [**30C10 + V-8**]$^+$ (666.4 m/z) and [**30C10 + V-9**]$^+$ (638.5 m/z).

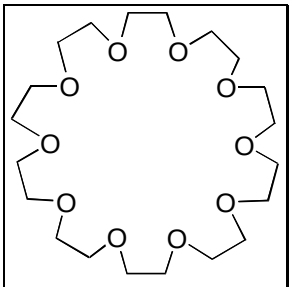

V-17

30C10

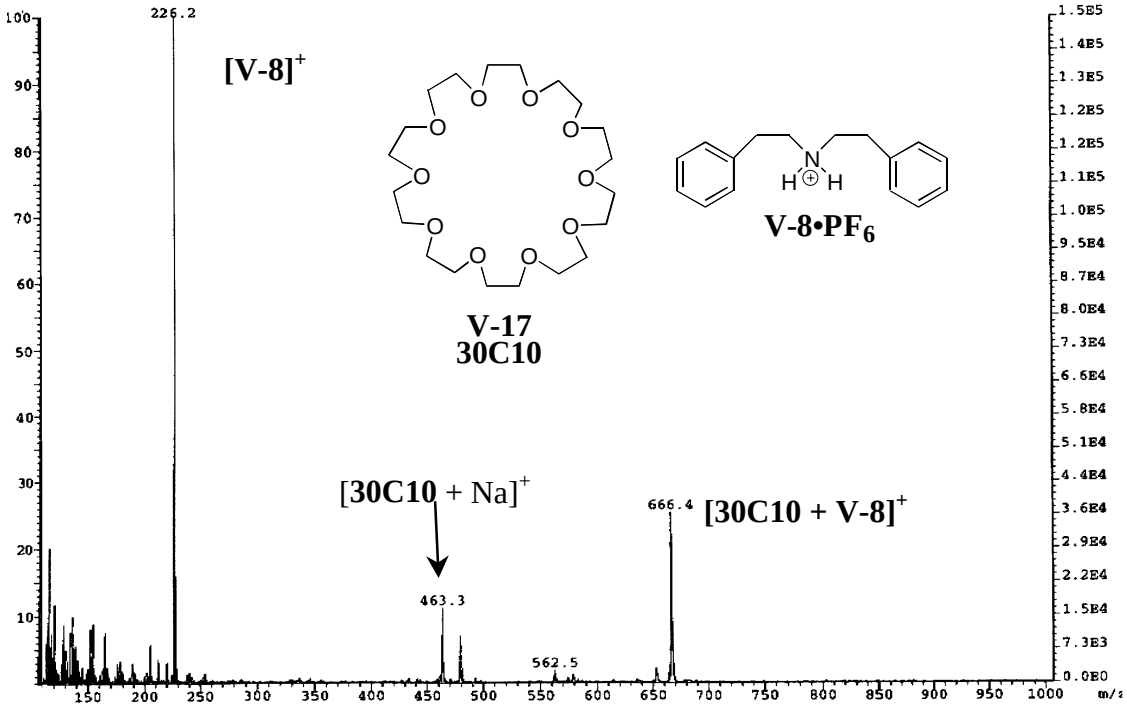

Figure V-40. ESI-MS of **30C10** + **V-8•PF$_6$**.

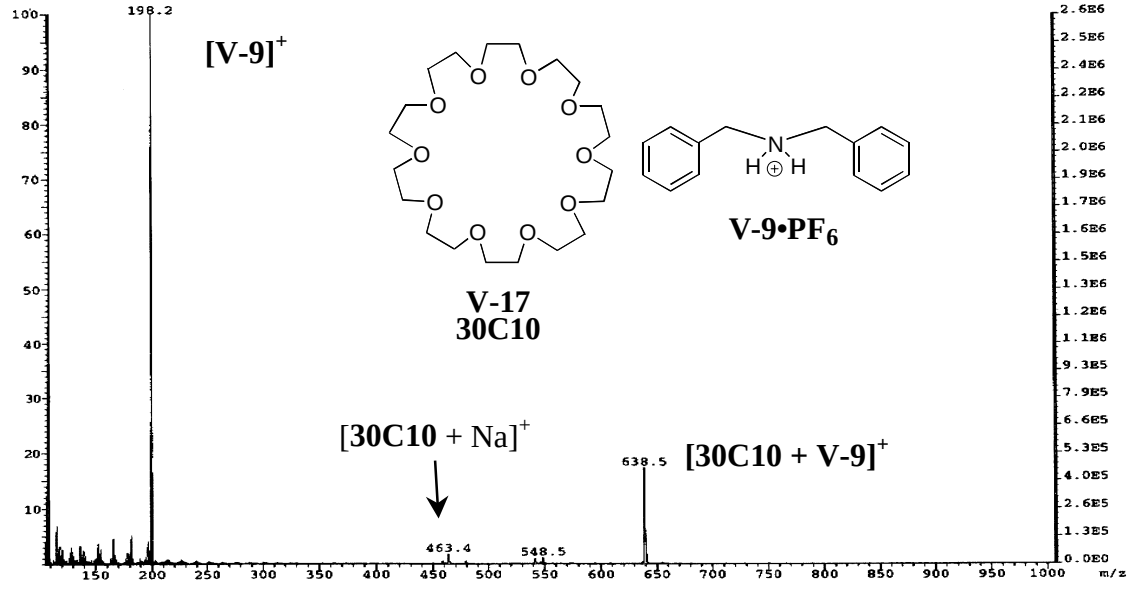

Figure V-41. ESI-MS of **30C10** + **V-9•PF$_6$**.

The determination of the stoichiometry for the complex formed between **30C10** and the dibenzyl ammonium salt **V-9•PF$_6$** was conducted using the mole ratio method in acetone-d$_6$ (**Figure V-42**). The break point occurs at a stoichiometric ratio higher than the expected 1:1 ratio (actually 1.3:1). This may be due to the high concentrations used in the ^{1}H NMR experiments. The three graphical methods, the Benesi-Hildebrand, Rose-Drago, and Creswell-Allred methods, were used to calculate the K_a value using the data from the mole ratio method (**Table V-12**). The Rose-Drago method returned an unreasonable answer, however. This suspect result may be due to the fact that the concentrations were not with in the Weber "probability of binding," **p**. Using the Δ_o value obtained from the Creswell-Allred graphical method the **p** values were calculated (**Table V-13**). Only the first two data entries are within the suggested Weber "probability of binding." Therefore, the data was considered to be "bad." However, based on previously discussed systems, the K_a value should increase for a suitable data set. Comparing the calculated K_a values in **Table V-12** with those in **Table V-10** for **DB24C8**:**V-9•PF$_6$** indicates that the binding is of the same magnitude.

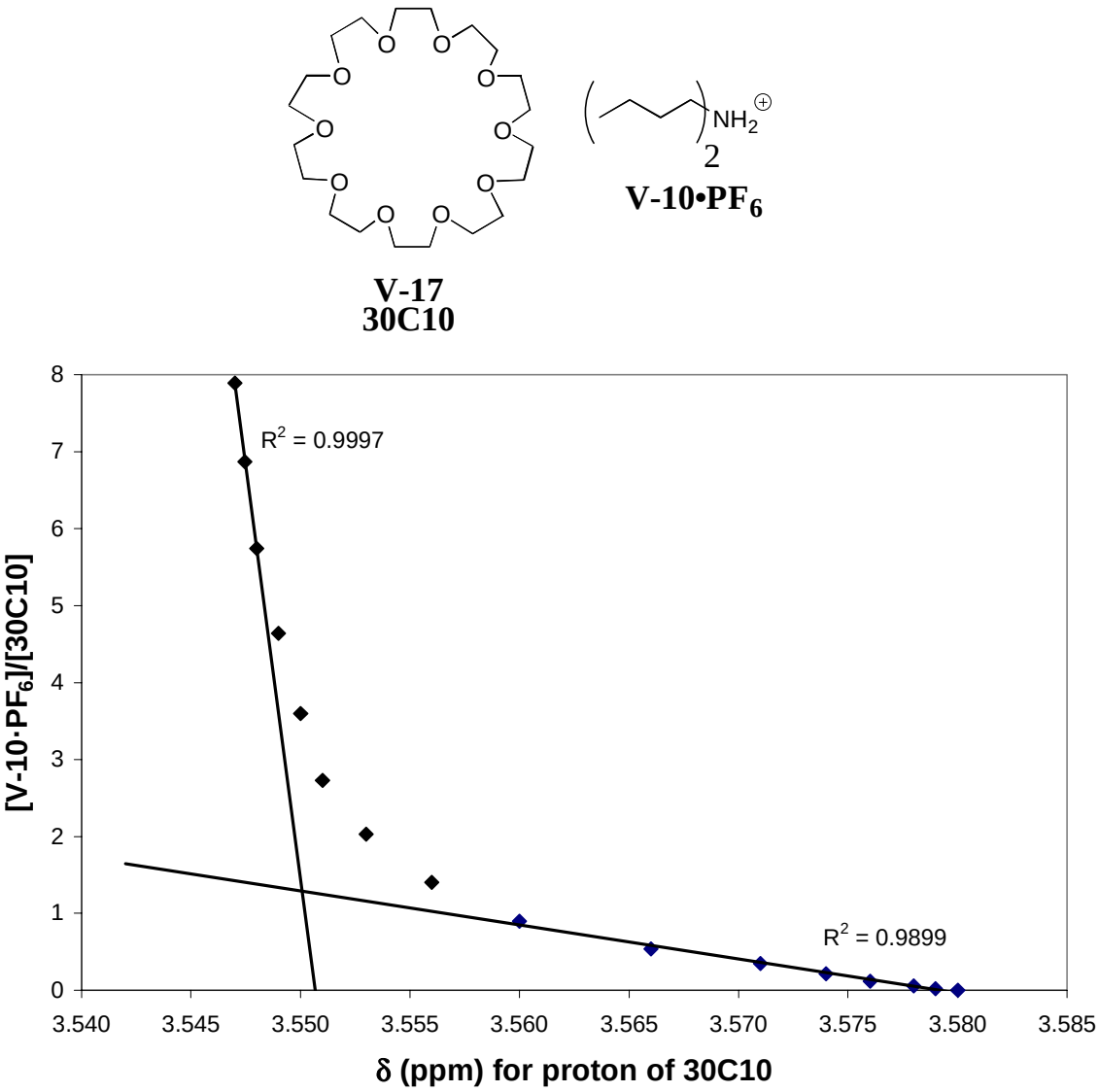

Figure V-42. Mole ratio plot for complex between **30C10** and **V-10•PF$_6$** in acetone-d$_6$.

Table V-12. Results from the graphical methods used to determine the 1:1 association constants for **30C10:V-9•PF_6** using the proton signal of **30C10** in acetone-d_6 (Temp = 23.0 ^oC). [a]Average for Benesi-Hildebrand and Creswell-Allred methods only.

Graphical Method	K_a **(M^{-1})** (R^2)	ΔG_{298K} **(kJ/mole)**
Benesi-Hildebrand	347 ± 15 (0.995)	-14.4
Rose-Drago	2320 ± 6365	-19.1
Creswell-Allred	363 ± 90 (0.982)	-14.5
Average[a]	355	-14.5

Table V-13. Data for determination of K_a from Creswell-Allred graphical method for complex of **30C10** (***R***) and **V-9•PF_6** (***S***) in acetone-d_6. (**p** = Δ/Δ_o), $[\boldsymbol{R}]_o$ 10.0 mM, $\delta_{\boldsymbol{R}}$ = 6.473 ppm, Temp(^oC) = 23.0.

$[S]_o$ **(mM)**	δ_{obs} **(ppm)**	Δ **(ppm)**	Δ_o **(ppm)**	**p**	$[RS]$ **(mM)**
14.05	3.556	0.024	0.0338	0.71	7.08
20.27	3.553	0.027		0.80	7.97
27.30	3.551	0.029		0.86	8.56
35.95	3.550	0.030		0.89	8.85
46.39	3.549	0.031		0.91	9.15
57.40	3.548	0.032		0.94	9.44
68.70	3.547	0.033		0.96	9.60

V.2.5 Complexation of 32-Membered Cryptand (V-18) with Dibenzyl ammonium hexafluorophosphate (V-9•PF_6)

The 32-membered bicyclic cryptand **V-18** (**32-Cryptand**) was synthesized to increase the binding of secondary ammonium ions over the monocyclic 32-membered crown ether **BMP32C10**. Due to the reduced conformational freedom of **32-Cryptand**, relative to **BMP32C10**, the entropy term for complexation should be lower for the binding of secondary ammonium ions with **32-Cryptand**.

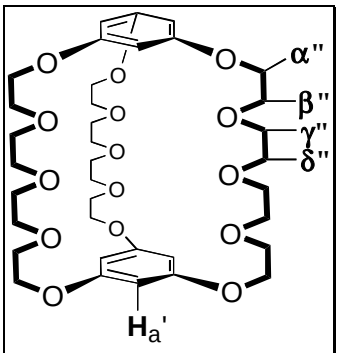

V-18

Again, ^{1}H NMR was used to determine if complexation occurred in solution. A change in the chemical shifts of the protons of both **32-Cryptand** and the dibenzyl ammonium salt **V-9•PF$_6$** was observed in an equimolar (0.010 M) solution in acetonitrile-d_3 (**Figure V-43**). The mole ratio method was used to elucidate the stoichiometry of the complex(s). The concentration of the dibenzyl ammonium salt **V-9•PF$_6$** was held constant while the 32-cryptand, **32-Cryptand**, was added in increasing amounts. However, the break point occurred at an unreasonable stoichiometry of 1:4 (**32-Cryptand**:**V-9•PF$_6$**) (**Figure V-44**). This unexpected result may indicate that more than one complex exists in solution. When the data were plotted using the Scatchard equation the fit was not good (**Figure V-45**). Therefore, it was assumed that more than the 1:1 complex existed in solution.

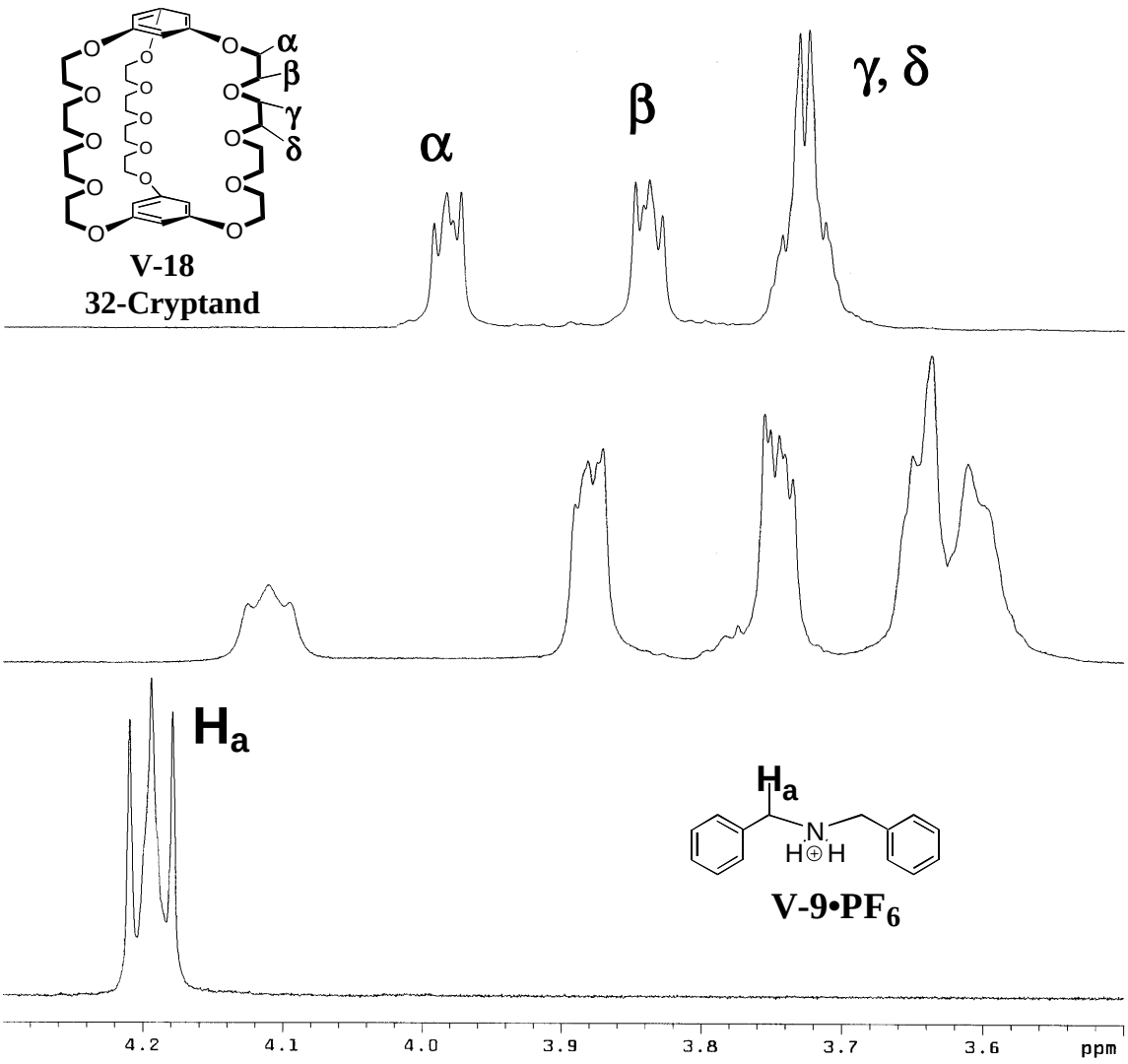

Figure V-43. Stacked ^{1}H NMR (400 MHz, $CDCl_3$:CD_3CN, 3:1, v:v) spectra of a) **32-Cryptand** (0.010 M), b) 1:1 solution of **32-Cryptand** and **V-9•PF$_6$** (0.010 M), and c) **V-9•PF$_6$** (0.010 M).

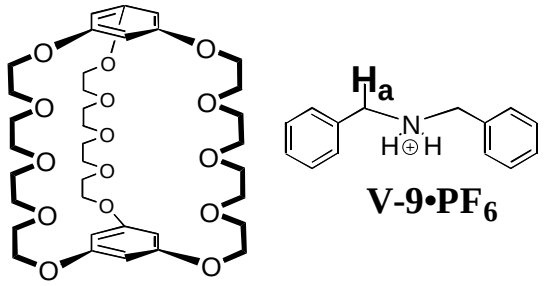

V-18
32-Cryptand

V-9•PF_6

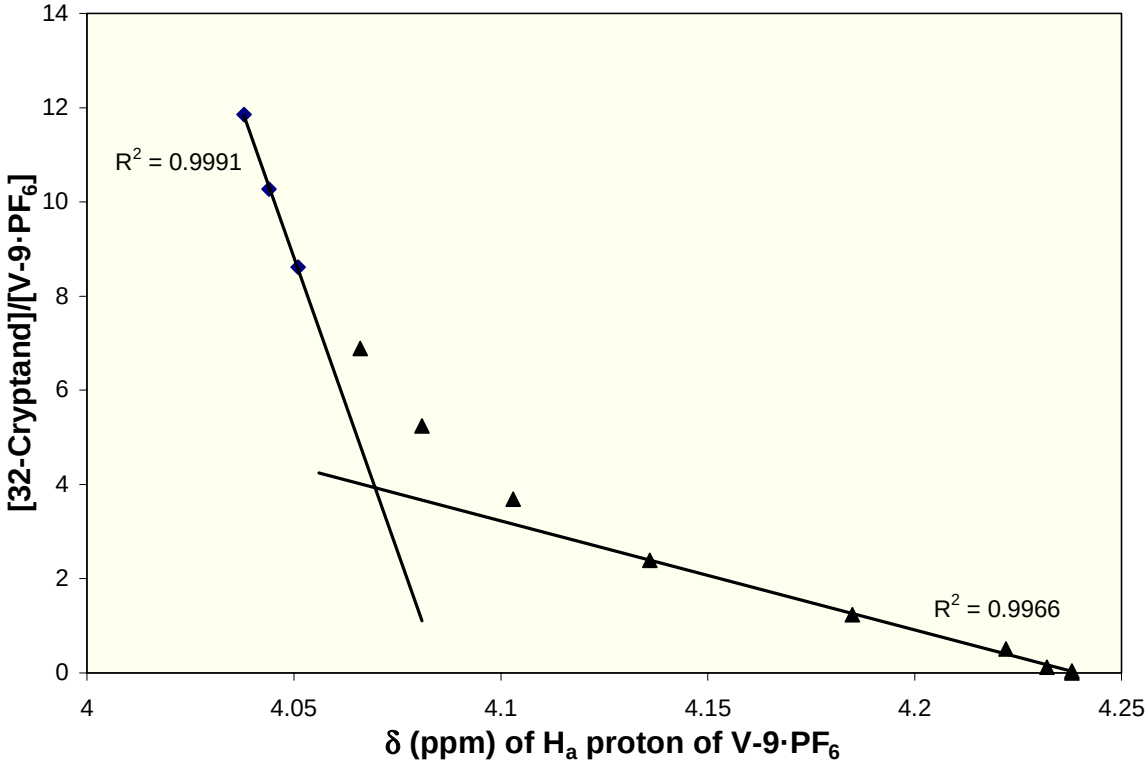

Figure V-44. Mole ratio plot for complex between **32-Cryptand** and **V-9•PF_6** in acetonitrile-d_3.

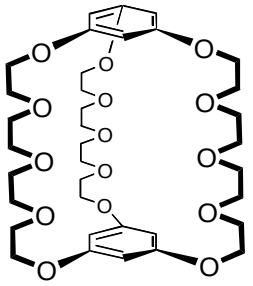

V-18
32-Cryptand

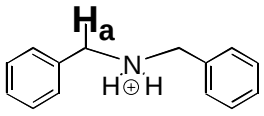

V-9•PF$_6$

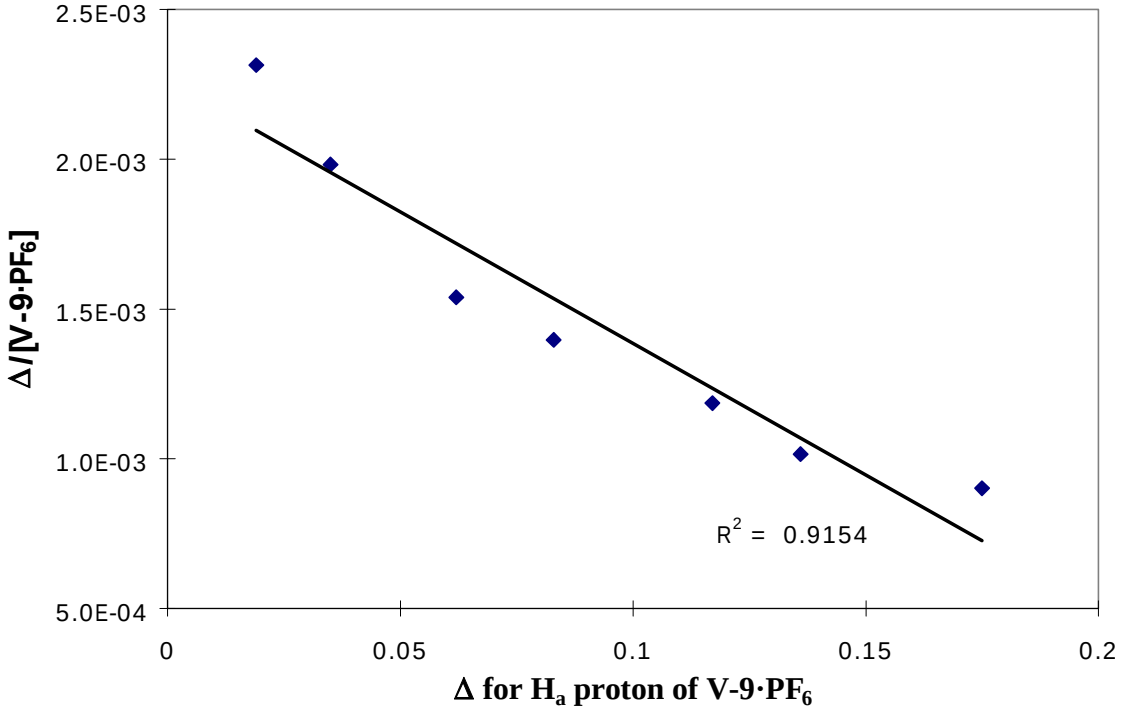

Figure V-45. Scatchard plot for **32-Cryptand** + **V-9•PF$_6$**.

Unlike what is observed for the complex between **BMP32C10** and the dibenzyl ammonium salt **V-9•PF$_6$** (**Figure V-46**), the change in the chemical shift for the H$_a$ proton of the dibenzyl ammonium salt **V-9•PF$_6$** is discontinuous (**Figure V-47**), i.e., some of the signals start to go upfield but then change direction and start to go downfield. Notice that the ammonium salt was added to the crown ether or cryptand. This observation gave further evidence that more than one type of complex occurs in solution.

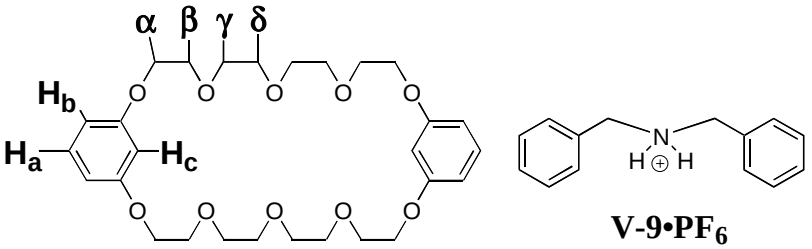

V-12
BMP32C10

V-9•PF$_6$

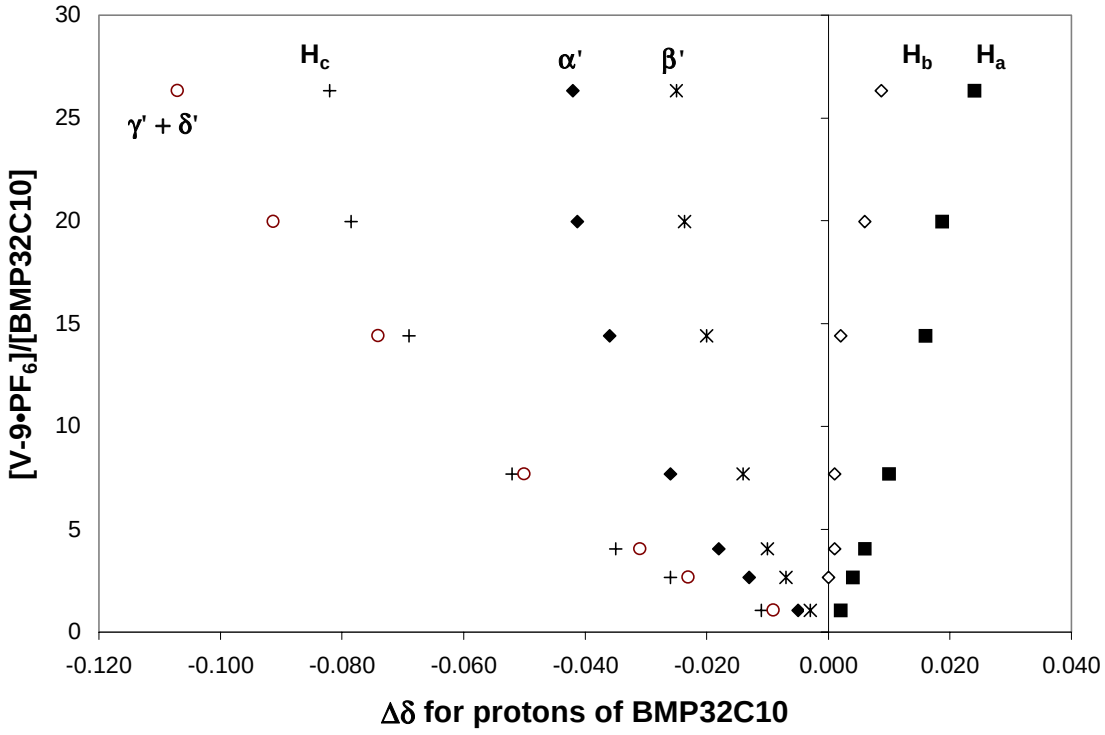

Figure V-46. Plot of [**BMP32C10**]:[**V-9•PF$_6$**] versus Δδ for protons of **BMP32C10**.

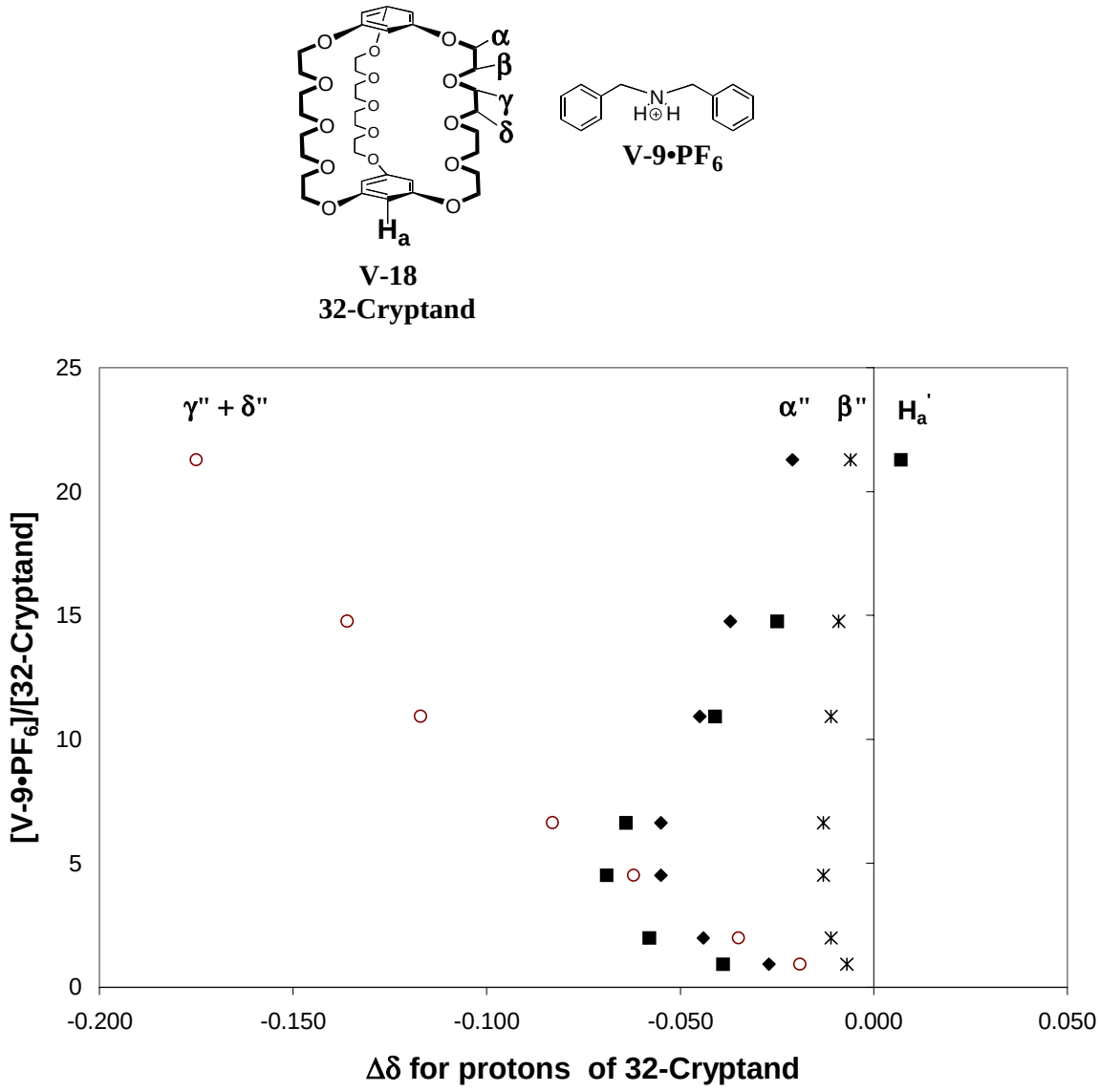

Figure V-47. Plot of **32-Cryptand:V-9•PF$_6$** versus Δδ for protons of **32-Cryptand**.

V.3 Conclusions

The complexation of several secondary ammonium ions with crown ethers and a cryptand was investigated. Special interest was placed on determining the stoichiometry of complexation as well as the association constant(s) in the solution phase using ^{1}H NMR spectroscopy. The stoichiometry for the complexes was established using the mole ratio (titration) method. Association constants were determined using several graphical methods (Benesi-Hildebrand, Creswell-Allred, and Rose-Drago). A summary of the stoichiometry and association constants for the complexes is given in **Table V-14**.

Two X-ray crystal structures revealed [2.1]pseudorotaxanes were formed with the two secondary ammonium salts, **V-8•PF$_6$** and **V-9•PF$_6$**, and the 32-membered bisphenylene crown ether **BMP32C10**. Another X-ray structure, however, revealed that the same crown ether can form an "exo," "cradled barbell," complex with the *m*-substituted diammonium salt, **V-14•PF$_6$**. All three solid state complexes were stabilized mainly due to hydrogen bonding with secondary stabilization occurring through π–π aryl interactions.

The information obtained from the complexation investigations discussed above revealed that the *meta*-substituted crown ethers are <u>not</u> suitable for making polypseudo- or polyrotaxanes having secondary ammonium ion units. The reasons are three-fold: 1) the smaller 26-membered crown ether, **BMP26C8**, does not complex with secondary ammonium ions, 2) the association constants are to low for the 32-membered crown ether, **BMP32C10**, and 3) the formation of a folded, "exo" complex instead of a pseudorotaxane in the solid state between **BMP32C10** and the the *m*-substituted diammonium ion, **V-14•PF$_6$** suggests that a polymeric system may not thread at all. Instead, it is suggested that the 24-membered crown ether, **DB24C8**, be used as the cyclic component in future polymeric systems. The synthesis of difunctional 24-membered dibenzo-crown ethers would result in a mixture of isomers; however, it is believed that the separation of the isomers would be possible.

The association constant for the complexation of **30C10** with the dibenzyl ammonium salt **V-9•PF$_6$** was of the same order as for **DB24C8** with the same salt.

Therefore, it is suggested that the **30C10** also be used as a cyclic component for the formation of polypseudo- and polyrotaxanes having secondary ammonium ion complexing moieties.

Table V-14. Summary of complexation in solution. T = 23.0 °C (25.0 °C for **BMP32C10** + **V-9**), nc = no complex, nm = not measured. Counterions = PF_6.

Receptor	***Substrate***	**Exchange Rate**	**Stoichiometry (*R*:*S*)**	K_a **(M^{-1})**
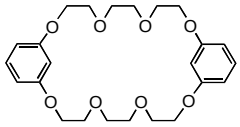 **V-7** **BMP26C8**	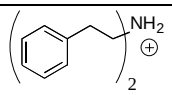 **V-8**	-	-	nc
	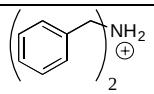 **V-9**	-	-	nc
	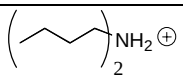 **V-10**	-	-	nc
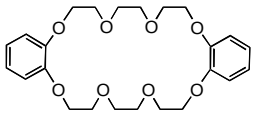 **V-3** **DB24C8**	**V-8**	SLOW	1:1	71[1]
			"	90[2]
			"	460[3]
	V-10	FAST	1:1	165[2]
	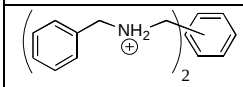 para, **V-13**	SLOW	2:1	K_{a1}[4] = 8.2 x 10^2 K_{a2} = 2.6 x 10^2
	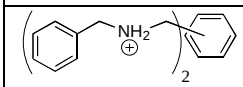 meta, **V-14**	SLOW	2:1	K_{a1}[4] = 43 K_{a2} = 4.6 x 10^2

[1] acetonitrile-d_3
[2] acetone-d_6
[3] chloroform-d
[4] chloroform-d:acetonitrile-d_6 (1:1, v:v)

Receptor	*Substrate*	Exchange Rate	Stoichiometry (*R*:*S*)	K_a (M^{-1})
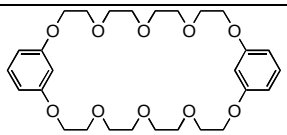 **V-12** **BMP32C10**	**V-8**	FAST	1:1	13.7[1]
	V-9	FAST	nm	nm
	V-14	FAST	1:1	257[2]
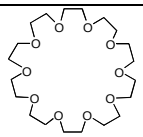 **V-17** **30C10**	**V-9**	FAST	1:1	355[2]
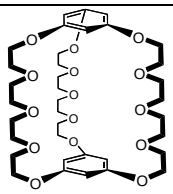 **V-18** **32-Cryptand**	**V-9**	FAST	?	?

V.4 Experimental

Chemical Reagents and Measurements

All deuterated solvents were used directly as received from Cambridge Isotopes. ^{1}H NMR spectra were obtained on a 400 MHz Varian spectrometer with tetramethylsilane as an internal standard. Mass spectrometry was provided by the Washington University Mass Spectrometry Resource, an NIH Research Resource (Grant No. P41RRR0954).

NMR Analyses

1. **BMP26C8 + V-9•PF_6**:

Three (3) NMR solutions were made in the appropriate deuterated solvent in a 1.0 mL volumetric flask: 1) **BMP26C8** (0.010 M, 4.5 mg), 2) **V-9•PF_6** (0.010 M, 3.4 mg), and 3) **BMP26C8** + **V-9•PF_6** (0.010 M: 0.010 M). Each solution was then analyzed directly by ^{1}H NMR (400 MHz, ambient T).

2. **BMP26C8 + V-10•PF_6**:

The same procedure was used as was for **BMP26C8 + V-9•PF_6** (solvent = acetonitrile-d_3). **BMP26C8** (0.010 M, 4.5 mg) and **V-10•PF_6** (0.010 M, 2.7 mg).

3. **BMP32C10 + V-9•PF_6**:

a) **Probe Exp**.:

The same procedure was used as was for **BMP26C8 + V-9•PF_6** (solvent = acetonitrile-d_3). **BMP32C10** (0.010 M, 5.4 mg) and **V-9•PF_6** (0.010 M, 3.4 mg).

b) **Mole Ratio Exp**.:

Two (2) separate stock solutions were made, STOCK A: 0.010 M solution of **V-9•PF_6**, and STOCK B: 0.2000 M solution of **BMP32C10** made using STOCK A. STOCK A: **V-9•PF_6** (6.9 mg, 0.020 mmol) was dissolved in acetonitrile-d_3 in a 2.0 mL volumetric flask. STOCK B: **BMP32C10** (107.3 mg, 0.2000 mmol) was dissolved in STOCK A solution in a 1.0 mL volumetric flask. In an NMR tube, STOCK A (0.422 g, 0.500 ml)

was added and analyzed by ^{1}H NMR. Small aliquots (column 3 of table) of STOCK B were then added to the initial solution via a Hamilton syringe (50 μl) (**Table V-15**). After each injection the solution was shaken to ensure complete mixing and the ^{1}H NMR of the solution was taken at the appropriate temperature. The volumes were assumed to be additive.

c) **Determination of Association Constant**:

BMP32C10 (51.8 mg, 0.0965 mmol) was dissolved in 10.0 mL of acetonitrile-d_3 in a volumetric flask ([**BMP32C10**] = 9.65 mM). A sample (~1.0 mL) was analyzed by ^{1}H NMR at 25.0, 33.0, 41.0, 49.0, and 57.0 ^{o}C. In seven (7) separate 1.0 mL volumetric flasks 3.5, 8.8, 13.4, 25.5, 47.7, 66.1, and 87.2 mg of **V-9•PF$_6$** were added. Each flask was filled with the **BMP32C10** solution above. The concentrations of **V-9•PF$_6$** are listed in the 3rd column of **Table V-5**. Each sample mixture was then analyzed by ^{1}H NMR at the aforementioned temperatures. A total of 40 ^{1}H NMR experiments were conducted.

Table V-15. Volumetric amounts titrated and resulting concentrations of **BMP32C10** for Mole the Ratio experiment for **BMP32C10 + V-9•PF$_6$**. [**V-9•PF$_6$**] = 10 mM.

Entry	Vol. (μl) of STOCK B added	Cumm. Vol. (μl) of STOCK B added	Total Vol. (μl)	[BMP32C10] (mM)
1	-	-	500	-
2	1	1	501	0.4
3	2	3	503	1
4	10	13	513	5.1
5	20	33	533	12
6	35	68	568	24
7	45	113	613	37
8	65	178	678	53
9	65	243	743	65
10	115	358	858	83.4
11	150	508	1008	101
12	200	708	1028	117
13	148	856	1356	126

4. **BMP32C10 + V-8•PF_6**:

The same procedure was used as was for **BMP26C8 + V-9•PF_6** (solvent = acetone-d_6). **BMP32C10** (0.010 M, 5.4 mg) and **V-8•PF_6** (0.010 M, 3.7 mg).

5. **BMP32C10 + V-14•PF_6**:

a) **Probe Exp**.:

The same procedure was used as was for **BMP26C8 + V-9•PF_6** (solvent = acetone-d_6). **BMP32C10** (0.010 M, 5.4 mg) and **V-14•PF_6** (0.010 M, 4.6 mg).

b) **Mole Ratio Exp**.:

Two (2) separate stock solutions were made, STOCK A: 0.0100 M solution of **BMP32C10**, and STOCK B: 0.200 M solution of **V-14•PF_6** made using STOCK A. STOCK A: **BMP32C10** (10.7 mg, 0.0200 mmol) was dissolved in acetone-d_6 in a 2.0 mL volumetric flask. STOCK B: **V-14•PF_6** (92.7 mg, 0.200 mmol) was dissolved in STOCK A solution in a 1.0 mL volumetric flask. In an NMR tube, STOCK A (0.436 g, 0.500 ml) was added and analyzed by ^{1}H NMR. Small aliquots (column 2 of table) of STOCK B were then added to the initial solution via a Hamilton syringe (50 μl) (**Table V-16**). After each injection the solution was shaken to ensure complete mixing and the ^{1}H NMR of the solution was taken at the appropriate temperature. The volumes were assumed to be additive.

Table V-16. Volumetric amounts titrated and resulting concentrations of **V-14•PF_6** for the Mole Ratio experiment for **BMP32C10 + V-14•PF_6**. [**BMP32C10**] = 10 mM.

Entry	Vol. (μl) of STOCK B added	Cumm. Vol. (μl) of STOCK B added	Total Vol. (μl)	[V-14•PF_6] (mM)
1	-	-	500	-
2	2	2	502	0.8
3	3	5	505	2
4	5	10	510	4
5	8	18	518	7
6	10	28	528	11
7	12	40	540	15
8	15	55	555	20
9	18	73	573	26
10	20	93	593	31
11	25	118	618	38
12	30	148	648	46

6. **DB24C8 + V-8•PF_6**:

The same procedure was used as was for **BMP26C8 + V-9•PF_6** in appropriate deuterated solvents. **DB24C8** (0.010 M, 4.5 mg) and **V-8•PF_6** (0.010 M, 3.7 mg).

7. **DB24C8 + V-10•PF_6**:

a) **Mole Ratio Exp**.:

Two (2) separate stock solutions were made, STOCK A: 0.010 M solution of **DB24C8**, and STOCK B: 0.149 M solution of **V-10•PF_6** made using STOCK A. STOCK A: **DB24C8** (9.3 mg, 0.020 mmol) was dissolved in acetone-d_6 in a 2.0 mL volumetric flask. STOCK B: **V-10•PF_6** (41.0 mg, 0.149 mmol) was dissolved in STOCK A solution in a 1.0 mL volumetric flask. In an NMR tube, STOCK A (0.665 g, 0.763 ml) was added and analyzed by ^{1}H NMR. Small aliquots (column 3 of table) of STOCK B were then added to the initial solution via a Hamilton syringe (50 μl) (**Table V-17**). After each injection

the solution was shaken to ensure complete mixing and the ^{1}H NMR of the solution was taken at the appropriate temperature. The volumes were assumed to be additive

Table V-17. Volumetric amounts titrated and resulting concentrations of **V-10•PF_6** for the Mole Ratio experiment for **DB24C8 + V-10•PF_6**. [**DB24C8**] = 10 mM.

Entry	Vol. (μl) of STOCK B added	Cumm. Vol. (μl) of STOCK B added	Total Vol. (μl)	[V-10•PF_6] (mM)
1	-	-	763	-
2	2	2	765	0.4
3	3	5	768	1
4	5	10	773	2
5	7	17	780	3
6	10	27	790	5.1
7	20	47	810	8.7
8	30	77	840	14
9	40	117	880	20
10	50	167	930	27
11	70	237	1000	35
12	100	337	1100	45.6
13	130	467	1230	56.6
14	170	637	1400	67.8
15	200	837	1600	77.9

8. **DB24C8 + V-13•2(PF_6) and V-14•2(PF_6)**:

The ^{1}H NMR experiments for the calculation of K were conducted as follows. In an NMR tube the appropriate salt (10 mmol) was dissolved in the NMR solvent mixture ($CDCl_3$:CD_3CN, 1:1, v:v) in a 1.0 mL volumetric flask to give a solution concentration of 0.010 M. An ^{1}H NMR spectrum was then taken. **DB24C8** (4.48 mg, 10.0 mmol) was added and another ^{1}H NMR spectrum was taken. **DB24C8** (44.8 mg, 100 mmol) was then added to the same NMR tube to make the final concentration of the crown equal to 0.10 M and an ^{1}H NMR spectrum was taken. This was done for all four salts **V-13•2(PF_6)**, **V-14•2(PF_6)**, **V-15•2(PF_6)**, and **V-16•2(PF_6)**. One more ^{1}H NMR experiment was

conducted on a 0.010 M (4.48 mg, 10.0 mmol) solution of **DB24C8** alone giving a total of 13 ^{1}H NMR experiments.

9. **30C10 + V-9•PF_6**:

a) **Probe Exp**.:

The same procedure was used as was for **BMP26C8 + V-9•PF_6** (solvent = acetone-d_6). **30C10** (0.010 M, 4.4 mg) and **V-9•PF_6** (0.010 M, 3.4 mg).

b) **Mole Ratio Exp**.:

Two (2) separate stock solutions were made, STOCK A: 0.010 M solution of **30C10**, and STOCK B: 0.150 M solution of **V-9•PF_6** made using STOCK A. STOCK A: **30C10** (8.8 mg, 0.020 mmol) was dissolved in acetone-d_6 in a 2.0 mL volumetric flask. STOCK B: **V-9•PF_6** (51.5 mg, 0.150 mmol) was dissolved in STOCK A solution in a 1.0 mL volumetric flask. In an NMR tube, STOCK A (0.658 g, 0.755 ml) was added and analyzed by ^{1}H NMR. Small aliquots (column 3 of table) of STOCK B were then added to the initial solution via a Hamilton syringe (50 μl) (**Table V-18**). After each injection the solution was shaken to ensure complete mixing and the ^{1}H NMR of the solution was taken at the appropriate temperature. The volumes were assumed to be additive.

Table V-18. Volumetric amounts titrated and resulting concentrations of **V-9•PF_6** for the Mole Ratio experiment for **30C10 + V-9•PF_6**. [**30C10**] = 10 mM.

Entry	Vol. (μl) of STOCK B added	Cumm. Vol. (μl) of STOCK B added	Total Vol. (μl)	[V-9•PF_6] (mM)
1	-	-	755	-
2	1	1	756	0.2
3	2	3	758	0.6
4	3	6	761	1
5	5	11	766	2
6	7	18	773	3
7	10	28	783	5.4
8	20	48	803	9.0
9	30	78	833	14
10	40	118	873	20
11	50	168	923	27
12	70	238	993	36
13	100	338	1093	46.4
14	130	468	1223	57.4
15	170	638	1393	68.7
16	200	838	1593	78.9

10. **32-Cryptand + V-9•PF_6**:

a) **Probe Exp**.:

The same procedure was used as was for **BMP26C8 + V-9•PF_6** (solvent = acetonitrile-d_3). **32-Cryptand** (0.010 M, 7.3 mg), 2) **V-9•PF_6** (0.010 M, 3.4 mg)

b) **Mole Ratio Exp**.:

Two (2) separate stock solutions were made, STOCK A: 0.010 M solution of **V-9•PF_6**, and STOCK B: 0.2000 M solution of **32-Cryptand** made using STOCK A. STOCK A: **V-9•PF_6** (6.9 mg, 0.020 mmol) was dissolved in acetonitrile-d_3 in a 2.0 mL volumetric flask. STOCK B: **32-Cryptand** (145.3 mg, 0.2000 mmol) was dissolved in STOCK A solution in a 1.0 mL volumetric flask. In an NMR tube, STOCK A (0.422 g, 0.500 ml) was added and analyzed by ^{1}H NMR. Small aliquots (column 3 of table) of STOCK B were then added to the initial solution via a Hamilton syringe (50 μl) (**Table V-19**).

After each injection the solution was shaken to ensure complete mixing and the ^{1}H NMR of the solution was taken at the appropriate temperature. The volumes were assumed to be additive.

Table V-19. Volumetric amounts titrated and resulting concentrations of **32-Cryptand** for the Mole Ratio experiment for **32-CRYPTAND + V-9•PF_6**. [**V-9•PF_6**] = 10 mM.

Entry	Vol. (μl) of STOCK B added	Cumm. Vol. (μl) of STOCK B added	Total Vol. (μl)	[32-Cryptand] (mM)
1	-		500	-
2	1	1	501	0.4
3	2	3	503	1
4	10	13	513	5.1
5	20	33	533	12
6	35	68	568	24
7	45	113	613	37
8	65	178	678	53
9	85	263	763	69
10	115	378	878	86.1
11	150	530	103	103
12	200	730	123	119

Mass Spectroscopic Analyses

For High Resolution FAB-MS equimolar solutions of both components were made in acetone and the solvent was allowed to evaporate slowly. The matrix was 3-NBA. For ESI-MS the samples were diluted to an unknown concentration in acetone/methanol (20/80%) and the fragmentor was run at a low potential of 27 V. High Resolution FAB-MS gave m/z = 674.3614 (dev. -11.7 ppm), 646.3384 (dev. 0.6 ppm), 578.3715 (dev. 3.8 ppm), 762.4224 (dev. 0.8 ppm), 1077.4785 (dev. -4.1 ppm), and 999.4364 m/z (deviation 0.6 ppm) for **BMP26C8:V-8$^+$, BMP26C8:V-9$^+$**, **BMP26C8:V-10$^+$**, **BMP32C10:V-8$^+$**, **BMP32C10:(V-9)$_2$·PF_6^+**, and **BMP32C10:V-14$^+$**, respectively.

ESI-MS analyses gave m/z = 674.6, 646.5, 578.5, 666.4, and 638.5 for **BMP26C8:V-8$^+$**, **BMP26C8:V-9$^+$**, and **BMP26C8:V-10$^+$**, **30C10:V-8$^+$**, and **30C10:V-9$^+$**, respectively.

X-ray Crystallography

All software and sources of the scattering factors are contained in the SHELXTL (version 5.03) program library (G. Sheldrick, Siemens XRD, Madison, WI). All other non-hydrogen atoms were refined with anisotropic displacement coefficients. All hydrogen atoms were treated as idealized contributions.

For **V-7 (BMP26C8)**: X-ray crystallographic data were obtained using a Siemens R3m/v single crystal diffractometer. See **Table V-20** for X-ray crystallographic data.

For **BMP32C10:(V-8)$_2$•2PF$_6$, BMP32C10:(V-9)$_2$•2PF$_6$,** and **BMP32C10:V-14•2(PF$_6$)**: X-ray crystallographic data were obtained using a Siemens CCD-detector-equipped P4 diffractometer (a four-circle SMART system). The systematic absences in the diffraction data were consistent for the reported space group for **BMP32C10:(V-8)$_2$•2(PF$_6$)**, **BMP32C10:V-14•2(PF$_6$)** and space groups $P\bar{1}$ and $P1$ for **BMP32C10:(V-9)$_2$•2(PF$_6$)**. Even though the E-statistics for the latter strongly suggested the non-centrosymmetric space group $P1$, both possibilities were explored, but only space group $P\bar{1}$ yielded chemically reasonable and computationally stable results and refinement. The structures were solved using direct methods, completed by subsequent difference Fourier synthesis and refined by full-matrix least-squares procedures. In both structures the crown ethers reside on inversion centers. In the case of **BMP32C10:(V-8)$_2$•2(PF$_6$)**, two carbon atoms (C(9) and C(10)) are disordered between two positions in a 2:1 ratio and were refined isotropically. See **Table V-20** for X-ray crystallographic data.

Table V-20. X-ray crystallographic data.

	V-7, BMP26C8	**BMP32C10: (V-8)$_2$·2PF$_6$)**	**BMP32C10: (V-9)$_2$·2(PF$_6$)**	**BMP32C10: V-14•2(PF$_6$)**
Formula	$C_{24}H_{32}O_8$	$C_{60}H_{80}F_{12}N_2O_{10}P_2$	$C_{56}H_{72}F_{12}N_2O_{10}P_2$	$C_{56}H_{78}F_{12}N_2O_{12}P_2$
Formula weight (g/mol)	448.51	1279.20	1223.10	1261.14
Lattice type	Monoclinic	Monoclinic	Triclinic	Monoclinic
Space Group	$P2_1/n$	$P2_1/n$	P-1	$P2_1/c$
***T*, K**	298(2)	243(2)	222(2)	173(2)
***a* (Å)**	11.382(3)	12.250(2)	11.0034(2)	10.2919(2)
***b* (Å)**	16.111(2)	11.294(4)	11.88170(10)	22.9186(5)
***c* (Å)**	12.8971(11)	23.473(3)	13.1435(2)	26.2672(4)
α (deg)	-	-	102.9690(1)	-
β (deg)	102.479(11)	98.522(5)	113.7160(10)	94.8390(10)
χ (deg)	-	-	96.0480(10)	-
***V* (Å^3)**	2309.2(7)	3211.8(12)	1495.81(4)	6173.7(2)
Z	4	2	1	4
***D*$_c$, (g cm^{-3})**	1.290	1.323	1.358	1.357
***F*(000)**	960	1344	1280	
μ (mm^{-1})	0.096	0.158	0.167	
Θ Range (deg)	2.05 – 22.50	4.0 - 45.0	3.5 - 56.2	4.0 - 56.0
No. of unique reflections:				
Measured	2913	4182	6409	
Observed		2264	5515	8503
No. of variables	290	388	370	
***R* (%)**	4.26	6.67	5.57	
***R*$_w$ (%)**	9.25	15.89	22.35	10.24

V.5 References

1) Pedersen, C. J. *J. Am. Chem. Soc.* **1967**, *89*, 2495.

2) Pedersen, C. J. *J. Am. Chem. Soc.* **1967**, *89*, 7017.

3) Cram, D. J.; Cram, J. M. *Science* **1974**, *183*, 803.

4) Cram, D. J.; Helgeson, R. C.; Sousa, L. R.; Timko, J. M.; Newcomb, M.; Moreau, P.; Jong, F. D.; Gokel, G. W.; Hoffman, D. H.; Domeier, L. A.; Peacock, S. C.; Madan, K.; Kaplan, L. *Pure Appl. Chem.* **1975**, *43*, 327.

5) Goldberg, I. *Complexes of Crown Ethers with Molecular Guests*; Goldberg, I., Ed.; Academic Press: London, 1984; Vol. 2, pp 261-335.

6) Bradshaw, J. S.; Izatt, R. M.; Bordunov, A. V.; Zhu, C. Y.; Hathaway, J. K. *Crown Ethers*; Bradshaw, J. S.; Izatt, R. M.; Bordunov, A. V.; Zhu, C. Y.; Hathaway, J. K., Ed.; Pergamon: Oxford, UK, 1997; Vol. 1, pp 35-95.

7) Vögtle, F.; Seel, C.; Windscheif, P.-M. *Cyclophane Hosts: Endoacidic, Endobasic, and Endolipophilic Large Cavities*; Vögtle, F.; Seel, C.; Windscheif, P.-M., Ed.; Pergamon: Oxford, UK, 1997; Vol. 2, pp 211-265.

8) Vögtle, F. *Supramolecular Chemistry; an Introduction*; John Wiley & Sons Ltd.: Chichester, UK, 1991.

9) Sutherland, I. O. *Chem. Soc. Rev.* **1986**, *15*, 63-91.

10) Stoddart, J. F. *Chiral Crown Ethers*; Stoddart, J. F., Ed.; John Wiley & Sons: New York, 1987; Vol. 17, pp 207-288.

11) Gokel, G. W. *Crown Ethers and Cryptands*; Gokel, G. W., Ed.; John Wiley & Sons Ltd.: Chichester, 1996, pp 263-307.

12) Gokel, G. W. *Crown Ethers and Cryptands*; The Royal Society of Chemistry: Cambridge, UK, 1991.

13) Ovchinnikov, Y. A.; Ivanov, V. T.; Shkrob, A. M. *Membrane Active Complexones*; Elsevier: New York, 1974.

14) Pressman, B. C. *Ann. Rev. Biochem.* **1976**, *45*, 501.

15) Goldberg, I. *Acta Crystallogr., Sect. B* **1975**, *31*, 2592.

16) Metcalfe, J. C.; Soddart, J. F.; Jones, G. *J. Am. Chem. Soc.* **1977**, *99*, 8317-8319.

17) Barrett, A. G. M.; Lana, J. C. A.; Tograie, S. *J. Chem. Soc., Chem. Commun.* **1980**, 300.
18) Barrett, A. G. M.; Lana, J. C. A. *J. Chem. Soc., Chem. Commun.* **1978**, 471.
19) Vögtle, F.; Weber, E. *Kontakte (Darmstadt)* **1977**, *No. 1*, 11.
20) Starks, C. M.; Liotta, C. L.; Halpern, M. *Phase-Transfer Catalysis: Fundamentals, Applications, and Industrial Perspectives*; Chapman & Hall: New York, 1994.
21) Ochiai, E. *Bioinorganic Chemistry: an Introduction*; Allyn and Bacon: Boston, 1977.
22) Heumann, K. G. *Top. Curr. Chem.* **1985**, *127*, 77.
23) *Proceedings of the Symposium on High Power, Ambient Temperature Lithium Batteries*; Electrochemical Society: Pennington, NJ, 1992.
24) Vögtle, F.; Weber, E. *The Chemistry of the Ether Linkage, Suppl. E, Part 1*; Wiley: Chichester, 1981.
25) Hancock, R. D. *Acc. Chem. Res.* **1990**, *23*, 253.
26) Kollman, P. A.; K. M. Merz, J. *Acc. Chem. Res.* **1990**, *23*, 246.
27) Brodbelt, J.; Maleknia, S.; Lin, C.; Lagow, R. *J. Am. Chem. Soc.* **1991**, *113*, 5913.
28) Brodbelt, J.; Maleknia, S.; Lagow, R.; Lin, T. Y. *J. Chem. Soc., Chem. Commun.* **1991**, 1705.
29) Maleknia, S.; Brodbelt, J. *J. Am. Chem. Soc.* **1992**, *114*, 4295.
30) Mecozzi, S.; Rebek, J. *Chem. Eur. J.* **1998**, *4*, 1016-1022.
31) Gokel, G. W.; Abel, E. *Complexation of Organic Cations*; Gokel, G. W.; Abel, E., Ed.; Pergamon: Oxford, UK, 1997; Vol. 1, pp 511-535.
32) Izatt, R. M.; Lamb, J. D.; N. E. Izatt; B. E. Rossiter, J.; Christensen, J. L.; Haymore, B. L. *J. Am. Chem. Soc* **1979**, *101*, 6273.
33) Lehn, J.-M.; Vierling, P. *Tetrahedron Lett.* **1980**, 1323.
34) Bovill, M. J.; Chadwick, D. J.; Johnson, M. R.; Jones, N. F.; Sutherland, I. O.; Newton, R. F. *J. Chem. Soc., Chem. Commun.* **1979**, 1065-1066.
35) Tsukube, H. *Bull. Chem. Soc. Jpn.* **1984**, *57*, 2685-2686.
36) Leigh, S. J.; Sutherland, I. O. *J. Chem. Soc., Perkin. Trans. 1* **1979**, 1089.

37) Pearson, D. P. J.; Leigh, S. J.; Sutherland, I. O. *J. Chem. Soc., Perkin Trans. 1* **1979**, 3113.

38) Johnson, M. R.; Sutherland, I. O.; Newton, R. F. *J. Chem. Soc., Perkin. Trans. 1* **1979**, 357.

39) Hodgkinson, L. C.; Sutherland, I. O. *J. Chem. Soc., Perkin Trans. 1* **1979**.

40) Hodgkinson, L. C.; Johnson, M. R.; Leigh, S. J.; Spencer, N.; Sutherland, I. O.; Newton, R. F. *J. Chem. Soc., Perkin Trans. 1* **1979**, 2193.

41) Chadwick, D. J.; Cliffe, I. A.; Newton, R. F.; Sutherland, I. O. *J. Chem. Soc., Perkin Trans. 1* **1984**, 1707.

42) Johnson, M. R.; Jones, N. F.; Sutherland, I. O. *J. Chem. Soc., Perkin Trans. 1* **1985**, 1637.

43) Timko, J. M.; Helgeson, R. C.; Newcomb, M.; Gokel, G. W.; Cram, D. J. *J. Am. Chem Soc.* **1974**, *96*, 7097.

44) Mageswaren, R.; Mageswaren, S.; Sutherland, I. O. *J. Chem. Soc., Chem. Commun.* **1979**, 722.

45) Johnson, M. R.; Sutherland, I. O.; Newton, R. F. *J. Chem. Soc., Perkin Trans. 1* **1980**, 586.

46) Meot-Ner, M. *J. Am. Chem. Soc.* **1983**, *53*, 4912.

47) Kotzyba-Hibert, F.; Lehn, J.-M.; Vierling, P. *Tetrahedron Lett.* **1980**, 941.

48) Kotzyba-Hibert, F.; Lehn, J.-M.; Saigo, K. *J. Am. Chem. Soc.* **1981**, *103*, 4266.

49) Kintzinger, J.-P.; Kotzyba-Hibert, F.; Lehn, J.-M.; Pagelot, A.; Saigo, K. *J. Chem. Soc., Chem. Commun.* **1981**, 833.

50) Abed-Ali, S. S.; Brisdon, B. J.; England, R. *J. Chem. Soc., Chem. Commun.* **1987**, 1565-1566.

51) Ashton, P. R.; Cambell, P. J.; Chrystal, E. J. T.; Glink, P. T.; Menzer, S.; Philp, D.; Spencer, N.; Stoddart, J. F.; Tasker, P. A.; Williams, D. J. *Angew. Chem., Int. Ed. Engl.* **1995**, *34*, 1865.

52) Ashton, P. R.; Chrystal, E. J. T.; Glink, P. T.; Menzer, S.; Schiavo, C.; Stoddart, J. F.; Tasker, P. A.; Williams, D. J. *Angew. Chem., Int. Ed. Engl.* **1995**, *34*.

53) Ashton, P. R.; Glink, P. T.; Martínez-Díaz, M.-V.; Stoddart, J. F.; White, A. J. P.; Williams, D. J. *Angew. Chem., Int. Ed. Engl.* **1996**, *35*, 1930.

54) Ashton, P. R.; Chrystal, E. J. T.; Glink, P. T.; Menzer, S.; Schiavo, C.; Spencer, N.; Stoddart, J. F.; Tasker, P. T.; White, A. J. P.; Williams, D. J. *Chem. Eur. J.* **1996**, *2*, 709.

55) Ashton, P. R.; Glink, P. T.; Stoddart, J. F.; Tasker, P. T.; White, A. J. P.; Williams, D. J. *Chem. Eur. J.* **1996**, *2*, 729.

56) Fyfe, M. C. T.; Stoddart, J. F. *Adv. Supramol. Chem.* **1999**, *5*, 1-53.

57) Kolchinski, A. G.; Busch, D. H.; Alcock, N. W. *J. Chem. Soc., Chem. Commun.* **1995**, 1289.

58) Ashton, P. R.; Glink, P. T.; Stoddart, J. F.; Menzer, S.; Tasker, P. T.; White, A. J. P.; Williams, D. J. *Tetrahedron Lett* **1996**, *37*, 6217.

59) Hubin, T. J.; Kolchinski, a. G.; Vance, A. L.; Busch, D. H. *Adv. Supramol. Chem.* **1999**, *5*, 237-357.

60) Nagvekar, D. S.; Yamaguchi, N.; Wang, F.; Bryant, W. S.; Gibson, H. W. *J. Org. Chem* **1997**, *62*, 4798.

61) Gibson, H. W.; Nagvekar, D. S.; Yamaguchi, N.; Wang, F.; Bryant, W. S. *J. Org. Chem.* **1997**, *62*, 4798-4803.

62) Gibson, H. W.; Delaviz, Y. *Polymer* **1994**, *34*, 1109.

63) Delaviz, Y.; Gibson, H. W. *Org. Prep. Proc. Int.* **1991**, *23*, 382.

64) Delaviz, Y.; Merola, J. S.; Berg, M. A. G.; Gibson, H. W. *J. Org. Chem.* **1995**, *60*, 516.

65) Nagvekar, D.; Gibson, H. W. *Org. Prep. Proced. Int* **1997**, *29*, 240.

66) Gibson, H. W.; Nagvekar, D. S. *Can. J. Chem.* **1997**, *75*, 1375 - 1384.

67) Yamaguchi, N.; Gibson, H. W. *J. Chem. Soc., Chem. Comm.* **1999**, 789-790.

68) Yamaguchi, N.; Gibson, H. W. *Polym. Mater. Sci. Eng. (Am. Chem. Soc. Div. Polym. Mater. Sci. Eng.)* **1999**, *80*, 217-218.

69) Yamaguchi, N.; Gibson, H. W. *Angew. Chem., Int. Ed. Engl.* **1999**, *38*, 143-147.

70) Yamaguchi, N.; Hamilton, L. M.; Gibson, H. W. *Angew. Chem. Int. Ed. Engl.* **1998**, *37*, 3275-3279.

71) Yamaguchi, N.; Nagvekar, D. S.; Gibson, H. S. *Angew. Chem. Int. Ed. Engl.* **1998**, *37*, 2361-2364.

72) Fyfe, M. C. T.; Stoddart, J. F. *Acc. Chem. Res* **1997**, *30*, 393.

73) Tsukube, H.; Furuta, H.; Odani, A.; Takeda, Y.; Kudo, Y.; Inoue, Y.; Liu, Y.; Sakamoto, H.; Kimura, K. *Comprehensive Supramolecular Chemistry*; J. E. D. Davies J. A. Ripmeester, Ed.; Pergamon: Oxford, UK, 1997; Vol. 8, pp 425-482.

74) Sutherland, I. O. *Pure Appl. Chem.* **1989**, *61*, 1547.

75) Sutherland, I. O. *Adv. Supramol. Chem.* **1990,** *1*, 65-108.

76) A. S. Meyer, J.; Ayres, G. H. *J. Am. Chem. Soc.* **1957**, *79*, 49.

77) Chriswell, C. D.; Schilt, A. A. *Anal. Chem.* **1975**, *47*, 1623.

78) Whitlock, B. J.; Whitlock, H. W. *J. Am. Chem. Soc.* **1990**, *112*, 3910.

79) Hanna, M. W.; Ashbaugh, A. L. *J. Phys. Chem.* **1964**, *68*, 811.

80) Benesi, H. A.; Hildebrand, J. H. *J. Am. Chem. Soc.* **1949**, *71*, 2703.

81) Deranleau, D. A. *J. Am. Chem. Soc.* **1969**, *91*, 4050.

82) Sahai, R.; Loper, G. L.; Lin, S. H.; Eyring, H. *Proc. Natl. Acad. Sci. USA* **1974**, *71*, 1499.

83) Wachter, H. N.; Fried, V. *J. Chem. Ed.* **1974**, *51*, 798.

84) Rose, N. J.; Drago, R. S. *J. Am. Chem. Soc.* **1959**, *81*, 798.

85) Creswell, C. J.; Allred, A. L. *J. Phys. Chem.* **1962**, *66*, 1469.

86) Horman, I.; Dreux, B. *Anal. Chem.* **1983**, *55*, 1219-1221.

87) Wilcox, C. S. *Frontiers in Supramolecular Chemistry and Photochemistry*; Wilcox, C. S., Ed.; VCH Publishers: New York, 1991, 123-143.

88) Person, W. B. *J. Am. Chem. Soc.* **1965**, *87*, 167-170.

89) Deranleau, D. A. *J. Am. Chem. Soc.* **1969**, *91*, 4044-4049.

90) Weber, G. *Molecular Biophysics*; Pullman, B.; Weissbluth, M., Ed.; Academic Press: New York, 1965, pp 369-397.

91) Hanson, I. R.; Hughes, D. L.; Truter, M. R. *J. Chem. Soc. Perkin Trans. II* **1976**, 972.

92) Allwood, B. L.; Spencer, N.; Shahriari-Zavareh, H.; Stoddart, J. F.; Williams, D. J. *J. Chem. Soc., Chem. Commun.* **1987**, 1058.

93) Allwood, B. L.; Spencer, N.; Shahriari-Zavareh, H.; Stoddart, J. F.; williams, D. J. *J. Chem. Soc., Chem. Commun.* **1987**, 1061.

94) Slawin, A. M. Z.; Spencer, N.; Stoddart, J. F.; Williams, D. J. *J. Chem. Soc., Chem. Commun.* **1987**, 1070.

95) Jorgensen, W. L.; D, L., Severance *J. Am. Chem. Soc* **1990**, *112*, 4768.

96) Grossel, M. C.; Cheetham, A. K.; Hope, D. A.; Weston, S. C. *J. Org. Chem.* **1993**, *58*, 6651.

97) Paliwal, S.; Geib, G.; Wilcox, C. S. *J. Am. Chem. Soc.* **1994**, *116*, 4497.

98) Izatt, R. M.; Lamb, J. D.; Izatt, N. E.; Rossiter, B. E.; Christensen, J. J.; Haymore, B. L. *J. Am. Chem. Soc.* **1979**, *101*, 6273.

99) Truter, M. R.; Bush, M. A. *J. Chem. Soc., Perkin Trans. II* **1972**, 345.

100) Ashton, P. R.; Fyfe, M. C. T.; Martínez-Díaz, M.-V.; Menzer, S.; Schiavo, C.; Stoddart, J. F.; White, A. J. P.; Williams, D. J. *Chem. Eur. J.* **1998**, *4*, 1523.

101) Reichardt, C. *Sovents and Solvent Effects in Organic Chemistry*; 2 ed.; VCH: Weinheim, 1988.